FINAL REPORT

# EMISSION FTIR ANALYSES OF THIN MICROSCOPIC PATCHES OF JET FUEL RESIDUES DEPOSITED ON HEATED METAL SURFACES

James L. Lauer
Peter Vogel

Department of Mechanical Engineering,
Aeronautical Engineering and Mechanics
Rensselaer Polytechnic Institute
Troy, NY 12180-3590

Prepared for

NATIONAL AERONAUTICS AND SPACE ADMINISTRATION
Lewis Research Center

Under Grant NAG3-205

May 30, 1986

## PREFATORY NOTE

Except for the Appendix this report is the same as the one submitted in January 1984. Subsequently the NASA Fuels Group was terminated. The work described in the final appendix was partly funded by a grant from Geo-Centers, Inc. (Subcontract Agreement No. 416-008, Geo Centers, Inc.) and partly with money still left from the NASA grant. It is therefore proper to include it in this FINAL REPORT.

James L. Lauer
May 30, 1986

TABLE OF CONTENTS

## FOREWARD

This work was funded by NASA-Lewis Grant NAG 3-205. Some support was also given by ARO Grant No. DAAG 2483K0058 and by AFOSR Grant No. AFOSR-81-0005. We are very thankful to our sponsors.

The "flow-fuel" deposits were provided to us by Dr. Gary Seng of NASA-Lewis, who directed the simulator work. Later the deposit simulator (JFTOT) was donated to us by NASA and we generated our own deposits. Dr. Seng's cooperation and comments and encouragements throughout this project are most gratefully acknowledged.

The assistance of Professor T.E. Furtak and his students in obtaining the Raman spectra is acknowledged.

We are also grateful to Mr. Tim Dues, Wright-Patterson AFB, Propulsion Laboratory for his direction of our contract with Geo-Centers, Inc.

## 1.0 SUMMARY

The objective of the investigation was to relate fuel stability with fuel composition and to develop mechanisms for deposit formation, which can account for the large influence of small concentrations of nonhydrocarbons. Fuel deposits reduce heat transfer efficiency and increase resistance to fuel flow and are therefore highly detrimental to aircraft performance. Infrared emission Fourier transform spectroscopy was chosen as the primary method of analysis because it was sensitive enough to be used in situ on tiny patches (1.0 mm diameter and less) of monolayers or of only a few molecular layers of deposits which generally proved completely insoluble in any nondestructive solvents.

The bulk of the deposits were produced by NASA on metal strips (shims) in a high pressure/high temperature fuel system simulator operated with aerated fuel at varying flow rates. The shims were mounted on a slightly heated holder in such a way that the deposits faced an all-reflecting microscope objective of high numerical aperture and long working distance, which was coupled to an FTIR spectrophotometer. Some deposits were also generated in a closed small corrosion bomb on different metal strips by heating a small amount of dodecane or toluene in air.

Deposits of four base fuels were compared; dodecane, a dodecane/tetralin blend, commercial Jet A fuel, and a broadened-properties jet fuel particularly rich in polynuclear aromatics. Every fuel in turn was provided with and without small additions of such additives as thiophene, furan, pyrrole and cooper and iron naphthenates.

While the deposit weights were highest for the aromatic fuel compositions, the band intensities of C-C and C-H bands were highest for dodecane. In all cases furan and pyrrole increased weights and band intensities very strongly. Significantly, the naphthenates and tetralin, increased the intensity of the "amorphous" component of the 725/730 $cm^{-1}$ methylene rocking mode of solid paraffinic structures.

Agruments are presented for a mechanism by which the additives are concentrated on the solid surfaces and interact with oxygenated hydrocarbon radicals to form amorphous polymers.

A very thin deposit formed on silver from dodecane in the corrosion bomb was also analyzed by surface-enhanced Raman spectroscopy (SERS). Its very sharp bands were of much help in determining deposit composition. Deposit spectra and therefore compositions generated in the corrosion bomb varied considerably for aluminum, silver, and stainless steel substrates.

When the NASA-Lewis Fuel Group was dissolved the JFTOT apparatus we inherited from them was put into operation at RPI in order to generate aircraft fuel deposits for analysis by infrared emission Fourier transform spectrophotometry. Improved sensitivity of the latter apparatus made it possible to obtain spectra directly from deposits accumulated on aluminum, or preferably,

stainless steel tubes. The latter provide a higher temperature gradient and more deposits than the aluminum tubes. Comparison of the new data for the ERBS fuel with data previously obtained for deposits collected on flat shims showed that some oxidative pyrolysis occurred already on surfaces upstream of the shims and this observation together with the stepwise mechanism found, now confirms a view of deposits formation in stages, the last one being the deposition of carbonyl-(carboxyl)-containing material.

Besides runs with the ERBS fuel, one with an aluminum and two with stainless steel tubes, a run each was made with a steel tube, one with Occidental Lite Shale and one with Shale JP-4. The deposits collected with these fuels were very different from those of the ERBS fuel. They were generally thin, they exhibited maximum thickness well ahead of the position of maximum temperature and their carbonyl band in the infrared spectrum peaked at lower wavenumber (perhaps indicative of an amide-type group). These characteristics point to a mechanism in which basic nitrogen compounds interact with peroxides. To fully elucidate the mechanism specific probe compounds would have to be added to the fuel and the resulting deposits analyzed. Such a study can now be performed readily.

The infrared spectra allowed an estimate to deposit thickness of 100 to 5000 A under standard operating conditions.

## 2.0 INTRODUCTION

Aircraft fuels containing oxygen often have a tendency to form hard, sticky, carbonaceous and generally insoluble deposits on contacting surfaces at elevated temperatures. Small concentrations of nonhydrocarbons, such as nitrogn- and sulfur-containing materials, often enhance the deposit-forming tendency. In aircraft gas turbine engines these deposits may clog critical passages in valves and nozzles and decrease heat transfer efficiency through heat exchanger surfaces. These problems may increase in newer engines due to the higher temperatures and longer residence times expected with higher compression ratios and staged fuel injection. Future fuels are likely to be richer in aromatics and nonhydrocarbons than present ones and therefore likely to aggravate the deposit problems even more.

Clearly there is a need for the testing of fuels for their deposit-forming tendencies. In the longer run, however, an understanding of the mechanisms leading to deposit formation must be developed so that future fuels and engines can be designed to minimize deposit problems. Most of the testing is done today with small flow systems allowing for fuel and surface heating and the injection of controlled amounts of air or oxygen into the flowing test fuel. These JFTOT systems (Jet Fuel Thermal Oxidation Testers) typically use stainless steel or aluminum tubes, about 15 cm long, and of 0.3 cm diameter on their fuel-immersed portion for deposit collection on their outer surface. These tubes are located in the stream of test fuel and are heated by the passage of electric current. A thermocouple in the center of their hollow interior records an average temperature, but this method of heating practically

insures a temperature gradient along the tube axis. Furthermore, the large curvature of the mantle surface on which fuel deposits are formed, is very inconvenient for most methods of nondestructive chemical analysis. A superior device for deposit collection was therefore constructed at NASA-Lewis, where the surfaces are flat and removable strips of metal (shims) and of relatively large size (about 2 $cm^2$), yet small enough compared to the overall flow systems to insure uniform surface temperature.

For the study reported here both these shim deposits and deposits formed in our own laboratory on similar shims in a small corrosion test bomb under stationary conditions, were used. The fuels for this study were selected to be typical of actual ones. They were used either neat or containing small concentrations of simple molecules representative of typical nonhydrocarbon contaminants. Not unexpectedly the deposits formed under stationary conditions were different from those formed under flow because of the difference in precursor or intermediate species availability. However, the former deposits were found to be different also when shims of different metals were simultaneously used and thus provided a simple--and inexpensive--procedure for evaluating substrates. Deposit formation from liquid fuels depend very strongly on the nature of the solid boundary surfaces.

In view of the complexity of the process and the very small quantities of deposits formed in reasonable test times, say a few hours, it is not surprising that the standard deposit evaluating procedure today is still visual comparison of the deposit color with those on a standard color chart. A JFTOT "Tube Deposit Rater" (TDR) by which the reflected color is compared, has also been used. Unfortunately the "color number" so found does not provide much information of a chemical nature and therefore tells us little or nothing about the nature or mechanism of deposit formation. The procedure used in this study was infrared emission Fourier microspectrophotometry (FIEMS), which is extremely sensitive and very powerful for the solution of problems in molecular and crystalline structure. Preliminary studies of aircraft fuel deposits by FIEMS were reported previously [1] so that the apparatus and its capabilities need only a brief description. The results of the flow experiments showed that both the quantity and the nature of the deposits are altered with change of fuel composition and to some extent, change of nonhydrocarbon additive ("spike"). A strong influence of the substrate was shown in the bomb experiments.

In one instance, surface-enhanced Raman spectroscopy (SERS) was used to analyze a bomb deposit formed from dodecane on a silver surface. Because it is the first application of SERS to a "real" material, the very respectable spectrum is communicated here also.

When most of this work was completed, the JFTOT apparatus at NASA was dismantled and shipped to R.P.I., where it was reassembled and the work described in the Appendix was carried out, partly with funds still left from this grant and partly with new funds under Subcontract Agreement No. 416-008 between RPI and Geo-Centers, Inc.

Both of these grants or contracts were overspent so that no further work is expected.

## 3.0 EXPERIMENTAL

### 3.1 Apparatus and Experimental Conditions of Deposit Collection

Figure 1 is a photograph of the Modified JFTOT Flat Sample Rig (MJFSR) [1]. For this work it is important to note that the test specimens (shims) had a rectangular area of 10 x 20 mm exposed to the flowing fuel. Since the deposit weights varied between 0.02 and 0.2 mg (Figure 9) and their density was estimated as close to unity (between polyolefins and phenolic resins), thicknesses of 1000 Å to 1 μm could be estimated. These values are similar to our previously estimated values of 1000 Å, which were arrived at by scanning electron microscopy (SEM, [2]). Since these weights were obtained by differential weighings and represent small differences between relatively large numbers, their accuracy is not high. The higher weights were usually observed when naphthenates had been added to fuels. These materials are surfactants and caused deposits to be formed on both sides of the shims.

The conditions of the MJFSR runs were: test duration 120 minutes and run temperature 250°C. Since the heat-up and cooling times were excluded from the formal test duration and the temperatures were recorded at different locations on the outlet side, the actual test conditions were deduced by interpolations or small extrapolations. In any case the same conditions were always achieved and maintained to better than one percent (± 1%).

Work is now in progress to determine deposit thicknesses by ellipsometry.

For the stationary experiments in our laboratory a standard 500 mℓ stainless steel corrosion bomb was used. It was provided with inert (silicone or Viton) gaskets and filled with 10 mℓ of hydrocarbon test fluid; then several shims were inserted, and the bomb was heated to and maintained at 250°C for three hours. The hydrocarbon was in large excess over the oxygen and complete combustion was excluded, in analogy to the situation of the MJFSR where aerated fuels are used. The conditions of the bomb experiments insured that the metal strips (shims) suspended within the bomb were at uniform temperature throughout and at the same temperature as the fuel. Differences in amount and character of the material deposited on these strips must therefore be attributed exlusively to differences in the strip material deposited on these strips must therefore be attributed exclusively to differences in the strip material and cannot be attributed to temperature gradients, for example.

The deposit samples obtained from the MJFSR were all collected on commercial stainless steel foil and the same foil was also employed in the bomb experiments. However, in the latter strips of aluminum foil and silver foil

were also used as deposit collectors. For the Raman experiment a microscope slide covered with a thin evaporated silver film ("island film") was momentarily dipped into the test fluid after the test. The bomb deposit samples were very much thinner than the MJFSR ones, for they were barely visible as a change of reflectivity. The roughness of the stainless steel foil was far greater (at least three times) than that of the aluminum and silver foils; the roughness of the aluminum foil was about 50% greater than that of the silver foil. These estimates are based on the graybody background intensities in infrared emission.

### 3.2 Test Fuels

Three base fuels were used in the MJFSR: 1) Jet A, a representative jet fuel consisting of about 17% by volume of mononuclear aromatics, 0.1% of olefins, 2% of naphthalenes, and the balance of saturates; 2) ERBS, an experimental broadened-properties reference fuel, consisting of 13% mononuclear aromatics, 12% dinuclear aromatics, 2% polynuclear aromatics, 0.3% olefins and the balance of saturates; and 3) dodecane, an essentially pure hydrocarbon (aromatic and olefinic impurities less than 0.03%). In addition, a few runs were made with a mixture of 80% dodecane and 20% tetralin. Tetralin is well known for its peroxide-forming tendencies and a preliminary study of its influence on the formation and composition of the deposits was thought to be worth including.

The "spikes" or additives were tested in the MJFSR in varying concentrations. They were thiophene, furan, pyrrole and copper and iron naphthenates. For Jet A and ERBS the concentrations were: pyrrole 0.1 wt%, thiophene and furan 1.0 wt%, copper naphthenate 2PPM and iron naphthenate 1 PPM. For dodecane all the amounts were twice the above. Thiophene and pyrrole were thought to be good initial representatives of nonhydrocarbon components in fuel. The naphthenates were used because it was thought that a portion of the metals present in fuels are in organometallic form. However, the naphthenates can behave like soaps and alter the flow pattern at boundary surfaces.

Only two hydrocarbon liquids were used in the bomb experiments, dodecane and toluene.

### 3.3 Spectroscopic Analyses

Our preferred method of analysis was essentially the same Fourier emission microspectrophotometry we had used previously [2]. The schematic drawing of Figure 2 was taken from our previous publication. However, a number of improvements were made. Thus, for example, the chopper and the blackbody were relocated to a position between the heated sample and the lens. The old position below the lens, chosen for reasons of space and convenience, would lead to increased background radiation as the lens would heat up and itself become a source of radiation. This problem became particularly acute when the sample temperature was raised from 40°C to 130°C to improve the signal/noise ratio of extremely thin deposits. The tuning fork chopper was replaced by a rotating wheel at 45 degrees with the optical axis of the lens to introduce sample and blackbody radiation alternatingly into the spectrometer. The wheel was more stable and a better reflector than the tuning fork tines. However, perhaps the most important innovation of primary importance for

the analysis of the extremely thin deposits produced in our bomb experiments was a heated sample holder that would allow the planes of the shims to be placed at a high angle with the optic axis. Doing that also required a lens of longer working distance than the one used previously. A large angle of emission is of great importance when very thin samples on metal surfaces are analyzed by infrared emission, for then the metal surfaces produce an intensity pattern that has its maximum at viewing angles of 70°-80° from the surface normal (Greenler [3]).

Introduction of a variable viewing angle thus added another element of complexity in our sample location system. It is not important to describe it in detail in this paper, but it should be mentioned that a region in a deposit sample can be reproducibly located by X,Y,Z and rotational adjustments in both a horizontal and a vertical plane to about ±0.05 mm and 0.1° of angle. To make use of this precision all the instrumentation is set on an optical table of high quality. Depending on the objective lens used the deposit area viewed can be varied from about 1 $cm^2$ to 100 $\mu^2$, so that small spots of deposit can be analyzed.

In the work reported here polarization modulation was not used. The viewing angle was kept between 45 and 75°, with respect to the surface normal. The influence of viewing angle on a typical deposit spectrum is shown in Figure 3. At 0° very little structural detail appears above the background. At 45° strong bands at 1470, 1610, 1730 and 1780 $cm^{-1}$ are very distinct. These bands can be assigned to be $CH_2$ scissoring mode, the asymmetrical stretch of carboxylic acid salts, and the C=O stretches of ketones and p-lactones, respectively. As pointed out by Greenler [2], the most intense emission bands from a material adsorbed in a thin layer on a metal surface are likely to be those originating from a transition dipole vector having a strong component vibrating perpendicularly to the surface.

Our slow-scanning Fourier spectrometer is ideally suited for the analysis of the very weak infrared emissions (small sample areas, sample temperature as low as 40°C with a room temperature detector and very thin samples on metal surfaces) [4], but practical considerations allow the averaging of only a few (three or four) spectra. In general, only the spectral region from 600 to 2000 $cm^1$ could be used because of the rapid radiation intensity fall-off at higher frequencies. Furthermore, it proved to be convenient to separate this spectral region into three parts of optical filtering (600-1200, 1100-1400, and 1300-2000 $cm^{-1}$) to reduce the dynamic range. Not all ranges were run for all the spectra. The reciprocal resolution was ±5 $cm^{-1}$. The last two ranges required complete removal of moisture and carbon dioxide from the spectrometer atmosphere.

The Raman spectra were obtained with a Spex spectrometer in the RPI Physics Department.

### 3.4 Calibration

Figure 4 shows an emission spectrum of a 2.5 μm thick film of Mylar at 60°C. It is included here not only to show that all the absorption bands are clearly distinguishable as emission bands and that they appear at the same frequencies but also the three spectral ranges we use, which are separated by optical filters of sharp cutoffs. That the spectrum was not ratioed to

the blackbody, is one reason that the relative intensitites of the various bands are not those observed in absorption. Another reason for the intensity differences is the effect of the substrate and polarization.

The Mylar spectra are single spectra, not averages of many spectra as has become common practice in Fourier infrared spectroscopy.

## 4.0 RESULTS AND DISCUSSION

### 4.1 Bomb Experiements

#### 4.1.1 Infrared Emission

Figures 5 and 6 contain three infrared emissions each of deposits from dodecane and toluene, which were collected simultaneously on stainless steel, aluminum and silver strips. Thickness data are lacking, but visual comparison with deposits on tubes, whose thickness was estimated by scanning electron microscopy, would seem to indicate that these strip deposits were less than 100 Å thick. The spectra of these figures were all normalized and displaced vertically in the order of background intensity, stainless steel furnishing the highest background, no doubt because it is the poorest reflector and had the roughest surface. It should also be pointed out that all these spectra were separately obtained in three separate wavenumber regions although the composite spectra of Figures 5 and 6 appear to be continuous. Casual comparison of the spectra shows that the contrast is highest for the aluminum deposits and lowest for the stainless steel deposits, the silver deposit spectra occupying an intermediate position. The order of the spectral contrasts parallels that of the reflectivity of the substrate in the infrared (in the infrared aluminum is a somewhat better reflector than silver).

The strongest and most outstanding emission band in the spectra of the aluminum deposits formed from both dodecane and toluene is peaking at 930 $cm^{-1}$ for the former and at 910 $cm^{-1}$ for the latter. A weaker band in this spectral range is also present in all the other spectra. For this reason and because of the wavenumber difference it is unlikely that this band is merely the alumminum oxide phonon described by Mertens [5]. The chances are that it is both due to this phonon and to the OH...O out-of-plane hydrogen deformation of the carboxyl dimer. This assignment is confirmed by a strong band at 1300-1310 $cm^{-1}$, which is present in all the dodecane deposit spectra but only in the toluene deposit spectrum for aluminum. This band is considered to be caused by the C-O stretch of the carboxyl. Another carboxyl dimer band, the C=O stretch expected to be located between 1680 and 1740 $cm^{-1}$ is strongly present in both of the aluminum deposit spectra. The aluminum deposit spectra also contain a strong band at 1580 $cm^{-1}$ and a weaker one at 1430 $cm^{-1}$, which are usually assigned to the asymmetric and symmetric stretching modes of carboxylic acid salts, as well as a strong band at 1650 $cm^{-1}$, which can be assigned to C=C (olefin) stretch. The presence of a carboxylic acid in the aluminum deposits from dodecane is also indirectly confirmed by the series of nearly equispaced bands between 1200 nd 1320 $cm^{-1}$, which represent the harmonics of the $CH_2$ wagging mode; these bands are usually particularly intense in paraffinic carboxylic acids and salts. On the other had, the toluene deposits on aluminum show characteristic bands near 1580 and 1630 $cm^{-1}$, at 710 $cm^{-1}$ and around 1450 and 1500 $cm^{-1}$, which can be assigned to

the phenyl group. A band near 710 $cm^{-1}$ in all the dodecane deposits is likely to be the $CH_2$ rock. A band near 1730 $cm^{-1}$ for the dodecane deposits and near 1700 $cm^{-1}$ for the toluene deposits must be assigned to carbonyl.

There is much less evidence for carboxylic acids and little if any, for salts in the silver deposits and essentially none for either in the stainless steel deposits. In the latter the most identifiable bands, i.e., 1260 and 1350 $cm^{-1}$ for dodecane are $CH_2$ and $CH_3$ deformations. The silver deposit spectra, however, do show carbonyl bands as well.

The spectra of the bomb deposits can therefore be summarized as follows: On aluminum the hydrocarbons were partly oxidized all the way to carboxylic acids and salts, and partly to aldehydes and ketones, on silver also partly to carboxylic acids and to aldehydes and ketones and on stainless steel probably mostly to hydrocarbon polymers. The latter spectra show little evidence of the presence of carbonyl groups.

How do these spectra compare with the MJFSR spectra? A good example is shown in Figure 7.

Dodecane deposits on stainless steel are compared for the two situations. If at all present the 1260 and 1350 $cm^{-1}$ bands of the bomb experiments are essentially absent for MJFSR. However the MJFSR spectrum does show possible evidence for C=O bands at 1700, 1730 $cm^{-1}$ and a strong band at 840 $cm^{-1}$ may be indicative of olefin epoxidation. Olefins are also very likely present, as evidenced by bands near 1600 $cm^{-1}$. It would appear therefore that oxidation went further in MJFSR than in our bomb.

Unfortunately our emission spectra regions do not extend beyond 2000 $cm^{-1}$ because the available energy is too low beyond that frequency. Others encountered the same limitation (Suetaka [6]).

#### 4.1.2 Surface Enhanced Raman (SERS) Spectrum

The Raman spectrum of Figure 8, obtained by momentarily dipping a silver-coated microscope slide into the partly oxidized dodecane after the bomb test, was surprising for its quality. The deposit was barely visible as a minute reflectivity change and was probably no more than a few molecular layers thick. It shows strong bands at 820, 960, 1130, 1250, 1380, 1560, 1600 and at 1640 (strong) $cm^{-1}$. The principal infrared emission bands in the dodecane deposit on silver (Figure 5) are at 850, 910, 980, 1130, 1180, 1260, 1600, 1650 (weak) and 1730 $cm^{-1}$. Perhaps the most outstanding difference between these spectra is the clear absence of a Raman band at 1700 $cm^{-1}$ and the presence of broad and strong Raman bands but weak infrared bands grouped near 1400 and 1640 $cm^{-1}$. Since the carboxylic acid dimer is centrosymmetric, the asymmetric carbonyl stretch would be expected to fall at 1700 $cm^{-1}$ and be infrared-active only and the symmetric stretch to fall at 1640 $cm^{-1}$ and be Raman-active only. An infrared band near 1600 $cm^{-1}$ and a Raman band near 1400 $cm^{-1}$ are similarly expected for the coupled oscillators in carboxylic acid salts. Other bands in both the infrared and Raman spectra can be assigned to olefins and alkanes as shown in Table 1, which summarizes the data.

There is a great deal of recent literature on different selection rules for SERS and for ordinary Raman spectroscopy [7]. Some authors consider chemisorption a prerequisite for SERS. Our data would still be consistent with the assignments made, but no conclusions should be made on the basis of relative band intensities.

## 4.2 Lewis Thermal Stability Rig (MJFSR) Spectra

### 4.2.1 Overview

Figure 9 is a comparison of the deposit weight on the standard 2 $cm^2$ stainless steel surface and the "greatest unnormalized amplitude" (GUA) of our infrared emission spectra in the 650 - 1250 $cm^{-1}$ wavenumber region. This region includes essentially only bands representing C-C or C-H vibrational modes and the overall intensity in this region would be expected to be related only to carbonaceous, i.e., not oxidized, material. Some of the bars for the deposit weights are only partly filled to indicate that the measurements are possibly invalid; material crept under the sample shim. It is clear that the spikes (i.e., the additives) increased deposit weights considerably, especially thiophene, furan, and pyrrole, but the naphthenates had only little influence, presumably because of their lower concentrations, if the questioned data are excluded. The GUA's parallel the deposit weights in a general way, e.g., the GUA for the blanks (i.e., deposits from the neat fuel) are relatively low, but they are not proportional to them. The ratio of GUA to weight is high for the blanks and the deposits from the naphthenate spikes, but is much lower for the other spikes. If the lengths of the bars for the GUA's are added for a given fuel, then dodecane comes out first, ERBS fuel second and JETA third, but if the same is done for the deposit weights, ERBS fuel is first and JETA and dodecane about the same. What these comparisons show is the different nature of the deposits, thick deposits do not necessarily give intense spectral bands. The aromatic fuels contain less hydrogen per unit mass than the paraffinic and also give rise to aromatic deposits whose infrared emission bands are therefore weaker in the C-H region. Visual inspection of the deposit layers on the shims shows the difference in their nature by slightly different colors.

### 4.2.2 Dodecane Spectra

Figure 10 shows 600 - 2000 $cm^{-1}$ emission spectra of dodecane deposits formed at MJFSR on stainless steel shims. These spectra are included to show the complexity and the effect of the additives. Perhaps the single most important difference to be noticed in these spectra is the enhancement of a band at 1580 $cm^{-1}$ relative to its neighbors by the additives furan and the naphthenates. With the copper naphthenate spike this band is already the strongest in the spectrum, but with iron naphthenate this band is the outstanding feature in the 1400 - 2000 $cm^{-1}$ spectral region.

As mentioned earlier, the 1580 $cm^{-1}$ band was assigned to carboxyl salts. Therefore, the naphthenates, in particular, would seem to concentrate in the deposits.

To show the effect of the spikes more clearly the difference spectra of Figure 11 were plotted by computer. These spectra take into account that different spectra have different overall intensities. In all cases the deposit

spectrum derived from pure dodecane was substracted from the spectra derived from dodecane containing the spikes. Contributions of the spikes are pointing up, subtractions down. It will be noticed that all the additives enhance bands near 770 $cm^{-1}$, 1400, 1450 and 1550 $cm^{-1}$. Iron naphthenate and furan resolve the 1550 $cm^{-1}$ band from its 1580 $cm^{-1}$ neighbor. These bands occur in the additives. Thus the spectra show an increased concentration of additive material in the deposits.

The first two small emission bands on the left right after the steep initial rise of the background (caused by the optical filter) should also be compared in the spectra of Figure 10. These bands, located at 720 and 730 $cm^{-1}$ represent the "amorphous" and "crystalline" components of the $CH_2$ rocking mode of paraffinic chains. In the liquid phase only the 720 $cm^{-1}$ component is present. The "crystalline" mode arises from interactions between neighboring chains. Clearly the naphthenates enhanced the 720 $cm^{-1}$ band but virtually wiped out the other component. Tetralin did the same. These bands may therefore be related to the relative stickiness of the deposits.

### 4.2.3 Jet A and ERBS Spectra

In Figures 12 and 13 600 - 2000 $cm^{-1}$ emission spectra and their differences for Jet A are shown. When the "blank" is compared with the deposits from the spiked fuels, it will be noticed that the 720, 780, 850 $cm^{-1}$ triplet corresponding to aromatic substitution is reduced in relative importance by the naphthenates (it should be remembered that these are normalized spectra) while the 1580 $cm^{-1}$ carboxyl salt band is relatively enhanced. Again the conclusion is that these spikes concentrate on the surface.

The conclusions drawn from the ERBS emission spectra of Figures 14 and 15 are similar. The spikes enhance the 1580 $cm^{-1}$ carboxyl salt band, showing their increased concentration there.

### 4.2.4 Effect of Deposition Temperature on the Spectrum of an ERBS Deposit

Figure 16 shows an ERBS deposit spectrum obtained at 500°F and one at 600°F in the MJFSR. The strong aromatic bands at 1600 (naphthalene) and 1150 (m-substitution) $cm^{-1}$ are similar in both spectra. However, the higher temperature deposit also show strong bands at 720 and 780 $cm^{-1}$ which, if they belong to the same species, are characteristic of vicinal trisubstituted benzenes (fused polyphenyls?). An enhancement of these materials would be expected in the deposit, but confirmation of this result will be required.

## 5. CONCLUSION

If the reader has got the impression of enormous complexity, he has got the correct impression. Even a relatively simple, pure hydrocarbon such as dodecane can give rise to various polymeric and oxidized reaction products in its deposits and the distribution of these products depends on the nature of the collecting surface as well. The basic mechanism of liquid phase oxidation, viz. formation of alkyl hydroperoxides by the reaction of alkylperoxy radicals with hydrogen atom donors, which can be the hydrocarbon itself, has been well established [8]. In some instances peroxides are formed instead

of hydroperoxides. The decomposition of these peroxides then leads to unsaturates, aldehydes, ketones and acids with the strong possibility of chain reaction stimulations leading to polymers. The metal substrate can influence the deposit reaction, such as salt formation with carboxylic acid group. Our bomb experiments showed that an aluminum surface favors carboxylic acid formation, in other words more oxidation, and oxidative properties of aluminum oxide have been reported [9]. Since all the substrates in the bomb experiments were at constant temperature, their influence on deposit composition could be distinguished.

The MJFSR deposits were more highly oxidized, e.g., had more carboxyl groups, than the stationary bomb deposits, presumably because (i) more oxygen was available (it was continuously injected into the stream) and (ii) oxidized intermediates could be carried by convection as well as by diffusion. Hence the different compositons can be easily accounted for.

The Raman spectra (SERS) came out surprisingly well and were very helpful in the interpretation of infrared deposit spectral data. However, the procedure is clearly not routine and seems to work only with silver substrates, which are not realistic.

Much more realistic is the effect of the additives or spikes. Furan, thiophene and pyrrole are all very "aromatic" in their chemical behavior. They all promote deposit formation; pyrroles, e.g., were found to react strongly with peroxides to form polymeric sediments [10], but the detailed mechanism is unknown. Tetralin also reacts with peroxy radicals, even with its own hydroperoxy radical by serving as a hydrogen atom door, to form hydroperoxides [11]. The soluble copper and iron naphthenates are oxidation catalysts as well as micelle-formers like soaps. Dissolved copper in lubricating oils was found to be a good chain-initiation catalysts, dissolved iron a good chain-branching catalyst. Micelle formation of dissolved copper has been considered the reason for the maximum oxidation rate observed with increased concentration. Thus the naphthenates would also promote carboxylic acid formation from fuel and these acids would chemisorb on metal surfaces.

As was shown by one example, temperature can have a profound influence on surface deposits; higher temperatures increase the oxidation rate.

Thus fuel composition, temperature, the nature of the boundary surfaces and small amounts of nonhydrocarbons can be of great importance with regard to fuel stability and wall deposits. Oxidation is the prime chemical cause. And the spectroscopic procedures of infrared emission and Raman (SERS) spectroscopy can assist in differentiating between good and bad actors and in establishing mechanims.

## REFERENCES


1. Cohen, S.M., "Fuels Research-Thermal Stability Overview," NASA Conference Publication 2146, pp. 161-168 (April 1980).

2. Lauer, J.L. and Keller, L.E., "Oxidized Aircraft Fuel Deposits on Metal Surfaces Studied by Polarization-Modulated Fourier Infrared Emission Microspectrophotometry," Applications of Surface Sciences, 15, 50-65 (1983).

3. Greenler, R.G., "Light Emitted from Molecules Adsorbed on a Metal Surface," Surface Science, 69, 647-652 (1977).

4. Griffith, P.R., Chemical Infrared Fourier Transform Spectroscopy, John Wiley & Sons, New York, 1975, pp. 311-317.

5. Mertens, F.P., "Infrared Reflectance Study of the Oxidation of Aluminum Single Crystals," Surface Sciences, 71, 161-173 (1978).

6. Wagatsume, K., Monma, K. Suetaka, W., "Infrared Emission Spectra of Thin Films on Metal Surfaces by a Polarization Modulation Method," Applications of Surface Science, 7, 281-285 (1981).

7. Chang, R.K. and Furtak, T.E., Surface-Enhanced Raman Scattering, Plenum Press, New York, 1982, 423 pp.

8. Bell, E.R., Raley, J.H., Rust, F.R., Seubold, F.H. and Vaughan, W.E., "Reactions of Free Radicals Associated with Low Temperature Oxidation of Paraffins," Discussions of the Faraday Society, 10, 242-249 (1951).

9. Chapman, I.D. and Hair, M.L., Proceedings of the Third International Congress on Catalysis, North-Holland, Amsterdam, 1965, p. 1091.

10. Oswald, A.A. and Noel, F., J. Chem. Eng. Data, 6(2), 294 (1961).

11. Hartman, G. and Seibert, F., Helv. Chim. Acta., 15, 1390 (1932).

TABLE 1

INFRARED EMISSION AND RAMAN BANDS OF DODECANE DEPOSITS FROM BOMB EXPERIMENTS

| Infrared | | | | Raman | |
|---|---|---|---|---|---|
| Aluminum Substrate | | Silver Substrate | | Silver Substrate | |
| $cm^{-1}$ | Assignment | $cm^{-1}$ | Assignment | $cm^{-1}$ | Assignment |
| 710 | $CH_2$ rock | 710 | $CH_2$ rock | | |
| 840 | Epoxy | 780 | $CH_2$ deformation | 820 | Secondary alcohol |
| 930 | Carboxyl | 850 | Epoxy | 960 | C-C stretches (alkanes) |
| 1180 | $CH_2$ wag (alkanes) | 910 | $CH_2$ wag of C=C | 1130 | C-C stretches (alkanes) |
| 1210 | $CH_2$ wag (alkanes) | 980 | $CH_2$ wag of C=C | 1250 | Epoxy |
| 1250 | $CH_2$ wag (alkanes) | 1130 | $CH_2$ wag (alkanes) | 1380 | Carboxylate salt |
| 1310 | $CH_2$ wag (alkanes) | 1180 | $CH_2$ wag (alkanes) | 1560 | Coupled C=C stretches (1540-1620) of polymers |
| 1350 | $CH_2$ wag (alkanes) | 1200 | $CH_2$ wag (alkanes) | 1600 | |
| 1380 | $CH_2$ wag (alkanes) | 1250 | $CH_2$ wag (alkanes) | 1640 | Symmetric C=C (alkyl) stretch and carboxylic acid dimer |
| 1430 | Carboxylate salt | 1290 | $CH_2$ wag (alkanes) | | |
| 1470 | $CH_3$ deformation | 1490 | $CH_3$ deformation | | |
| 1580 | Carboxyl (salt) | 1600 | Carboxyl (salt) | | |
| 1650 | Olefin C=C stretch | 1650 | Olefin C=C stretch | | |
| 1720 | Carbonyl | 1700 | Ketone or ester carbonyl | | |
| 1740 | Carbonyl | | | | |

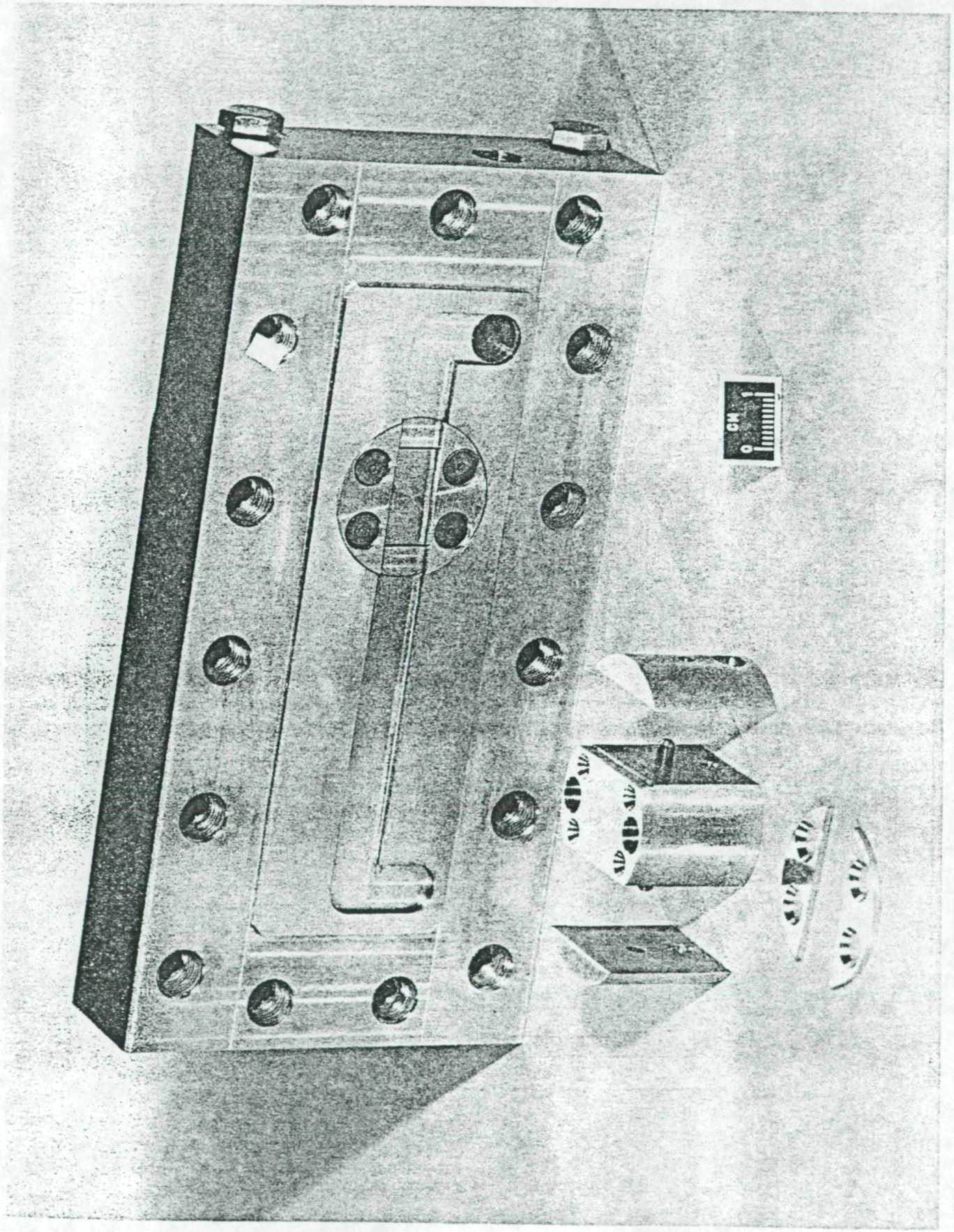


Figure 1 NASA Lewis MJF8R Deposit Sample Holder.

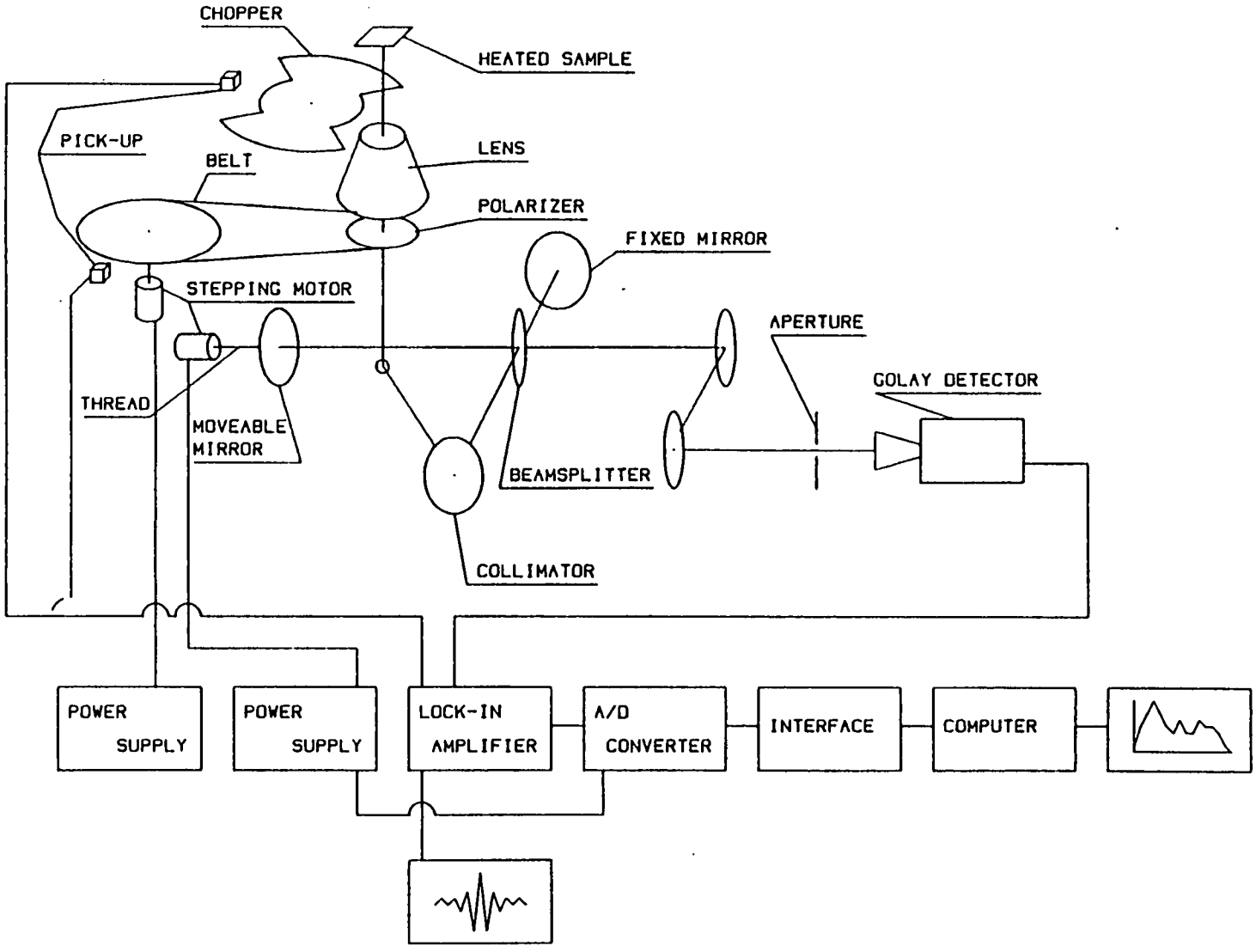


Figure 2 Schematic Drawing of Fourier Emission Microspectrophotometer

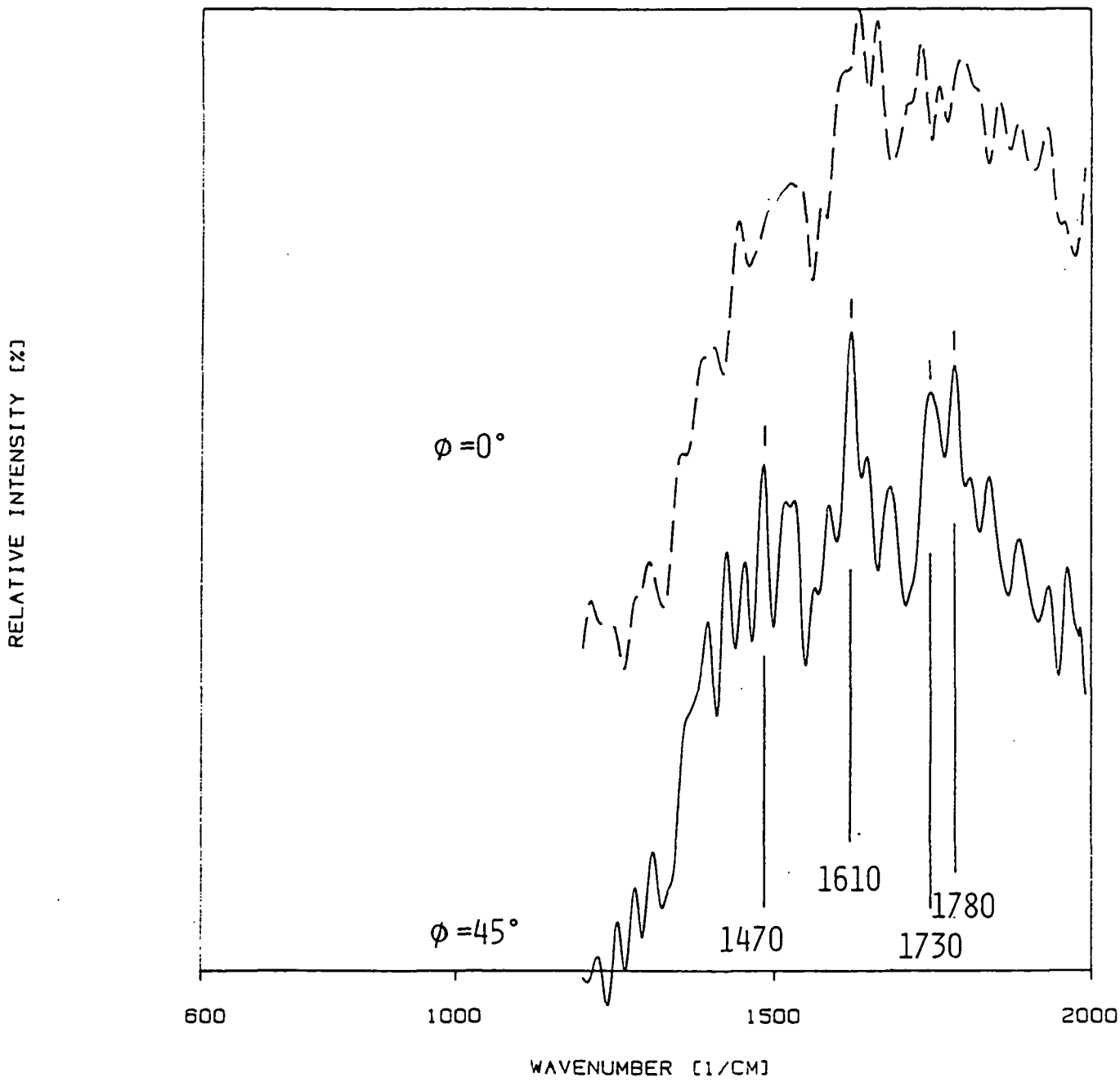


Figure 3 Change of Spectrum with Observation Angle

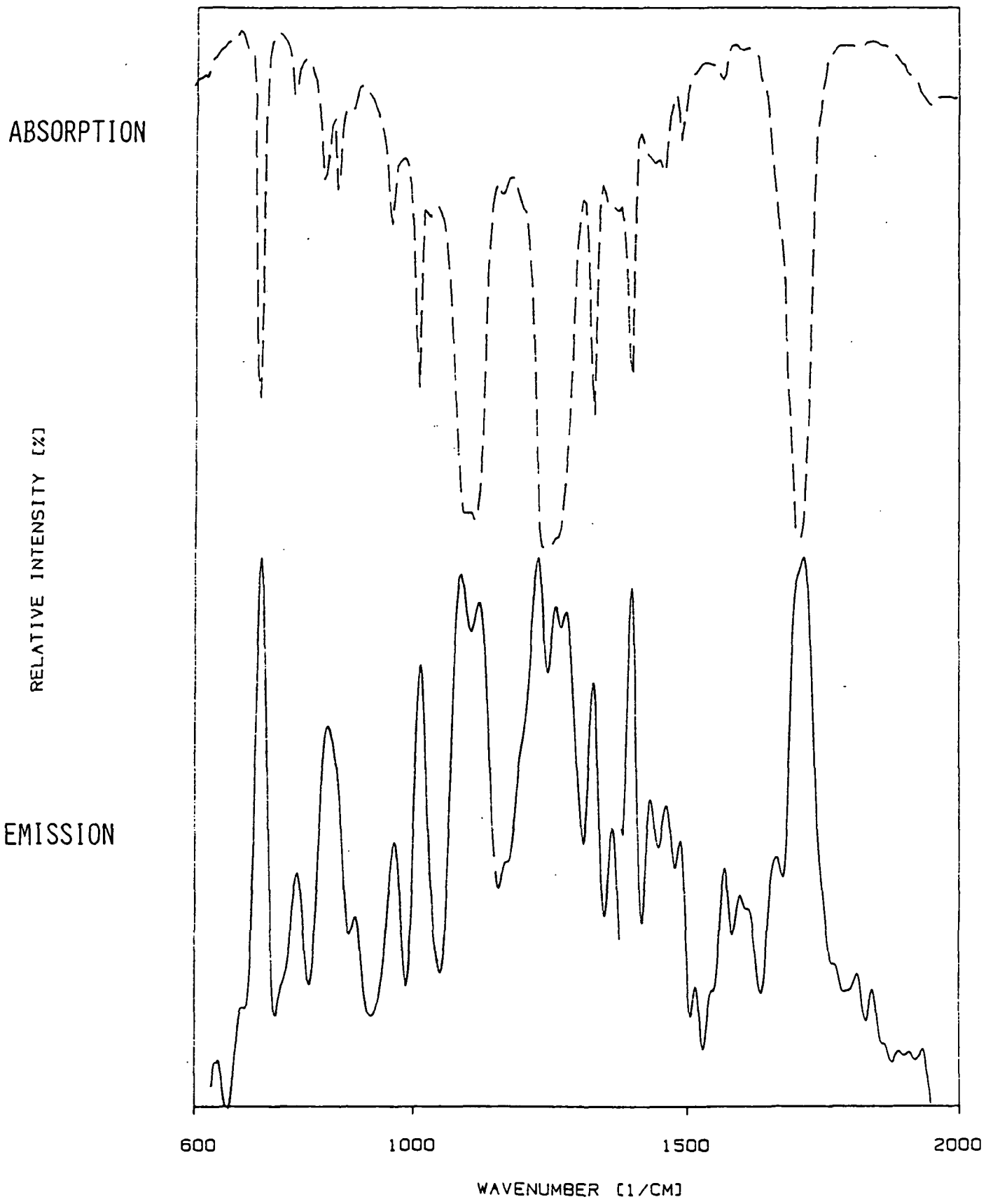


Figure 4 Absorption and Emission Spectrum of Mylar

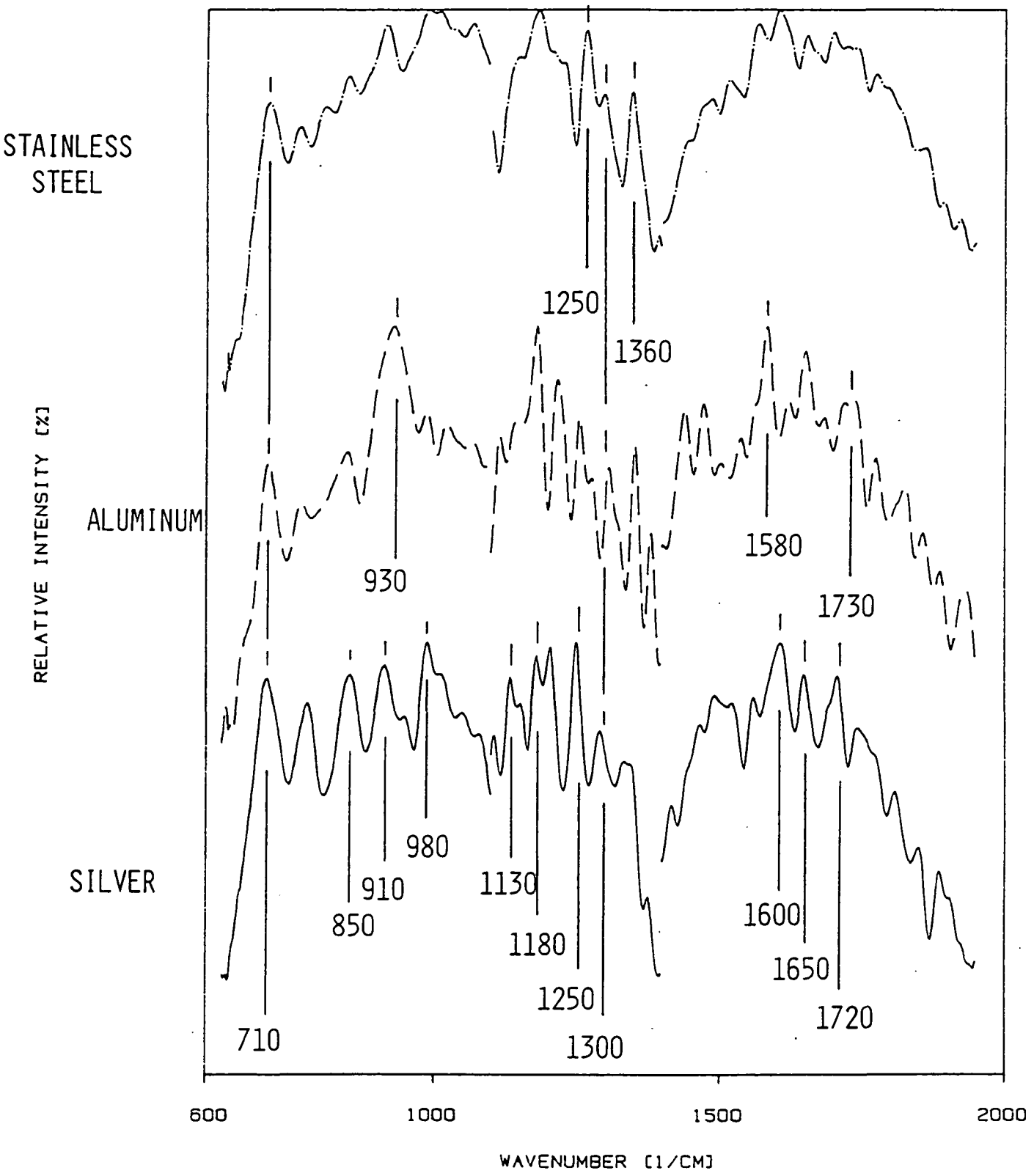


Figure 5 Emission Spectra of Dodecane Deposits Collected on Three Different Metals in a Corrosion Bomb

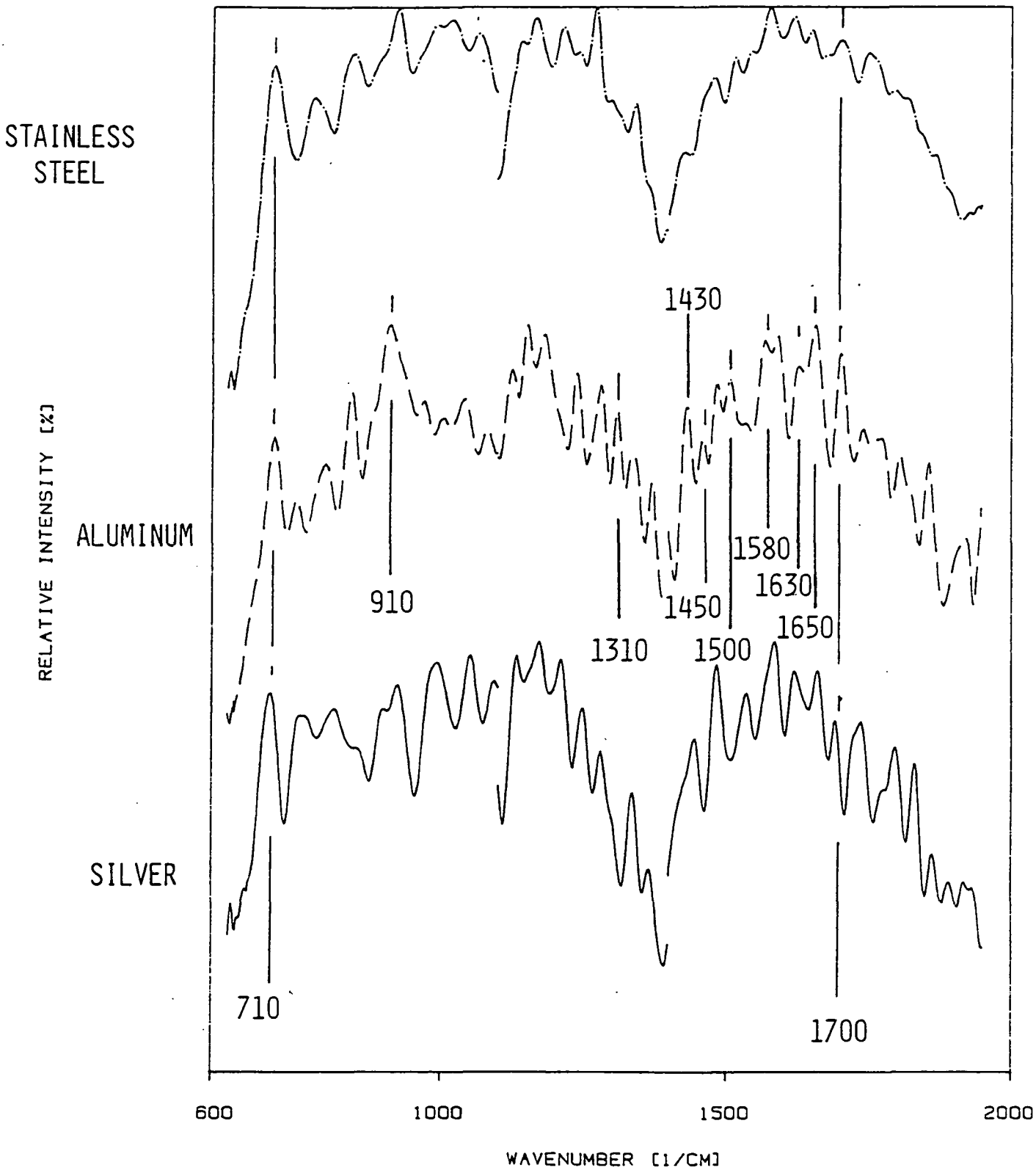


Figure 6 Emission Spectra of Toluene Deposits Collected on Three Different Metals in a Corrosion Bomb

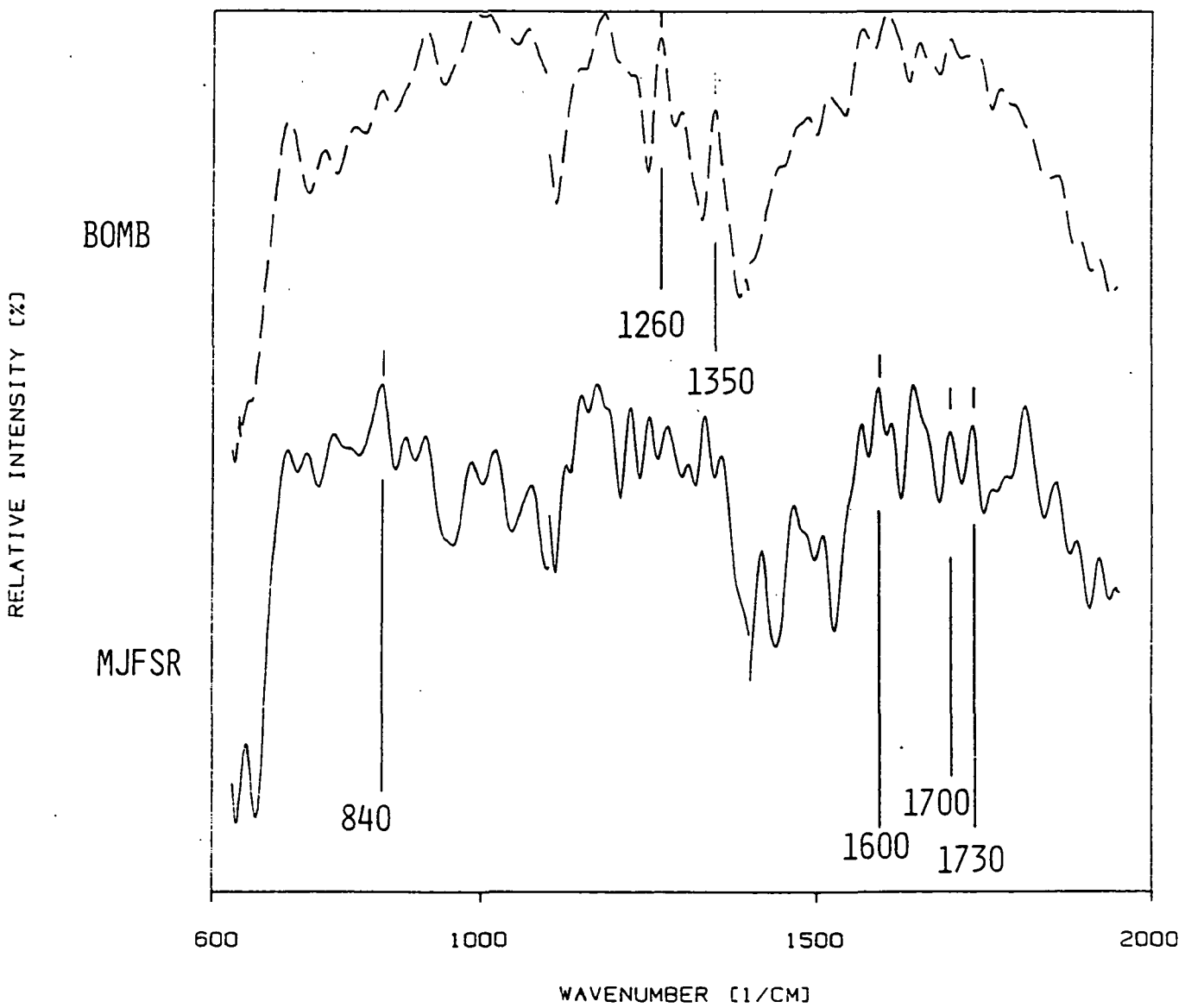


Figure 7 Comparison of Spectra from Dodecane Deposits Collected on Stainless Steel in the MJFSR and the Stainless Steel Bomb

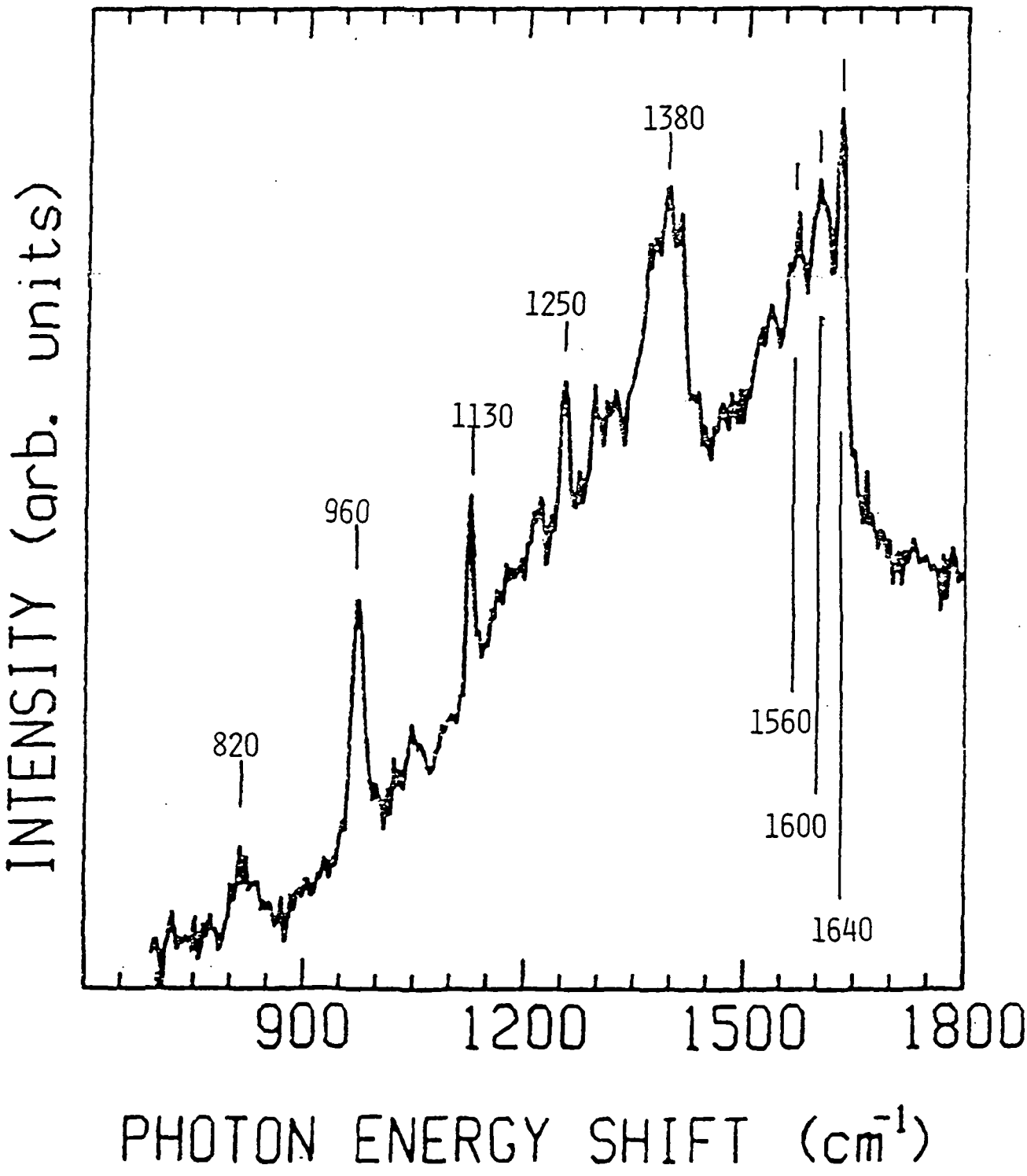


Figure 8 Raman Spectrum of a Dodecane Deposit Collected on Silver in a Stainless Steel Bomb

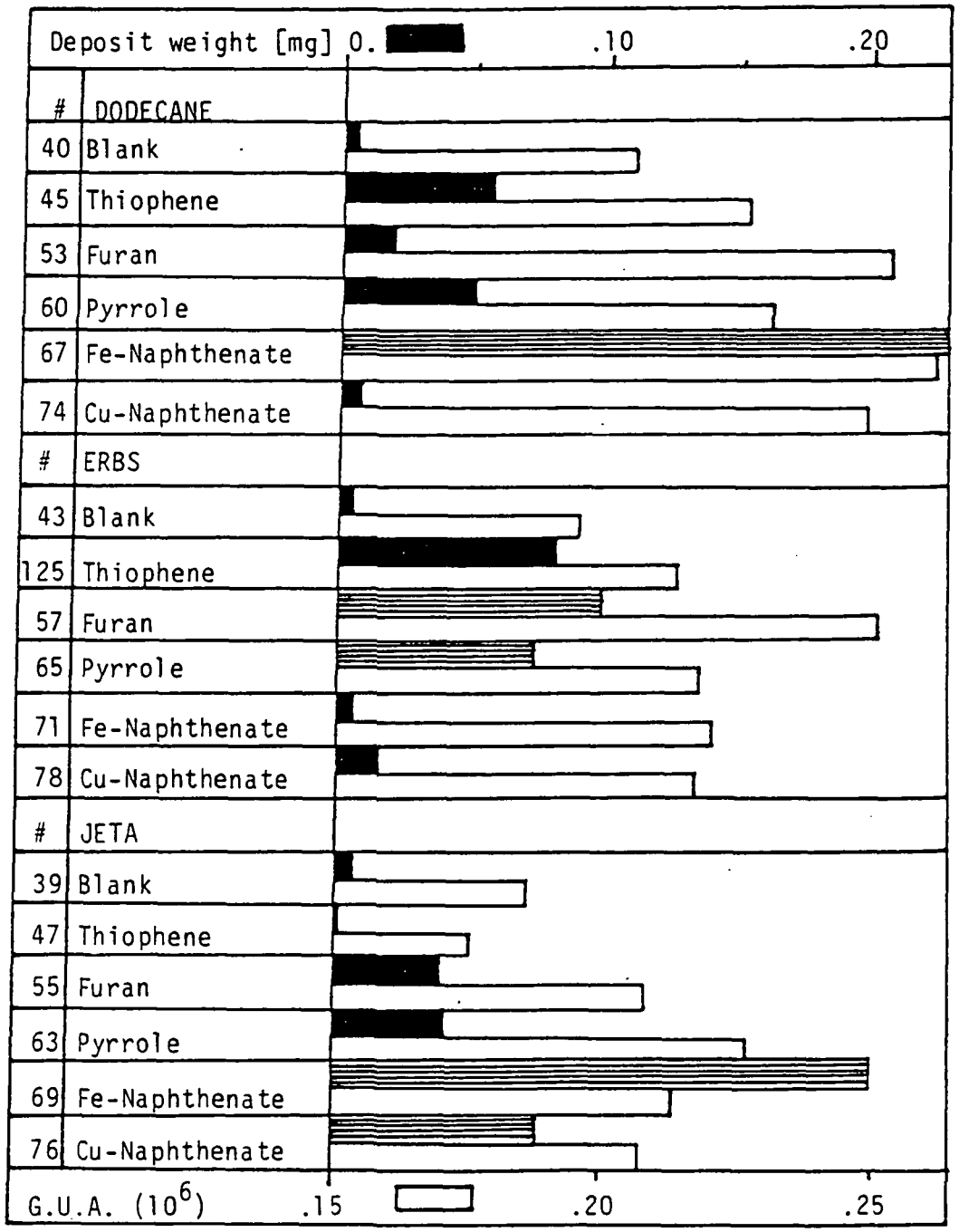


Figure 9 Comparison of MJFSR Deposit Weights and Infrared Emission Intensity (GUA). (The bars containing the horizontal lines represent weights of deposits formed on both sides of the collecting strip)

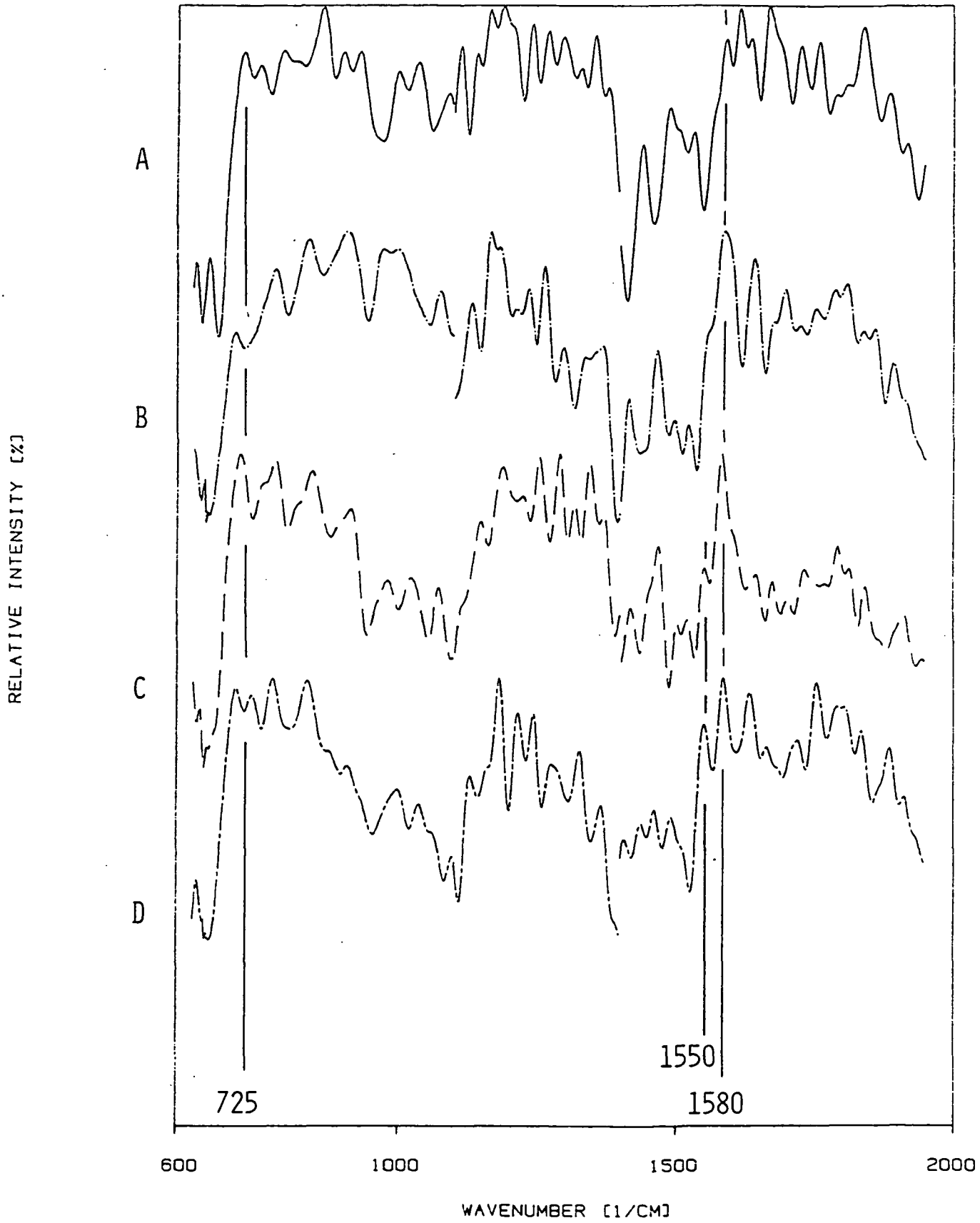


Figure 10 Emission Spectra of Dodecane Deposit on MJFSR Stainless Steel Shims (A: neat fuel, B: with copper naphthenate, C: with iron naphthenate, D: with furan)

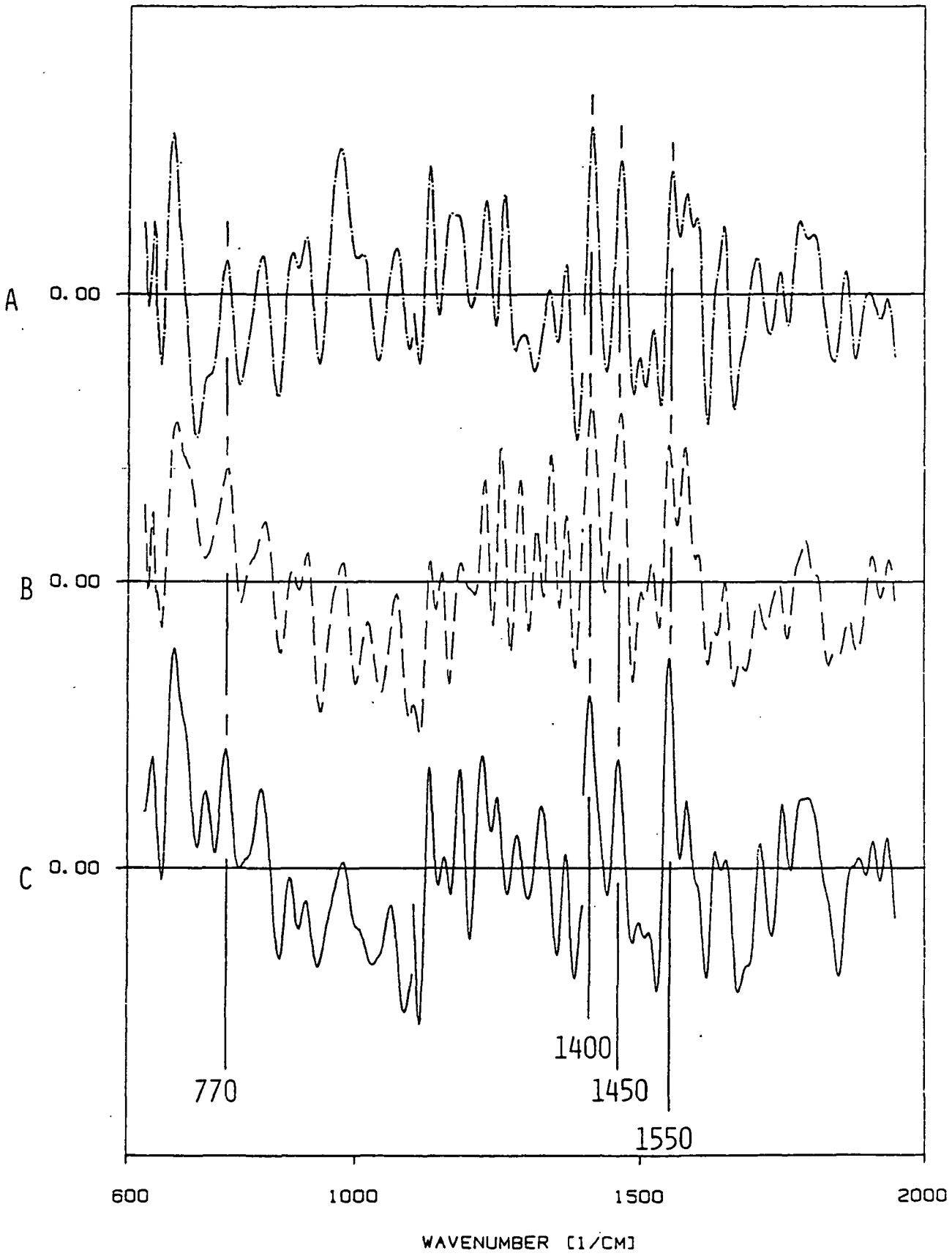


Figure 11 Difference Spectra of MJFSR Deposits from Dodecane with Additives and those of the Straight Fuel (A: with copper naphthenate minus neat, B: with iron naphthenate minus neat, C: with furan minus neat)

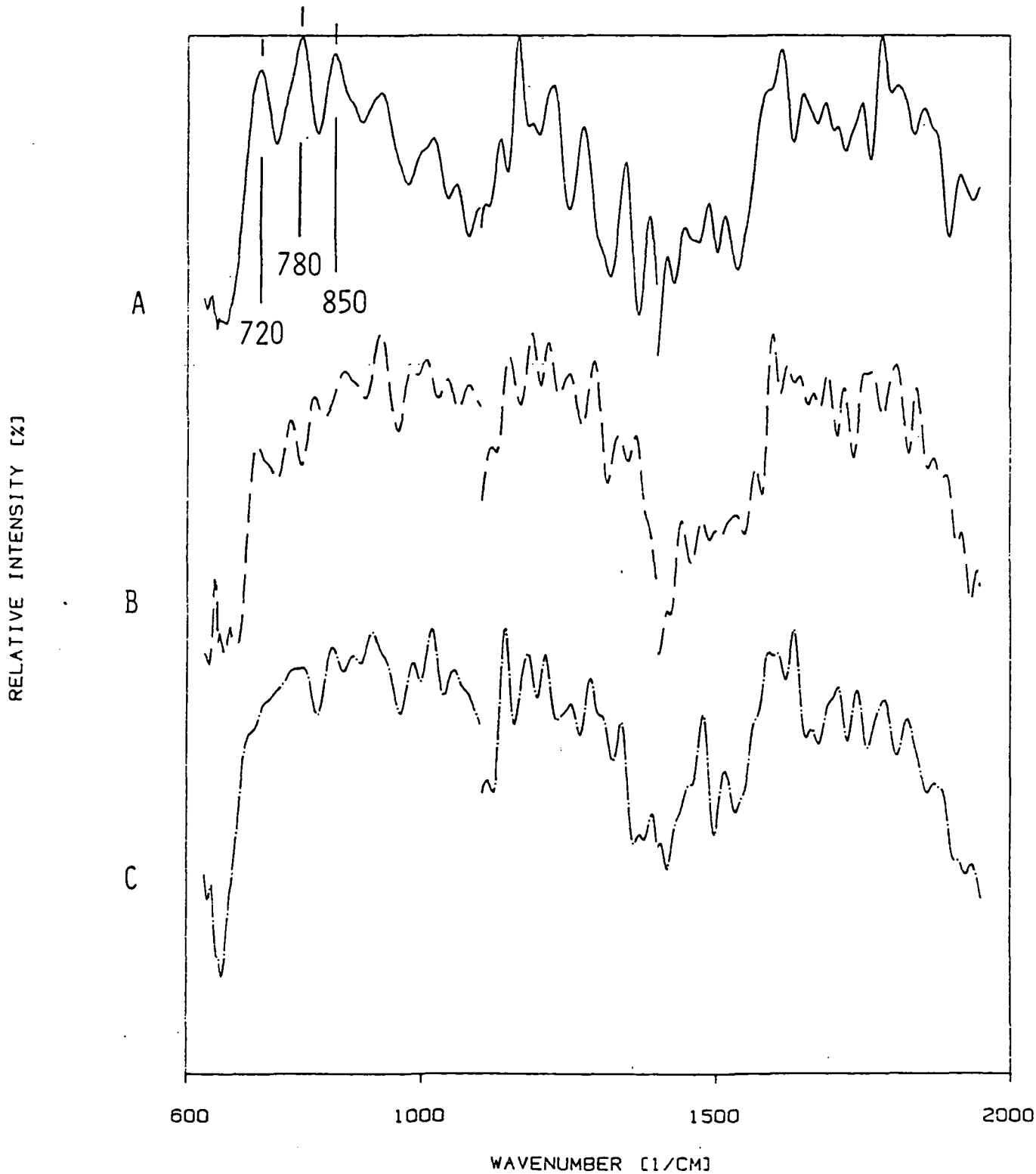


Figure 12 Emission Spectra of Jet A Fuel Deposits on MJFSR Stainless Steel Shims (A: neat fuel, B: with copper naphthenate, C: with iron naphthenate)

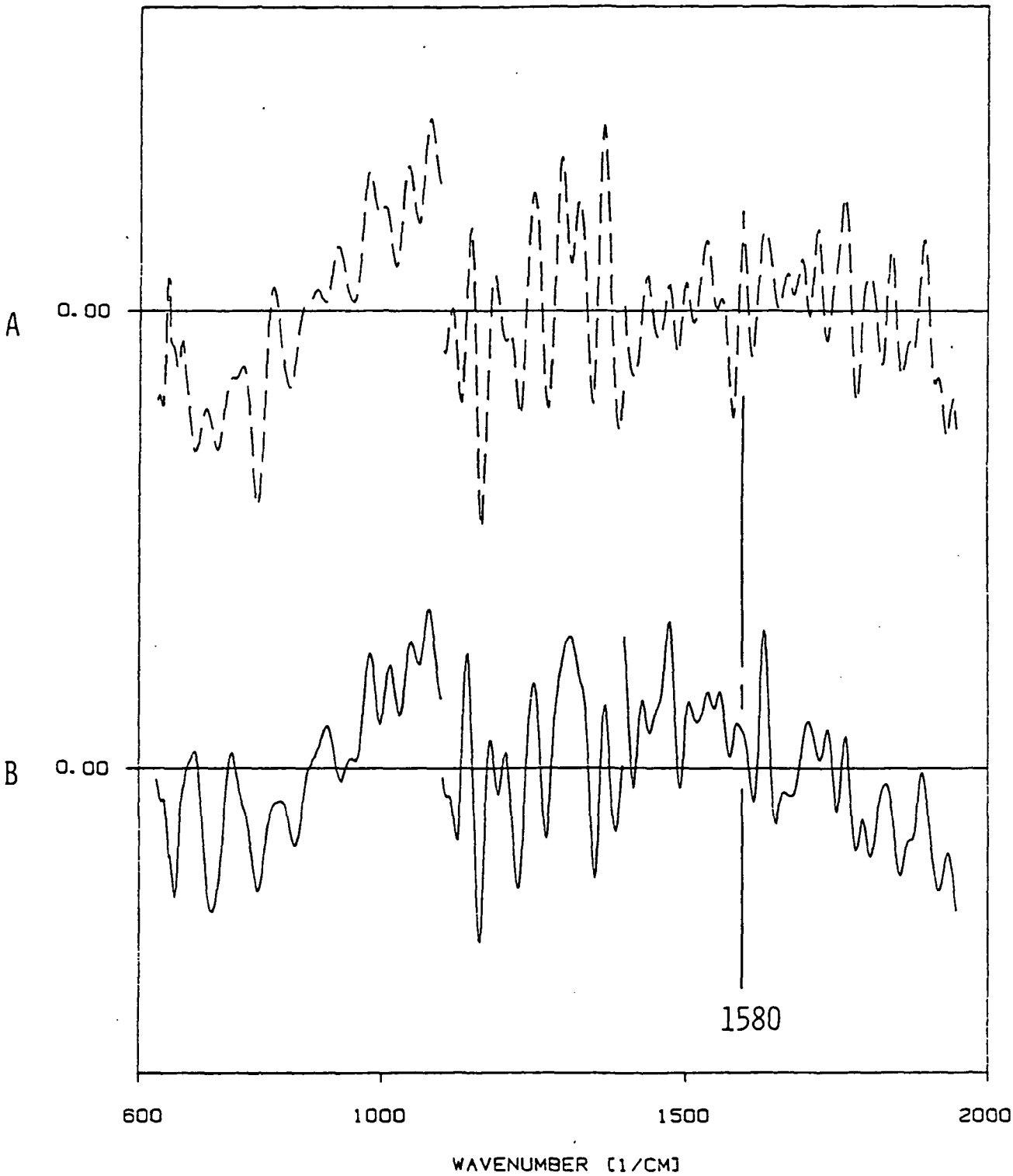


Figure 13 Difference Spectra of MJFSR Deposits from Jet A fuel with Additives and those of the Straight Fuel (A: with copper naphthenate minus neat, B: with iron naphthenate minus neat)

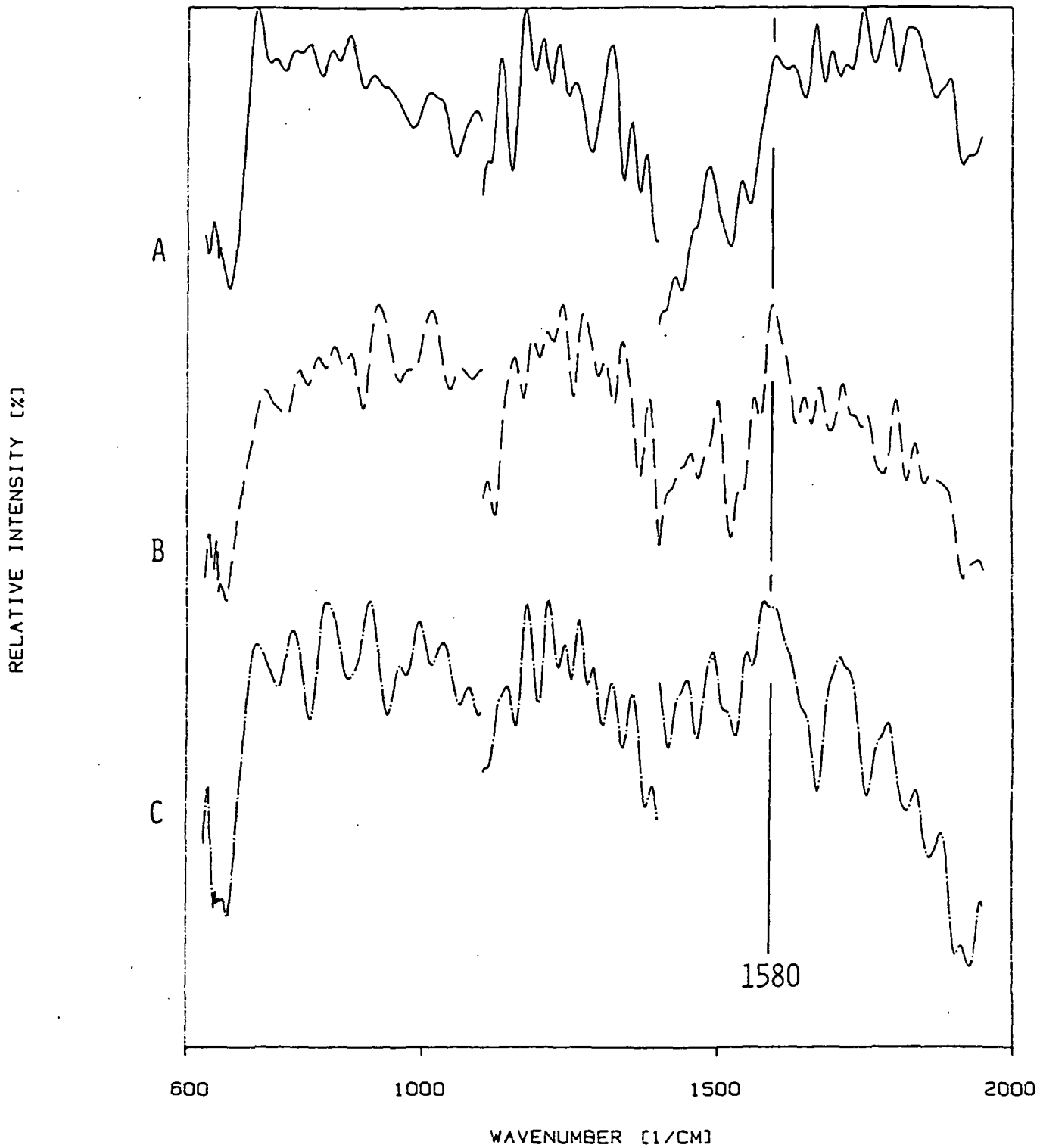


Figure 14 Emission Spectra of ERBS Fuel Deposit on MJFSR Stainless Steel Shims (A: neat, B: with copper naphthenate, C: with iron naphthenate)

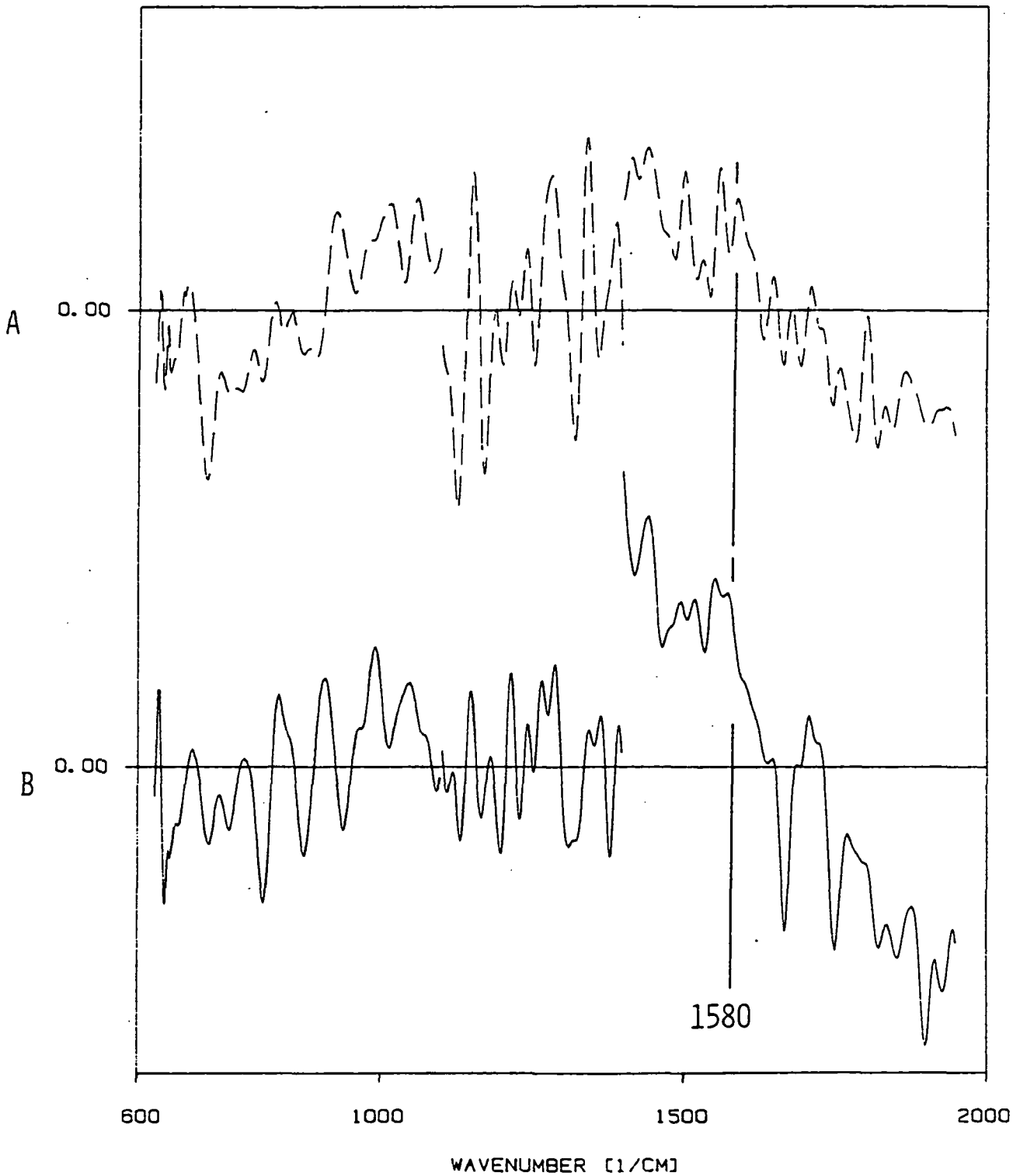


Figure 15 Difference Spectra of MJFSR Deposits from ERBS Fuel with Additives and those of the Straight Fuel (A: with copper naphthenate minus neat, B: with iron naphthenate minus neat)

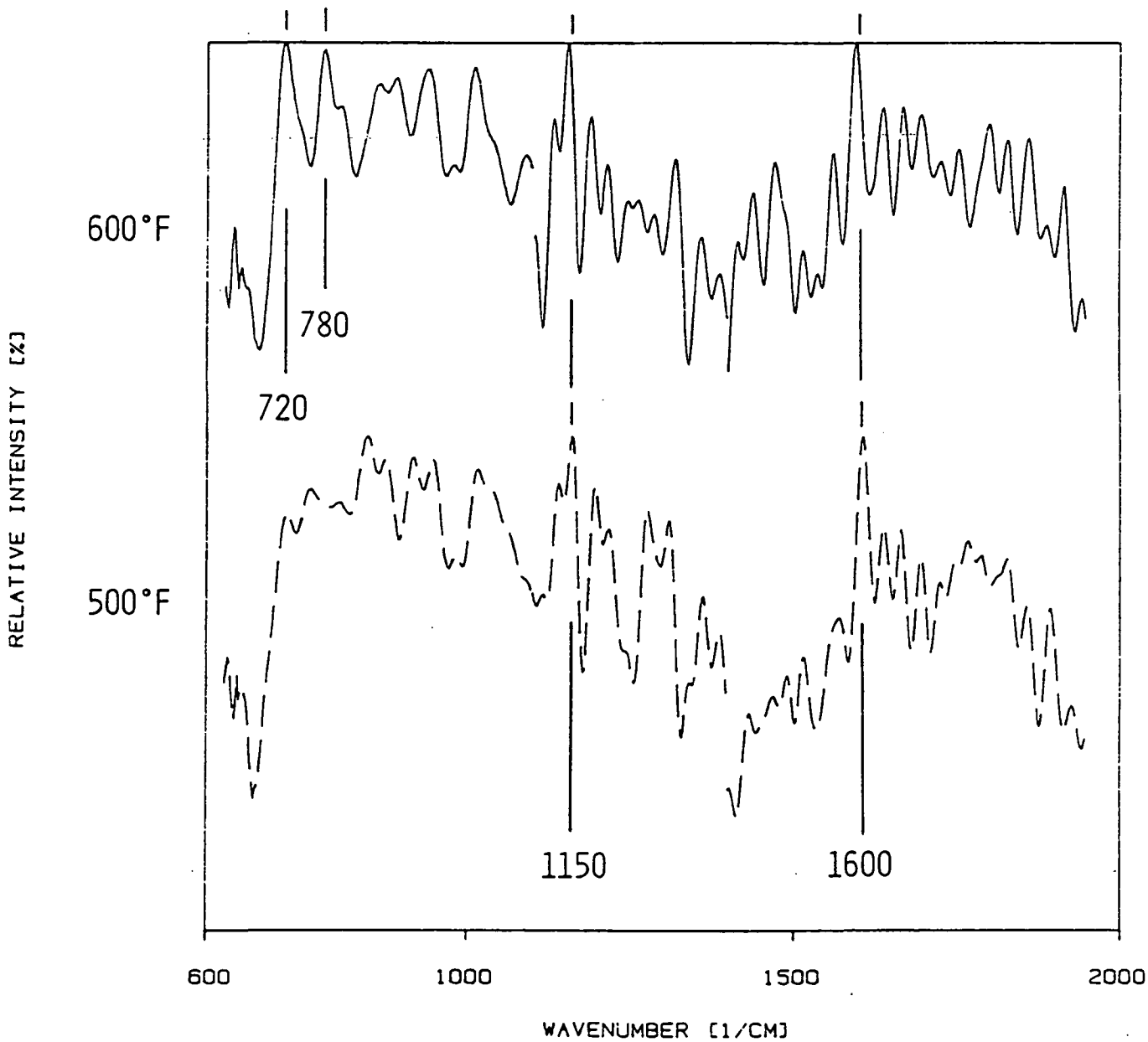


Figure 16 Emission Spectra of An ERBS Fuel Deposit Collected at 500 and 600°F

# APPENDIX

## FINAL REPORT

Subcontract Agreement No. 416-008
Between Geo-Centers, Inc and
Rensselaer Polytechnic Institute

## PREFATORY NOTE

The work reported in this report was completed in October 1985. Following discussions with Mr. Dues additional fuel samples were to be sent us for further research and it was for this reason that we had asked for an extension of the project time. These samples never came. Furthermore the work already done had resulted in a cost overrun which we had to cover and no further money could be authorized.

I am therefore submitting this report as our Final Report.

James L. Lauer
Principal Investigator

May 30, 1986

## SUMMARY

When the NASA-Lewis Fuel Group was dissolved the JFTOT apparatus we inherited from them was put into operation at Rensselaer Polytechnic Institute in order to generate aircraft fuel deposits for analysis by infrared emission Fourier transform spectrophotometry. Improved sensitivity of the latter apparatus made it possible to obtain spectra directly from deposits accumulated on aluminum or, preferably, stainless steel tubes. The latter provide a higher temperature gradient and more deposits than the aluminum tubes. Comparison of the new data for the ERBS fuel with data previously obtained for deposits collected on flat shims showed that some oxidative pyrolysis occurred already on surfaces upstream of the shims and this observation together with the stepwise mechanism found, now confirms a view of deposit formation in stages, the last one being the deposition of carbonyl-(carboxyl)-containing material.

Besides runs with the ERBS fuel, one with an aluminum and two with stainless steel tubes, a run each was made with a steel tube, one with Occidental Lite Shale and one with Shale JP-4. The deposits collected with these fuels were very different from those of the ERBS fuel. They were generally thin, they exhibited maximum thickness well ahead of the position of maximum temperature and their carbonyl band in the infrared spectrum peaked at lower wavenumber (perhaps indicative of an amide-type group). These characteristics point to a mechanism in which basic nitrogen compounds interact with peroxides. To fully elucidate the mechanism specific probe compounds would have to be added to the fuel and the resulting deposits analyzed. Such a study can now be performed readily.

The infrared spectra allowed an estimate of deposit thickness of 100 to 5000 Å under standard operating conditions.

# 1. INTRODUCTION

This project was late to get started, first for administrative reasons and then because of leaks and missing parts in the JFTOT apparatus we inherited from NASA's now defunct Fuel Group. We also had to build a fixture to obtain emission spectra from JFTOT tubes rather than the flat shims. The tubes are more difficult to position than the shims because of their smaller surface area, but we felt the substitution important enough to warrant the additional labor. The tubes provide a more realistic picture of thermal stability. Another change was the collection of deposits on stainless steel rather than on aluminum tubes. Stainless steel has a lower thermal conductivity than aluminum, which subjects the fluids passing over it to greater thermal stresses.

Oxidation plays a very important role in the nature and amounts of deposits. The deposits of all of the three fluids studied, ERBS (experimental broadened properties reference fuel), Occidental Light Shale Oil, and Shale JP-4, exhibit prominent bands of oxygen-containing functional groups in their infrared emission spectra. However, these spectra are very different and so are the spectral changes with temperature or, in other words, the spectra at particular tube positions. Possible reasons for these differences are discussed in the body of the report.

# 2. EXPERIMENTAL SETUPS AND PROCEDURES

## 2.1 Fuels and Surfaces Used

Three different fuels were used in this study. An experimental broadened-properties reference fuel (ERBS-3B-12.8) was used in three runs. Occidental Lite Shale Oil (83-POSF-0968) and Shale JP-4 (85-POSF-2193) were used in one run each.

The standard JFTOT aluminum tube was used as received in the first test runs. 316 Stainless steel JFTOT tubes were used in all the other runs. These tubes had to be cleaned in an alkaline detergent solution (RBS-35) because they were contaminated with lubricants from the manufacturing process.

Stainless steel tubes were selected because fuel deposits form more readily on stainless steel than on aluminum. We observed this behavior in an earlier study of fuel deposit formation [1].

## 2.2 Apparatus For Deposit Collection

For deposit collection both the regular JFTOT-Apparatus and the NASA Modifed Jet Fuel Oxidation Flat Sample Rig (MJFSR) were considered.

The MJFSR consists basically of a large heated metal block with a narrow channel of rectangular cross section for the fuel to flow. For deposit collection a metal shim is mounted in line with the flat channel.

Due to the fact that the whole metal block is heated, there are several disadvantages inherent to this design. Because the flow is very slow the fuel is at the same temperature as the metal shim, unlike the conditions in the heat exchangers. Deposits will not only form on the shim but on the inlet and outlet regions as well. So the fuel reaching the shim might be different from the fuel entering the sample rig. Removing these deposits from the fuel channel is very difficult. Therefore it is questionable that the starting conditions for each run are always the same.

For the above reasons it was decided to use the standard round JFTOT tubes for the experiments. Due to the temperature gradient along the tube axis deposits formed at different temperatures will be on one single tube. This might gradually change the fuel composition. But this is similar to the conditions in heat exchangers and corresponds to ALCOR's basic design.

## 2.3 Sample Holder and Fixture for IR-Emission Spectroscopy

A special sample holder was designed for the JFTOT tubes. It consists of a large block of aluminum mounted on an X-Y-Z-positioning stage. The sample holder is heated electrically to 110°C. The temperature is controlled to ± 1°C. To provide good heat conduction the tube is completely surrounded by the aluminum block except for a slit along the tube axis. A spring loaded counterblock presses the tube against the slit and allows for quick sample changes (Fig. 1).

The emitted infrared radiation is collected through the slit by an all reflecting microscope lens. By flipping a mirror the sample can be viewed through an optical microscope. This way very precise positioning can be achieved.

For the data processing reference spectra are needed. The references are incorporated into the sample holder to keep them at exactly the same temperature as the JFTOT tubes. The blackbody reference consists of an area coated with a solar black lacquer. A highly polished aluminum area serves as the second reference.

## 2.4 Data Collection

The infrared radiation emitted from the heated JFTOT was analyzed with a SIRIUS 100 FTIR spectrometer from Mattson Instruments, Inc. The interferometer was equipped with a liquid nitrogen-cooled mercury cadmium telluride detector. The bench temperature was stable to 0.5°C. The instrument was purged with dry air to remove water vapor.

1024 scans were averaged at a spectral resolution of 8 $cm^{-1}$. The spectrum of a deposit is obtained by substracting the spectrum of the JFTOT tube measured at a position where no deposit has formed from the total spectrum.

## 2.5 Infrared Spectra Recording

Infrared emission spectra of very thin films (thickness less than 10% of the wavelength detected) on metal surfaces depend strongly on the viewing angle. Greenler [2] has shown that the maximum emission intensity occurs at angles around 85 degrees from the surface normal. The emission vertical to the surface from such a film is essentially zero. Furthermore only radiation originating from molecular vibrations with a dipole component vertical to the surface is detectable.

The very small diameter of the standard JFTOT tube of only 1/8 inch requires the use of a microscope objective to obtain the necessary spatial resolution. The size of the all-reflecting microscope limits the maximum possible viewing angle to 45° degrees. Therefore the detectivity of very thin films is somewhat reduced. Nevertheless we were able to obtain reasonable infrared emission spectra, considering the small amount of deposit present in an area of 0.5 mm diameter with a thickness in the order of 1000 Å.

## 2.6 Estimated Deposit Thickness

First it was tried to analyze the infrared emission of a deposit in a direction normal to the surface. This way no discrete spectrum was obtained. From our theoretical analysis [4] we know that this means the deposit thickness is less than 1% of the wavelength of the radiation (e.g less than .1 μm for a wavelength of 10 μm). The maximum possible viewing angle with the microscope lens required to obtain the spatial resolution is 45° degrees. Under this angle a distinct spectrum of the deposit showed up with a peak emittance of about 2%. In this case the estimated film thickness is in the order of .1% of the wavelength which corresponds to 100 Å. From the maximum measured

emittance (about 40%) of all the samples in this study a maximum film thickness of .5 μm can be estimated.

## 3. INFRARED EMISSION SPECTRA OBTAINED

### 3.1 Extended Frequency Range

For the thickest deposits from each fuel the spectrum was plotted up to 3000 $cm^{-1}$ (Fig. 2). The spectrum becomes increasingly noisy at higher wavenumbers. Nevertheless there is an indication of the $CH_2$ band around 2900 $cm^{-1}$. But a better signal to noise ratio is essential for interpreting data in the extended wavenumber range. More signal could be obtained by increasing the temperature of the sample. But at the temperatures required for a significant improvement the sample may further oxidize. The only way to obtain good emission spectra in the higher wavenumber region is by the substitution of an InSb/MCT sandwich detector for our present MCT detector. We are now considering the purchase of such a device. (Its cost is high for us; about $8,000.)

### 3.2 Series of Spectra Obtained From Deposits at Different Tube Positions

#### 3.2.1 Run #1: ERBS on Aluminum

The first run on an aluminum tube was done to test the JFTOT setup. The ERBS fuel was used to compare the results to our previous study [3]. The temperature controller was set to 275°C with the thermocouple at the standard position of 38.7 mm. There were no measureable pressure drops across the fuel particle filter for the standard duration of the test of 150 min.

The visual inspection of the aluminum tube revealed no deposit. Nevertheless an infrared spectrum of a deposit could be measured (Fig. 3). A broad spectral feature is present of 1050-1250 $cm^{-1}$. Despite the noise in the

higher wavenumber region there is an indication of bands around 1600 and 1730 $cm^{-1}$. This spectrum is typical for deposits from the ERBS fuel. As a matter of fact it is very similar to the spectrum of the deposit from Run #2 (see below) at position 40 mm [Fig. 4].

### 3.2.2 Run #2: ERBS on 316 Stainless Steel (58 Minutes Run Time)

A 316 stainless steel tube was used for the second run. Because of the small amount of deposit obtained in Run #1, the temperature for this run was increase to 300°C measured at the standard position of 38.7 mm. The pressure over the filter increased readily and the JFTOT apparatus automatically shut off after 58 min, when the pressure reached 250 MM Hg.

The visual inspection of the tube showed some deposit symmetrically around the 45 mm position. There was no visible deposit between positions 0 and 30 mm. Infrared emission spectra were measured at positions 10, 20, and 30 mm and thereafter every 5 mm (Fig. 5). The spectra are rather noisy because the emittance is less than 2%. The strongest spectrum was obtained at position 45 mm, the visible center of symmetry of the deposit. This spectrum contains the strongest carbonyl band of the entire series (at 1730 $cm^{-1}$). The thickest deposit is expected at the position of the temperature maximum. This leads to the conclusion that the temperature profile for steel tubes is quite different from that of the aluminum tubes and that a strong carbonyl band develops only for deposits above a certain minimum thickness.

The most outstanding spectral features in all the spectra are the bands at 1080, 1180, 1610 and 1730 $cm^{-1}$. The normalized spectra from positions beyond 35 mm (Figs. 6 to 11) are basically identical. Therefore the deposited material is the same, only the thickness varies with position. The spectra are very similar to the early deposits (#126 and #142) in the time series of our previous study [3].

### 3.2.2 Run #3: ERBS on 316 Stainless Steel (150 Minutes Run Time)

The deposits obtained in Run #2 were very thin. Therefore the same fuel was used for Run #3, but for the standard time of 150 min. The manometer was bypassed to prevent the automatic shut off. The temperature was set to 300°C at the standard position of 38.7 mm. After 30 min. the temperature profile was measured. The maximum temperature was found to be 325°C at position 50 mm. The temperature profile for steel tubes differs from that of the standard aluminum tubes (50 mm vs. 45 mm for the aluminum tube).

The visual inspection showed almost symmetrical peacock rings around the 47 mm position. Around the center of symmetry they were covered with a thick brown overcoat. There was no visible deposit between the positions 0 and 25 mm.

Infrared emission spectra were measured at positions 10, 20, and 30 mm and thereafter every 5 mm (Figs. 12 to 19). The strongest spectrum was observed at position 45 mm. The spectral quality is excellent due to the high emittance of almost 45%. The most outstanding spectral features are again bands at 1080, 1180, 1610 and 1730 $cm^{-1}$. These bands seem to be typical for deposits from ERBS fuel. Other bands are at 600, 635, 760, 970, 1245, 1380, 1450 and 1775 $cm^{-1}$. The normalized spectra up to position 45 mm are almost identical. Therefore the material deposited in the region of the tube with a positive temperature gradient seems to be the same. At the position (50 mm) of the maximum temperature the band at 1730 $cm^{-1}$ is more intense compared to the other bands. This observation confirms a similar one for Run #2. Beyond 50 mm the 1610 and 1730 $cm^{-1}$ bands are comparatively much weaker.

### 3.2.3 Run #4: Lite Shale Oil on 316 Stainless Steel

For all further runs with stainless steel tubes the temperature was set to 325°C at position 50 mm in accordance with the measured temperature profile. Surprisingly enough no pressure rise over the filter was measured during the standard run time of 150 min.

The visual inspection showed deposits distributed over the whole tube starting with a purple ring at position 10 mm. A peacock ring structure is centered at 18 mm (well ahead of the temperature maximum). Two distinct areas with dark brown deposits followed up to the end of the tube.

Infrared emission spectra were measured at positions 5, 9.7, 15.4, 20, 25, 30, 36, 40.1, 45 and thereafter every 5 mm (Figs. 20-30). The strongest spectrum was observed at the 20 mm position. The most outstanding spectral feature is the band at 1715 $cm^{-1}$. Several weak bands are standing out of the flat top between 1200 and 1550 $cm^{-1}$. The normalized spectra up to the 20 mm position are basically identical. Positions 25 and 30 mm show a completely different spectrum. The dominant band is at 555 $cm^{-1}$. A weaker structure is between 700 and 750 $cm^{-1}$. Positions 36, 40.1 and 45 mm again show a different spectrum. A broad band is centered at 1220 $cm^{-1}$ and an indication of a band around 1600 $cm^{-1}$ can be made out. The spectra at the last two positions show an increasing emittance with wavenumber.

### 3.2.4 Run #5: Shale J-4 on 316 Stainless Steel

For this run the temperature was again set to 325°C at position 50 mm. The pressure over the filter gradually rose to about 200 mm Hg at the end of the standard run time of 150 min. Another temperature profile was measured this run to check for consistency.

The visual inspection showed the deposit concentrated around position 43 mm. There was no visible deposit between positions 0 and 20 mm.

Infrared emission spectra were measured at positions 10, 15, 23, 30, 34, 39, 41, 43, 45, 50 and 55 mm (Figs. 31-41). The strongest spectrum was observed at position 43 mm (just barely ahead of the temperature maximum). The maximum emittance of 21% resulted in a good quality spectrum. The dominant spectral features are the bands at 1455, 1610 and 1715 $cm^{-1}$. Two weaker bands are at 1385 and 1665 $cm^{-1}$. The normalized spectra up to the 45 mm position are basically identical. Bands around 720, 1020 and 1600 $cm^{-1}$ seem to be present in the spectra measured at 50 and 55 mm.

## 4. INTERPRETATION OF THE INFRARED SPECTRA

The strongest band in the ERBS spectra is at 1730 $cm^{-1}$. This band can be attributed to dialkyl ketones or six membered lactones. Unconjugated esters have a strong band at 1730 $cm^{-1}$ as well as at 1175 $cm^{-1}$. Both bands are present in the ERBS spectra. The presence of lactones is supported by a band at 1775 $cm^{-1}$, which might be due to five-membered lactones. The second strongest band is at 1610 $cm^{-1}$. 1,3 diketones in the enol form have a strong band at this wavenumber. Carboxyl salts also contribute to this band as well as to the band at 1380 $cm^{-1}$. The $CH_2$ group produces bands at 2920, 2860 and 1450 $cm^{-1}$. The same bands with the addition of a 1380 $cm^{-1}$ band can be attributed to the $CH_3$ group. Aromatics will contribute to the bands at 1610, 1450, 1175, 1080 and 760 $cm^{-1}$. The oxirane ring will show at 1245 and 760 $cm^{-1}$. The presence of an alcohol group is indicated by the band at 1055 $cm^{-1}$.

The spectra of the deposits from the shale JP-4 and the Occidental Lite Shale Oil fuel are very similar to each other but distinctly different from the spectra of the ERBS fuels. The strongest band is at 1715 $cm^{-1}$. It can

be attributed to various molecular groups like dialkyl ketones, six membered lactones, conjugated esters, and the nitrogen-containing carbamates, imides or five-membered lactams. In addition to this band, cyclic imides have a weak band at 1760 $cm^{-1}$, which is present as a shoulder in the spectra. The presence of nitrogen bonds in the form of the lactams and amides is indicated by the band or the shoulder at 1665 $cm^{-1}$, which is due to disubstituted amide or the six-membered lactam ring. The second strongest band is again at 1610 $cm^{-1}$ and it may be due to 1,3 diketone in the enol form and carboxyl salt with the additional band at 1380 $cm^{-1}$. As in the spectra of the ERBS deposits, the $CH_2$ and $CH_3$ groups show up at 1450 and 1380 $cm^{-1}$. Much less of the compounds that give rise to the bands in the region between 1000 and 1200 $cm^{-1}$ is present in the deposits from the shales.

## 5. DISCUSSION

### 5.1 ERBS Deposits

According to the infrared emission spectra the composition of the deposits from the ERBS fuel is independent of the tube position or the equivalent tube temperature in the region with a positive temperature gradient up to the position where the thickest deposit was formed. The thickest deposit is generally located before the position of maximum temperature. The intensity of the carbonyl band (1730 $cm^{-1}$) compared to the 1055 $cm^{-1}$ band is higher for the longer run. This is in agreement with our findings in the previous study, where the carbonyl contents also increase with deposition time. Deposits formed beyond the point of maximum temperature show less carbonyl content and compare to the deposits obtained for the shorter deposition time. This also explains the fact that the present deposits contain relatively more carbonyls than those of our previous study, because there in the flat sample rig the fuel already formed deposits on the inlet channel before reaching the sample. The spectra of run #2 compare well to #126 and #142 of our previous

study. The spectra of run #3 are similar to #246 of the previous study which contained thiophene for accelerated oxidation.

It would appear, therefore, from this and the previous study, that the composition of the deposits is not just a function of surface temperature but depends on the availability of precursors in the flowing fluid. The final stage in the oxidative pyrolysis is the deposit with a high concentration of carbonyl (1730 $cm^{-1}$, most likely conjugated esters and lactones). The hydroperoxide-peroxide mechanism generally proposed is consistent with our findings.

## 5.1 Shale Deposits

The most significant difference between the spectra of the shale and ERBS deposits is the shift of the carbonyl peak from 1730 to 1715 $cm^{-1}$ and the absence of the bands in the region from 1000 to 1200 $cm^{-1}$ for the former. Furthermore the valley between the carbonyl band (1715 $cm^{-1}$) and the band at 1610 $cm^{-1}$ is more or less filled. This is the region where the nitrogen bonds in the compounds like lactams and disubstituted amides show up. The shift of the carbonyl band to 1715 $cm^{-1}$ and the absence of the 1715 $cm^{-1}$ band indicate that esters are present in the conjugated form rather than the unconjugated form as in the ERBS deposits. The oxidation peak is closer to the fuel inlet region and therefore occurs at lower temperatures than for the ERBS fuels. This means that fuels from shale oils are more readily oxidized, especially to carbonyl (at 1175 $cm^{-1}$). Another point worth repeating here is the absence of particles clogging the fuel filter in the case of Occidental Lite Shale Oil. This observation points to more oxidation and less carbonization. The absence of the 1055, 1080 and 1175 $cm^{-1}$ bands is significant in this respect. These bands are likely to relate to particle formation and indeed we assigned them to alcohol radicals and primarily to aromatic and oxirane rings. In line with this reasoning the shale oil deposits

are also thinner, giving a lower overall emittance than the ERBS deposits.

This study appears to be unique in that we report less deposit for shale than for a regular hydrocarbon fuel. The difference lies in the highly aromatic nature of ERBS. Another point is that carbonyl is likely to be part of a nitrogen-containing functional group and that there are several definite stages of oxidative pyrolysis. It would seem that the acid hydroperoxides are sequentially neutralized by the nitorgen bases as well as oxidized further. The only real way to elucidate the mechanism is by a detailed study with known components.

## 6. CONCLUSION

Based on the limited number of data it would seem that the shale fuel gives less particles and deposits, but provides a much higher level of oxidation on the surface at lower temperatures. This result could not have been obtained with the previous NASA setup and therefore consitutes a significant advance of our knowledge. More work will be needed to learn the mechanisms leading to there observations, so that better insight into prospective fuel compositions can be gained. The differences between the spectra of the ERBS deposits and those of the shale fuels (Fig. 42) are indicative of a different oxidation mechanism.

## REFERENCES

1. Lauer, J.L., and Vogel, P., "Emission FTIR Analysis of Thin Microscopic Patches of Jet Fuel Residues Deposited on Heated Metal Surfaces," NASA Contractors Report 168331 under Grant No. NAG 3-205, 30 pp., 1984.

2. Greenler, P.R., "Light Emitted from Molecules Adsorbed on a Metal Surface," Surface Science, 69, 647-652, (1977).

3. Lauer, J.L., and Vogel, P., "Emission FTIR Analyses of Jet Fuel Deposits," Presented at the 188th National American Chemical Society Meeting, Philadelphia, August 26-31, 1984, Preprints-Symposia, General Papers, Petroleum Division, Vol 29, 101526 (1984).

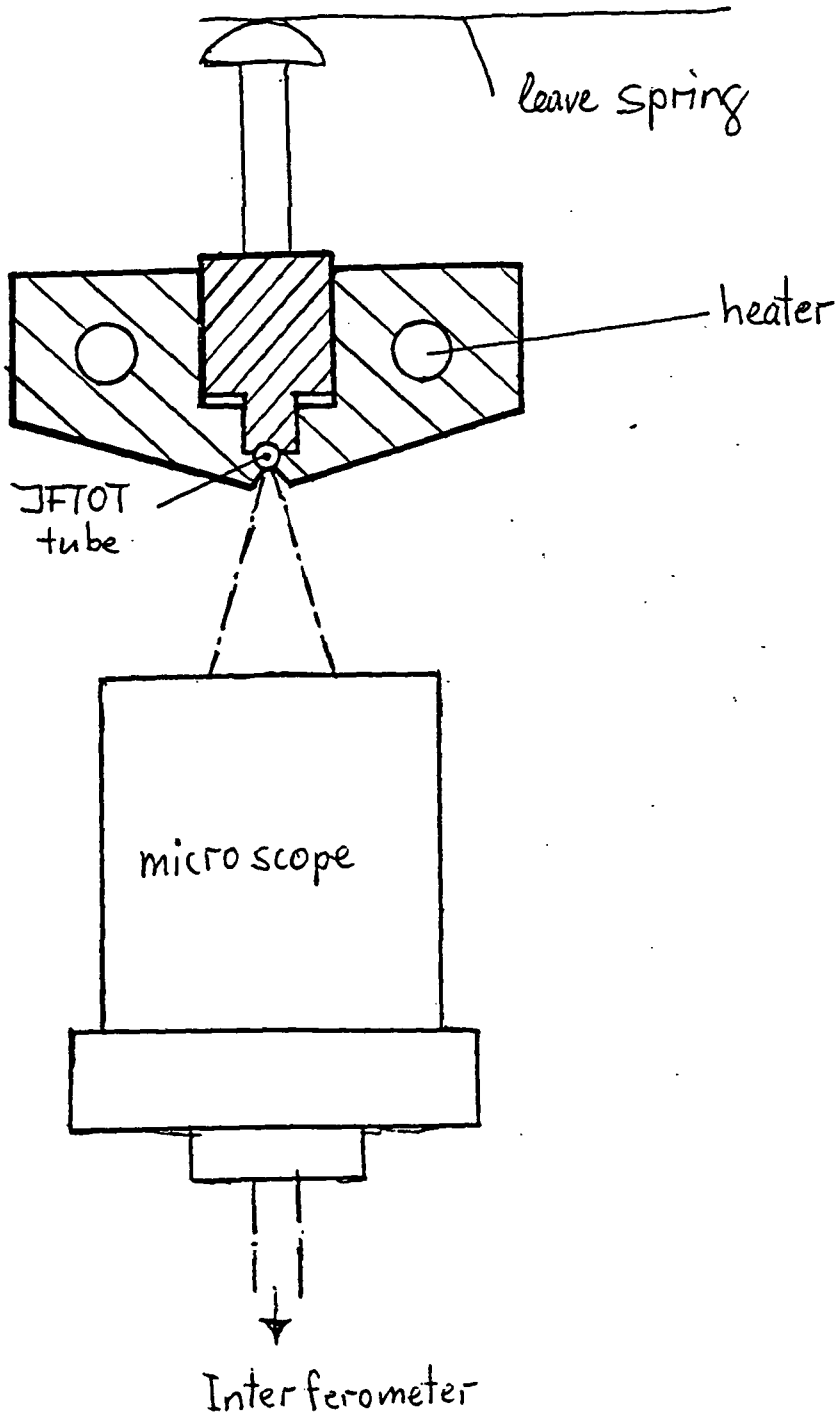
leave spring
heater
JFTOT
tube
micro scope
Inter ferometer

Figure 1

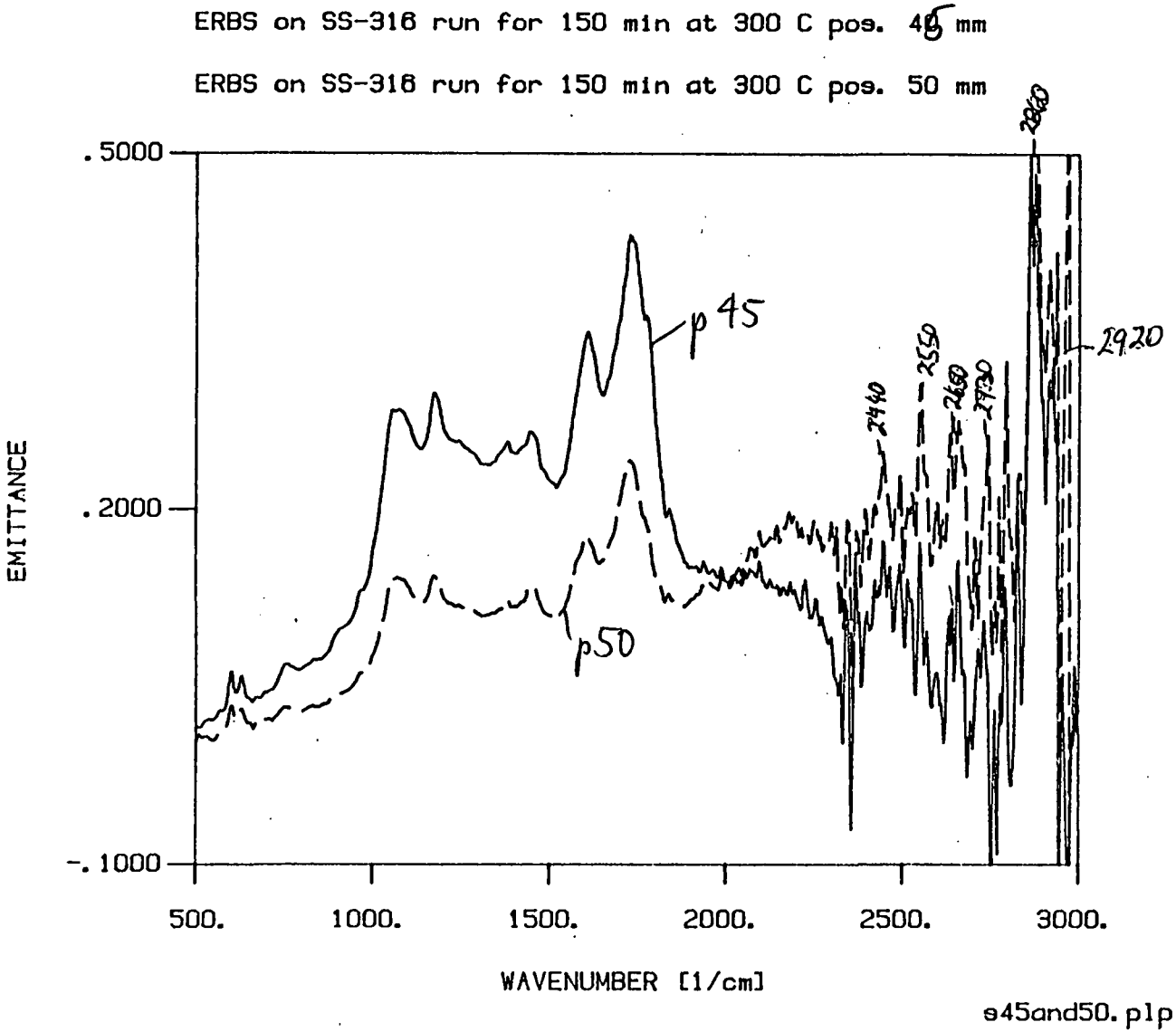
ERBS on SS-316 run for 150 min at 300 C pos. 45 mm
ERBS on SS-316 run for 150 min at 300 C pos. 50 mm
.5000
.2000
-.1000
EMITTANCE
500.
1000.
1500.
2000.
2500.
3000.
WAVENUMBER [1/cm]
p45
p50
2440
2550
2660
2730
2860
2920
s45and50.plp

Figure 2(a)

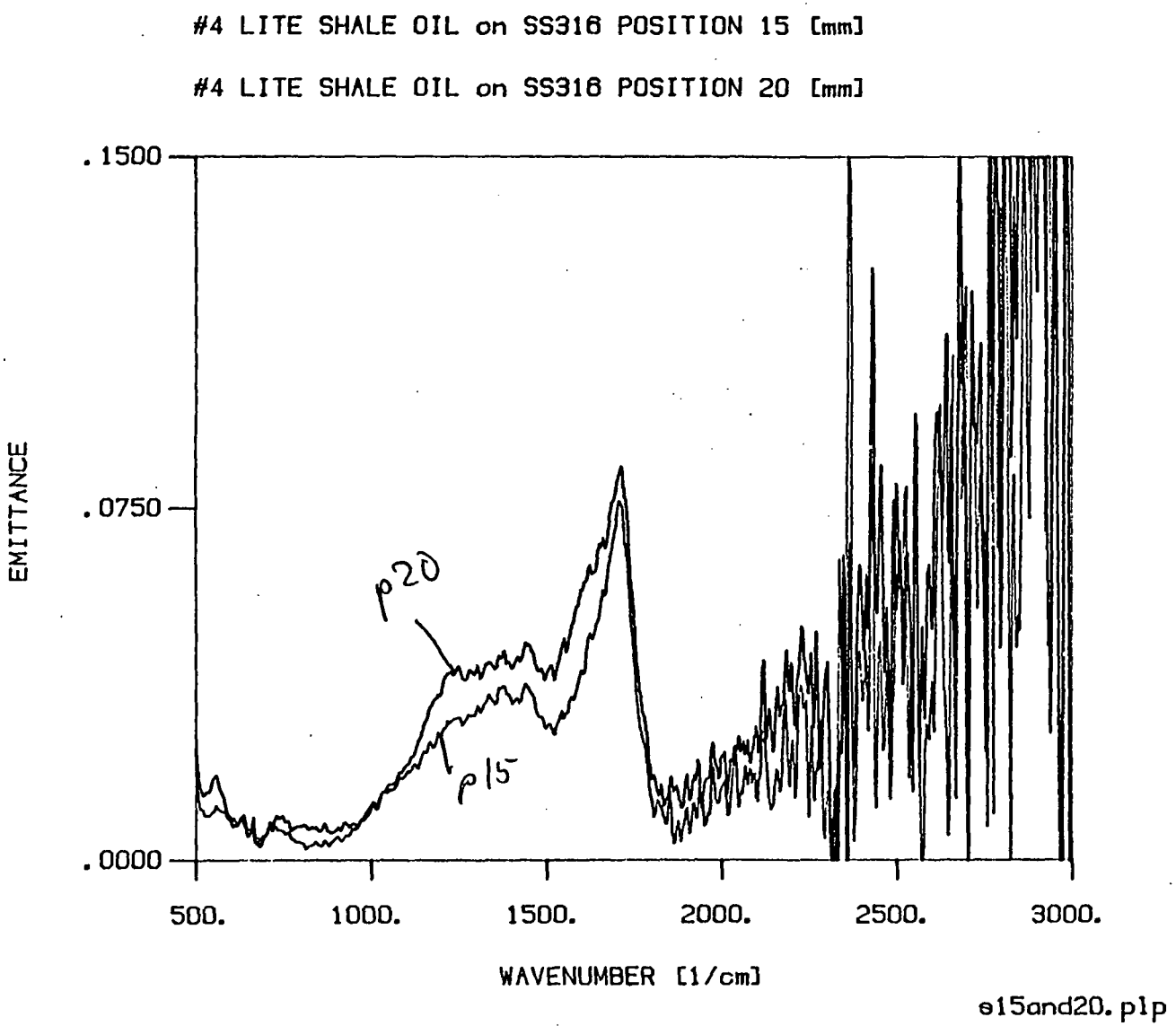
#4 LITE SHALE OIL on SS316 POSITION 15 [mm]
#4 LITE SHALE OIL on SS316 POSITION 20 [mm]
.1500
.0750
.0000
EMITTANCE
p20
p15
500.
1000.
1500.
2000.
2500.
3000.
WAVENUMBER [1/cm]
s15and20.plp

Figure 2(b)

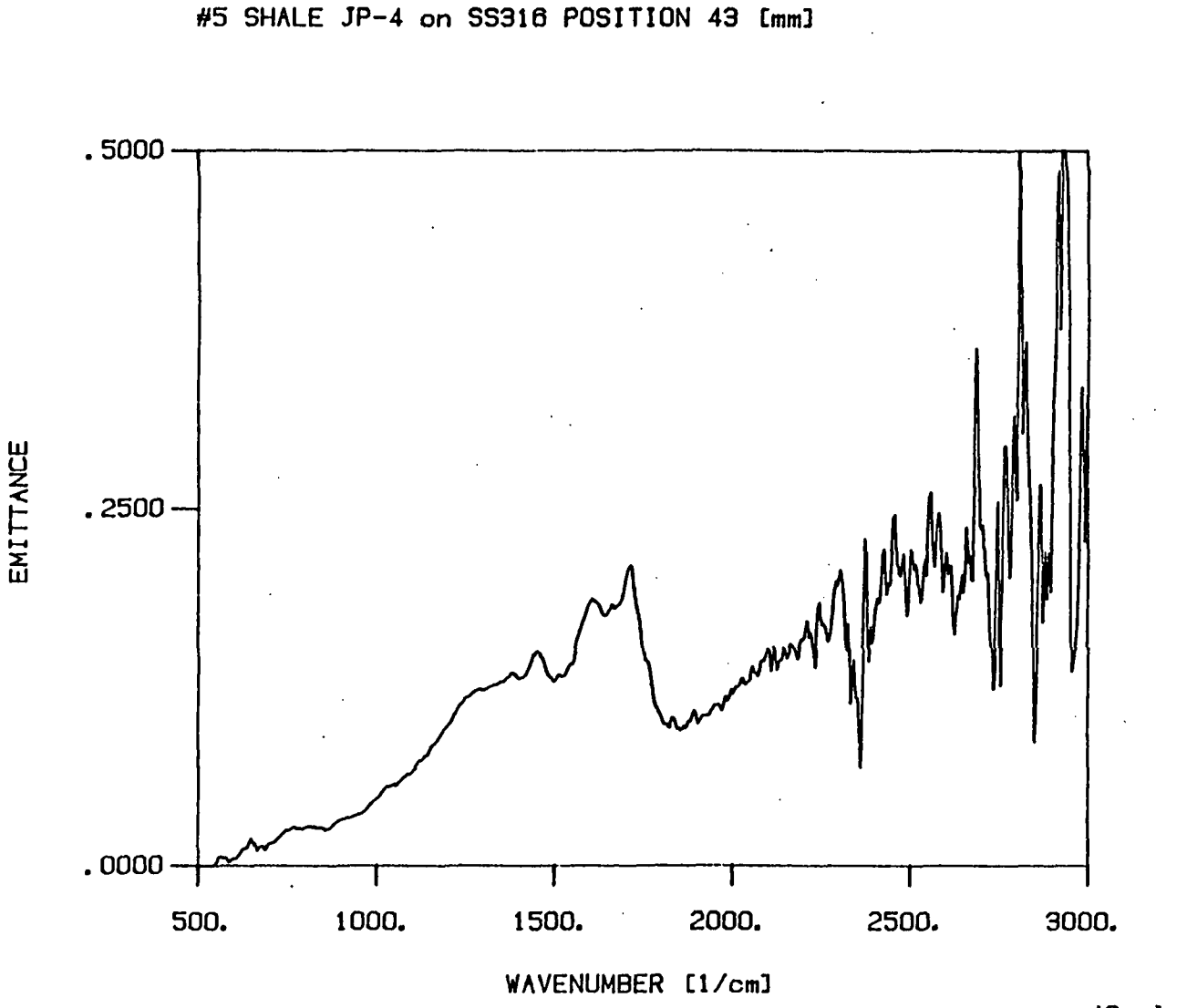
#5 SHALE JP-4 on SS316 POSITION 43 [mm]
.5000
.2500
.0000
EMITTANCE
500.
1000.
1500.
2000.
2500.
3000.
WAVENUMBER [1/cm]
e43.plp

Figure 2(c)

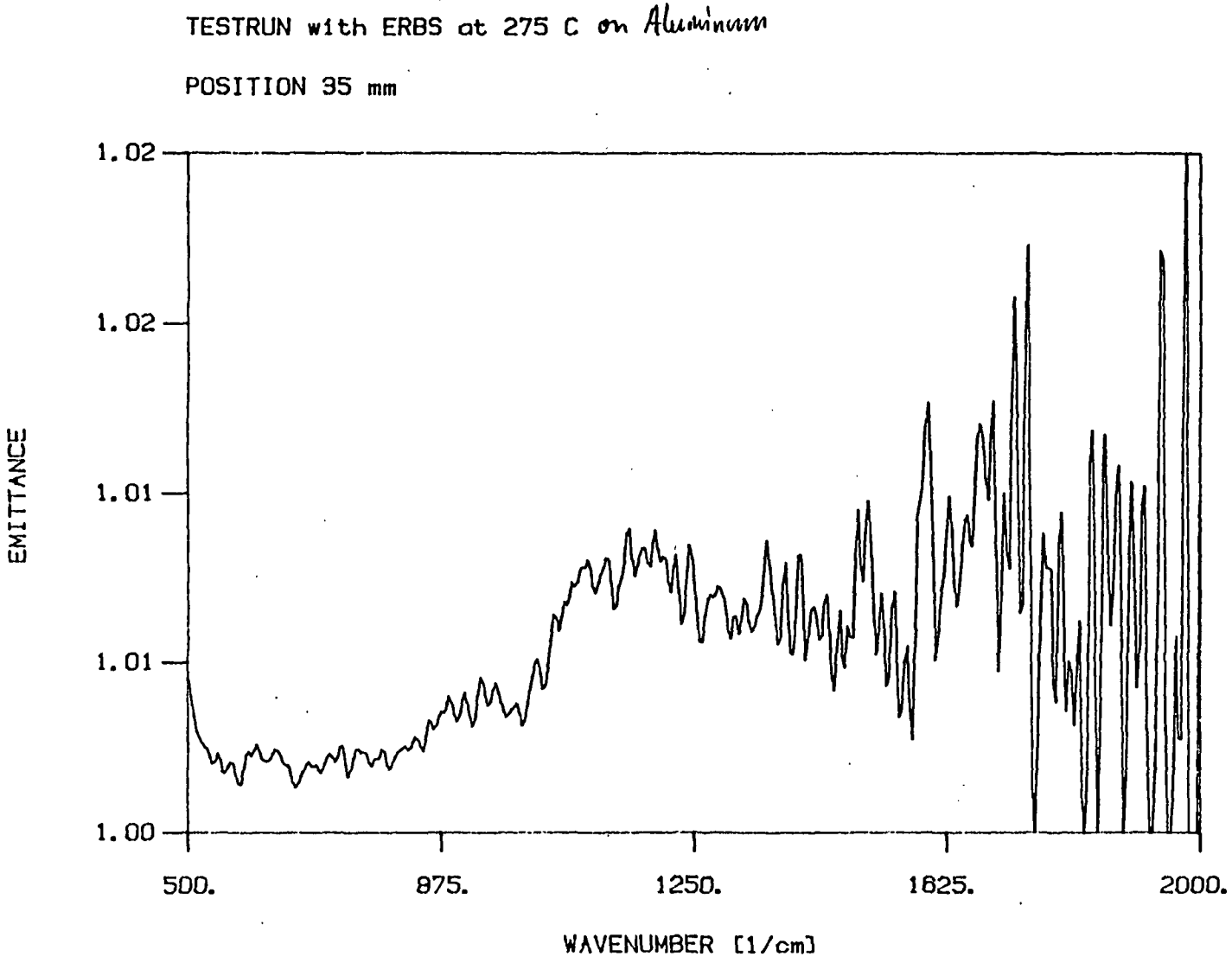
TESTRUN with ERBS at 275 C on Aluminum
POSITION 35 mm
1.02
1.02
1.01
1.01
1.00
EMITTANCE
500.
875.
1250.
1625.
2000.
WAVENUMBER [1/cm]

Figure 3

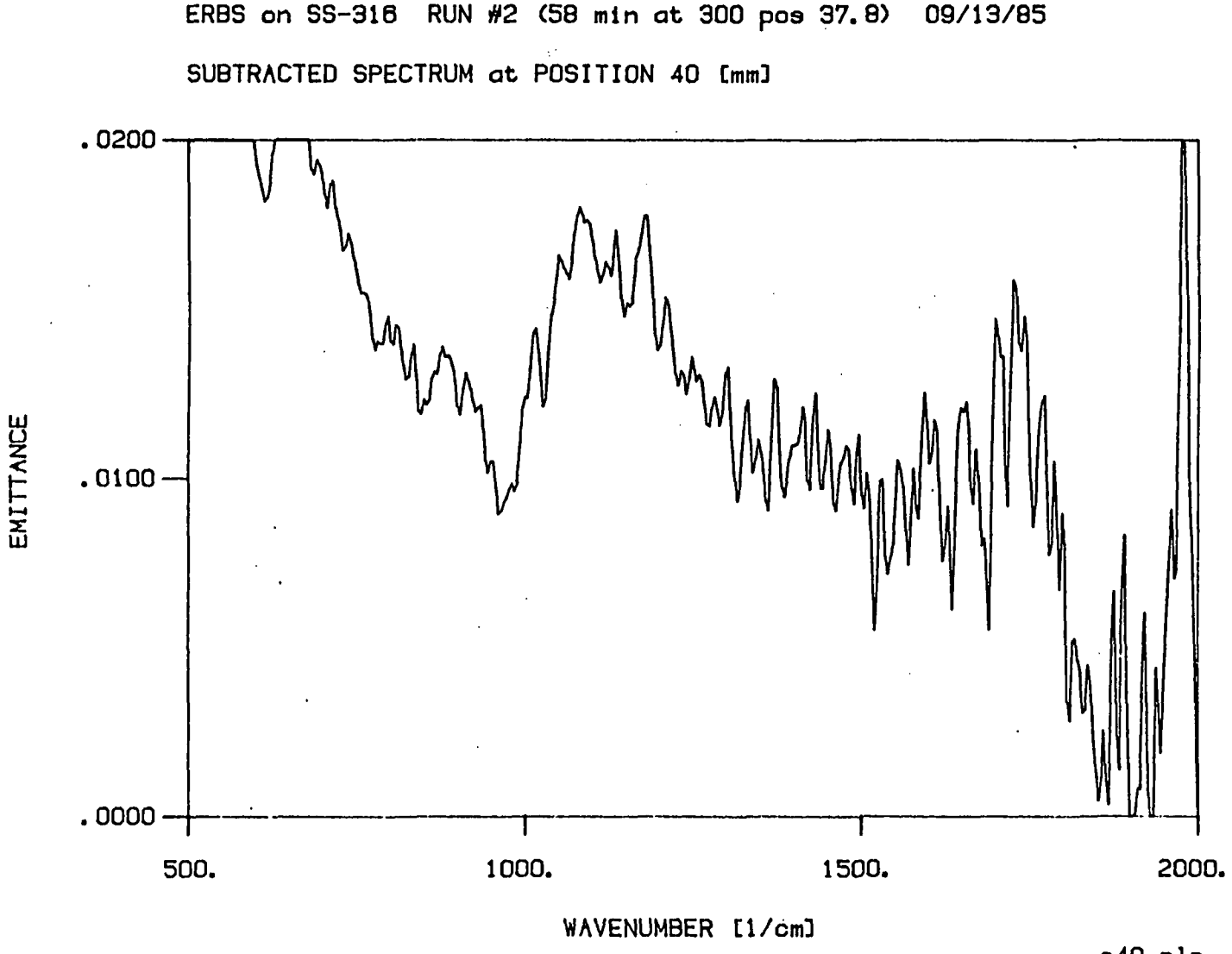
ERBS on SS-316 RUN #2 (58 min at 300 pos 37.8) 09/13/85
SUBTRACTED SPECTRUM at POSITION 40 [mm]
.0200
.0100
.0000
EMITTANCE
500.
1000.
1500.
2000.
WAVENUMBER [1/cm]
e40.plp

Figure 4

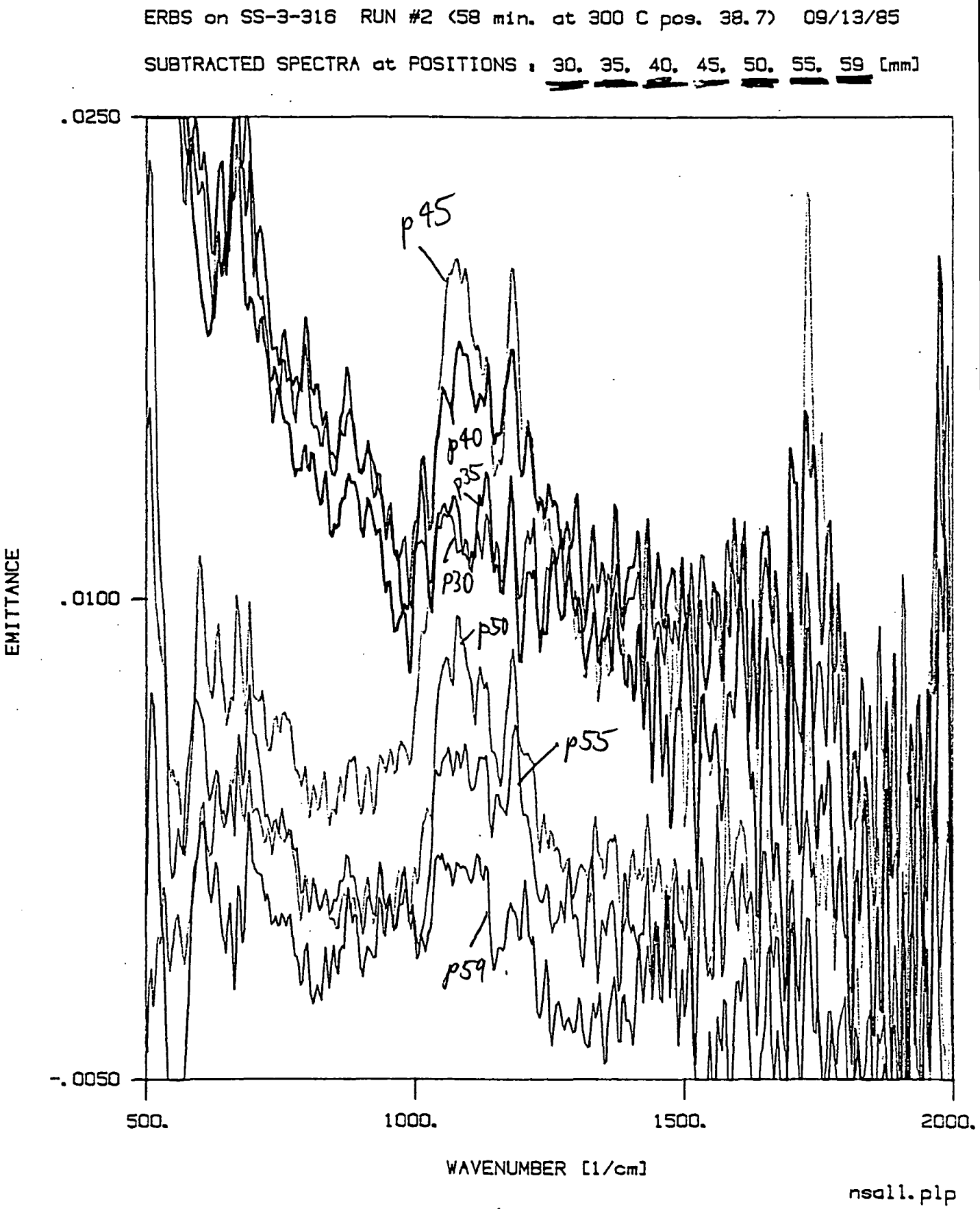
ERBS on SS-3-316 RUN #2 (58 min. at 300 C pos. 38.7) 09/13/85
SUBTRACTED SPECTRA at POSITIONS : 30. 35. 40. 45. 50. 55. 59 [mm]
.0250
.0100
-.0050
EMITTANCE
p45
p40
p35
p30
p50
p55
p59
500.
1000.
1500.
2000.
WAVENUMBER [1/cm]
nsall.plp

Figure 5

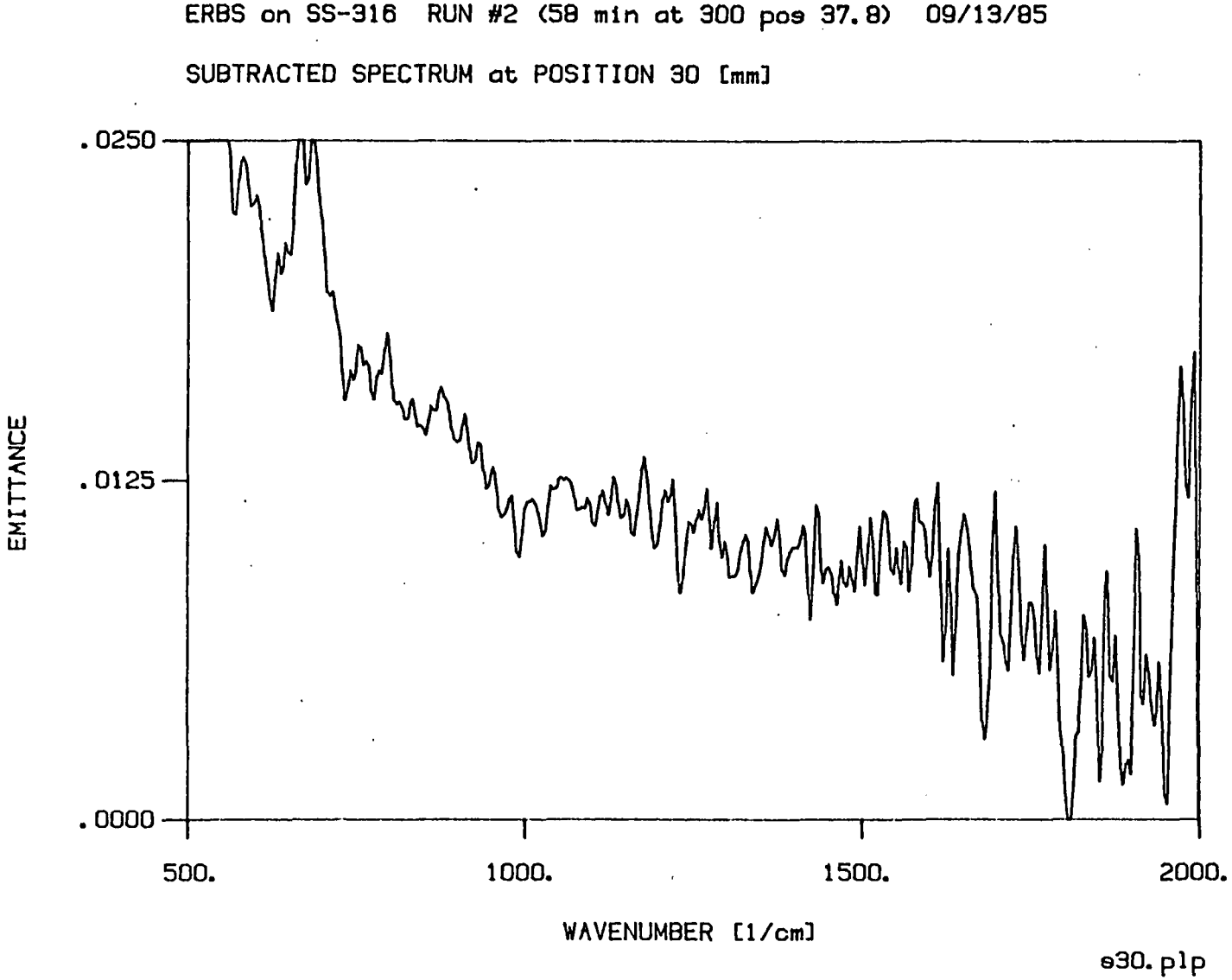
ERBS on SS-316 RUN #2 (58 min at 300 pos 37.8) 09/13/85
SUBTRACTED SPECTRUM at POSITION 30 [mm]
.0250
.0125
.0000
EMITTANCE
500.
1000.
1500.
2000.
WAVENUMBER [1/cm]
s30.plp

Figure 6

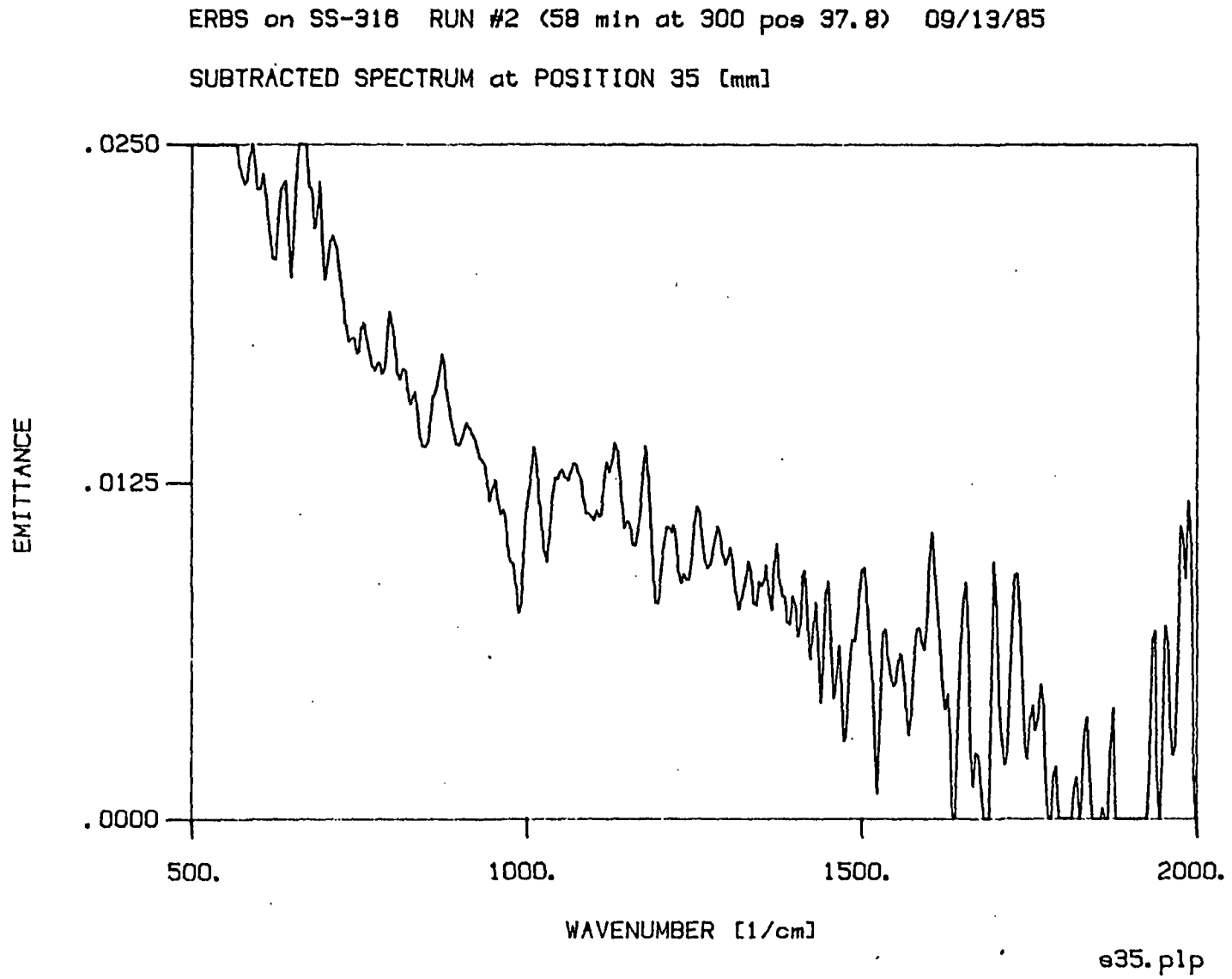
ERBS on SS-316 RUN #2 (58 min at 300 pos 37.8) 09/13/85
SUBTRACTED SPECTRUM at POSITION 35 [mm]
.0250
.0125
.0000
EMITTANCE
500.
1000.
1500.
2000.
WAVENUMBER [1/cm]
e35.plp

Figure 7

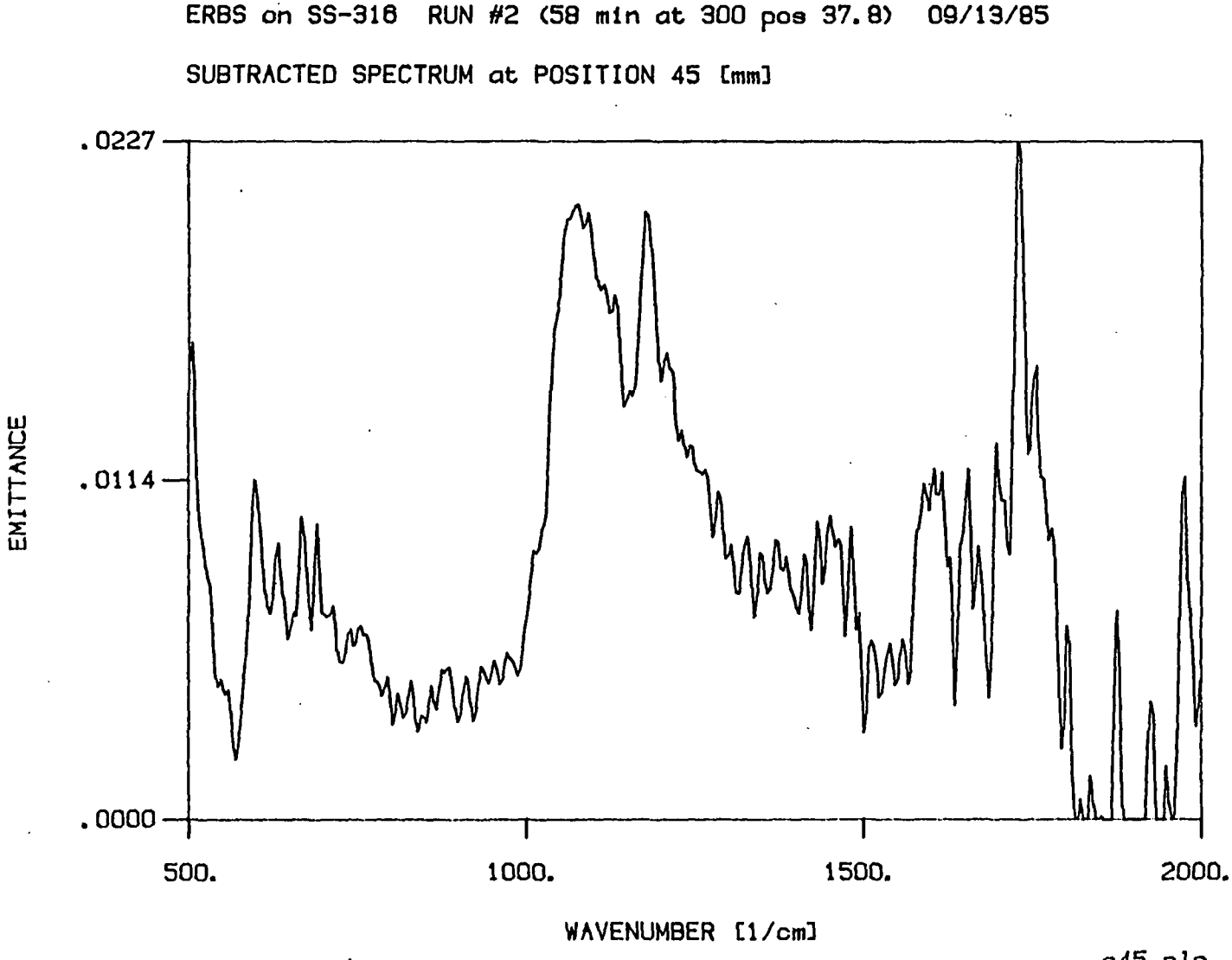
ERBS on SS-316 RUN #2 (58 min at 300 pos 37.8) 09/13/85
SUBTRACTED SPECTRUM at POSITION 45 [mm]
.0227
.0114
.0000
EMITTANCE
500.
1000.
1500.
2000.
WAVENUMBER [1/cm]
s45.plp

Figure 8

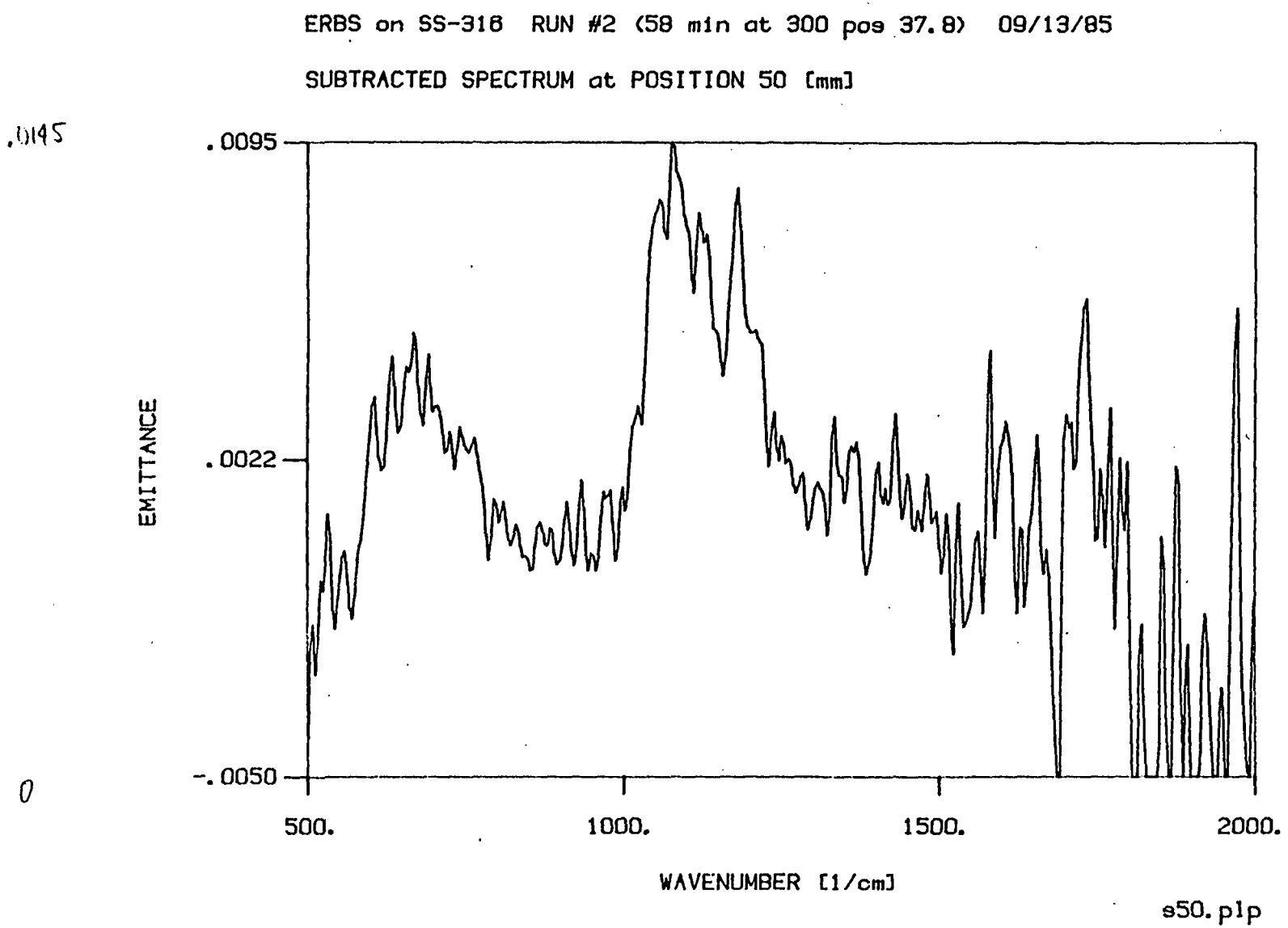
ERBS on SS-316 RUN #2 (58 min at 300 pos 37.8) 09/13/85
SUBTRACTED SPECTRUM at POSITION 50 [mm]
.0095
.0022
-.0050
EMITTANCE
500.
1000.
1500.
2000.
WAVENUMBER [1/cm]
s50.plp

Figure 9

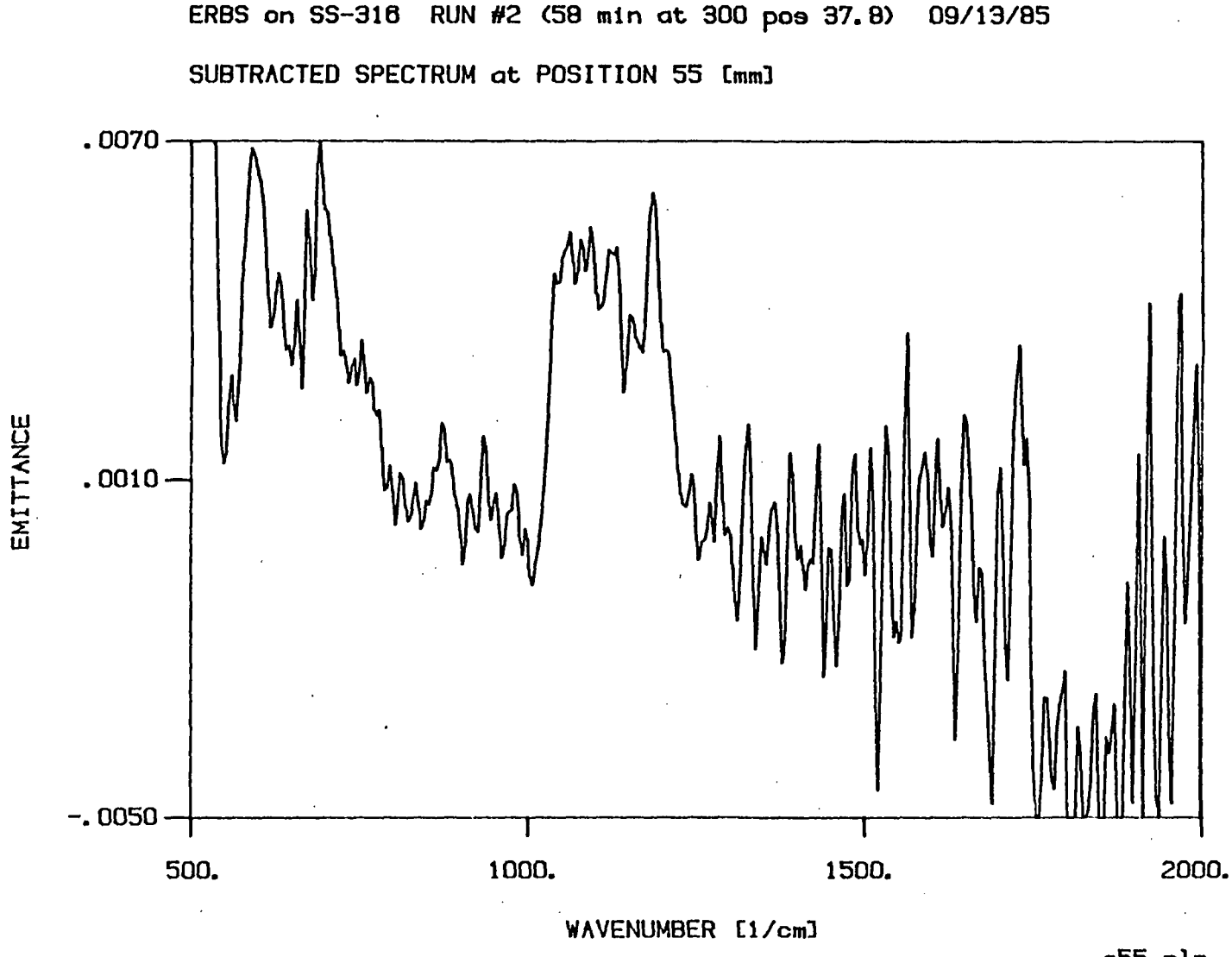
ERBS on SS-316 RUN #2 (58 min at 300 pos 37.8) 09/13/85
SUBTRACTED SPECTRUM at POSITION 55 [mm]
.0070
.0010
-.0050
EMITTANCE
500.
1000.
1500.
2000.
WAVENUMBER [1/cm]
s55.plp

Figure 10

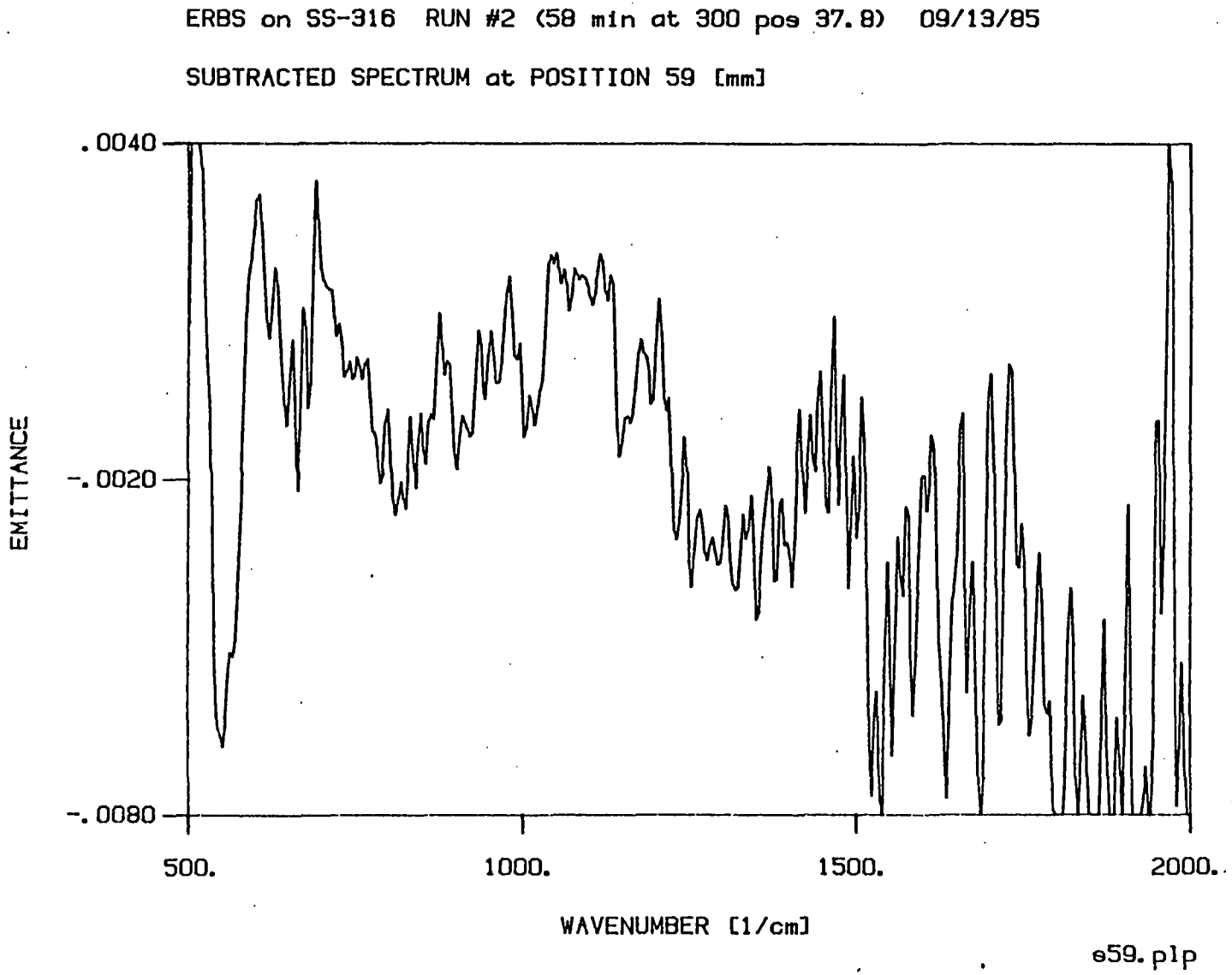
ERBS on SS-316 RUN #2 (58 min at 300 pos 37.8) 09/13/85
SUBTRACTED SPECTRUM at POSITION 59 [mm]
.0040
-.0020
-.0080
EMITTANCE
500.
1000.
1500.
2000.
WAVENUMBER [1/cm]
e59.plp

Figure 11

ERBS on SS-316 RUN #3 (150 min. at 300 C) 09/24/85

SUBTRACTED SPECTRA at POSITIONS : 30. 35. 40. 45. 50. 55. 59 [mm]

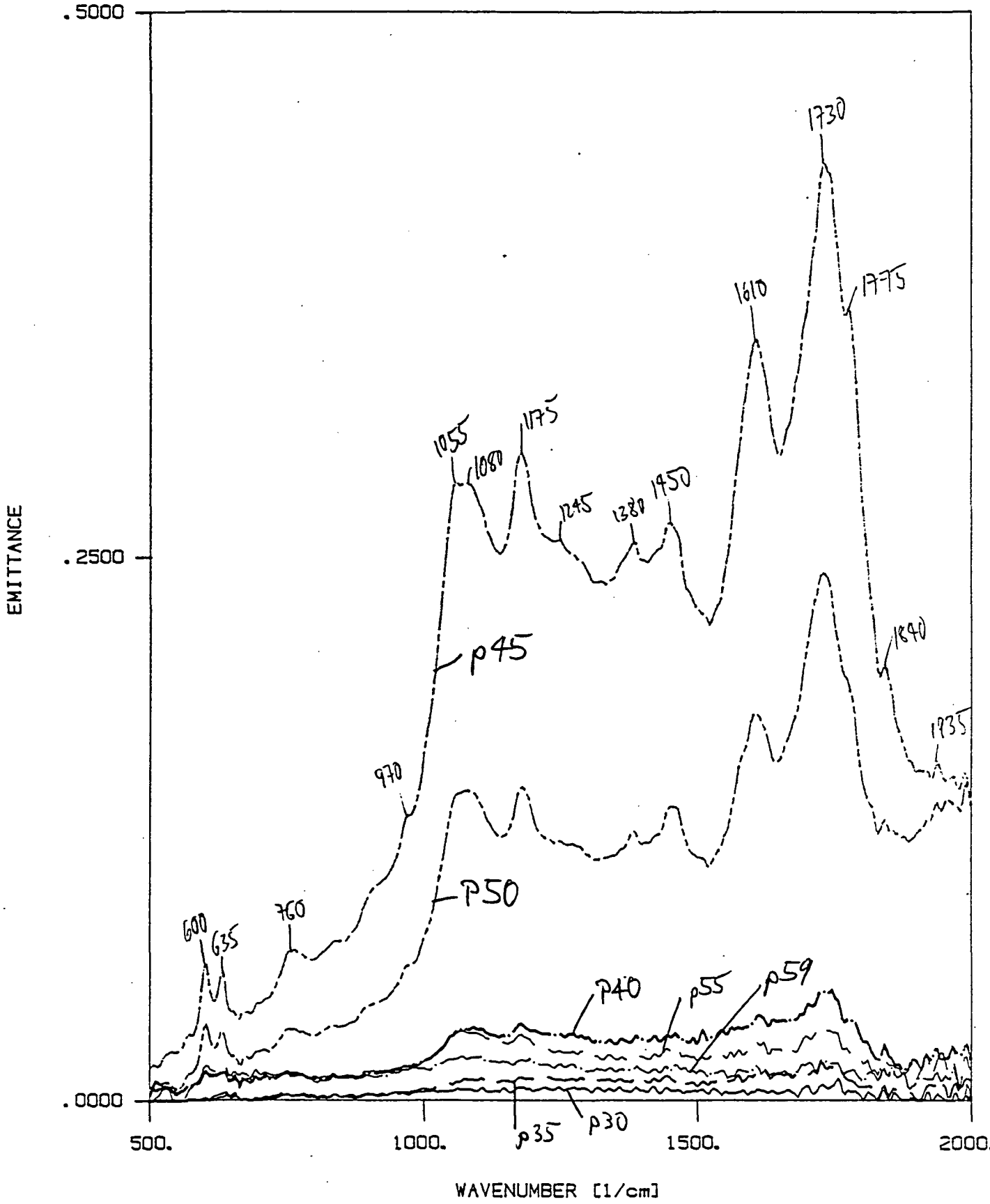


Figure 12

Sall.plp

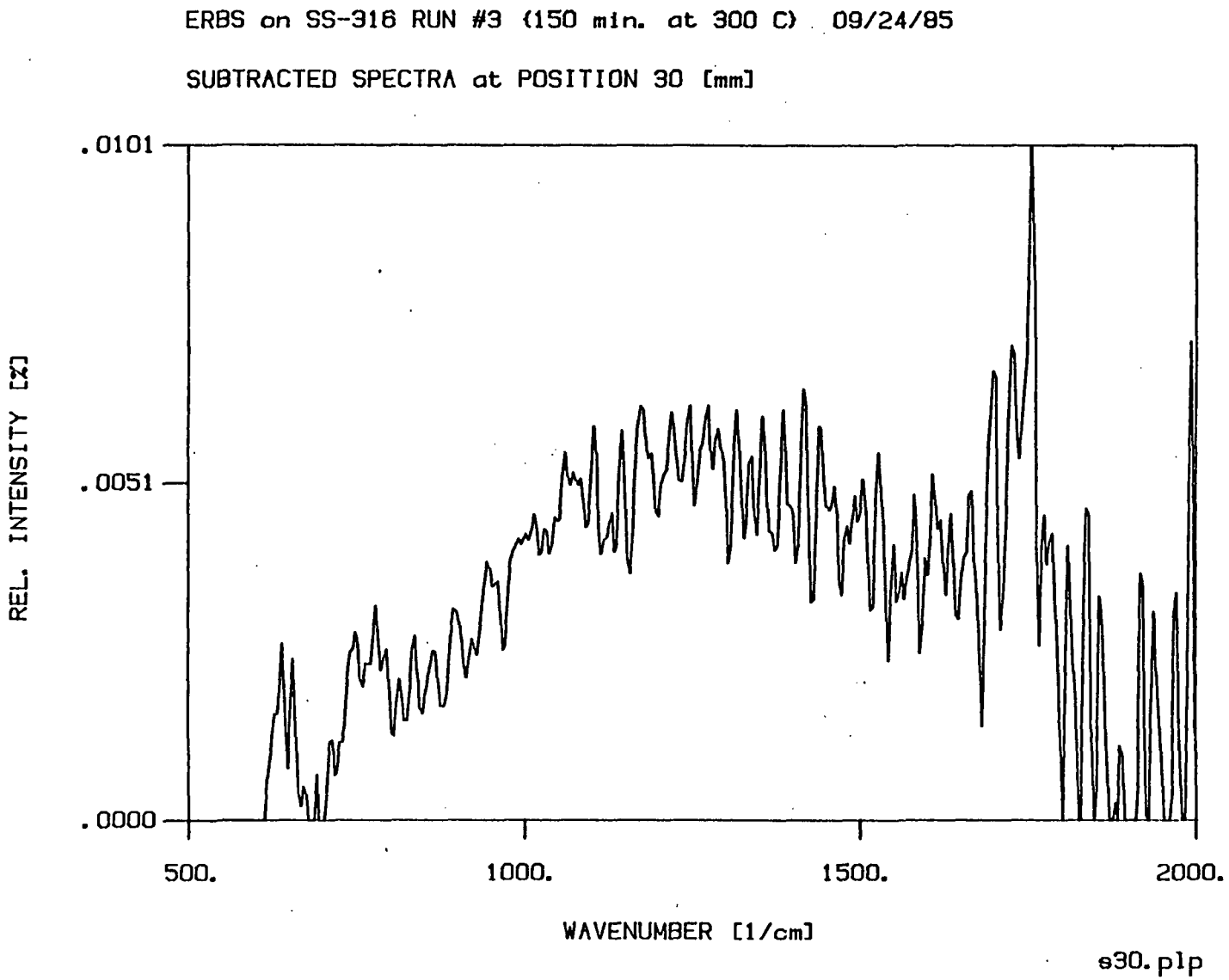
ERBS on SS-316 RUN #3 (150 min. at 300 C) 09/24/85
SUBTRACTED SPECTRA at POSITION 30 [mm]
.0101
.0051
.0000
REL. INTENSITY [%]
500.
1000.
1500.
2000.
WAVENUMBER [1/cm]
s30.plp

Figure 13

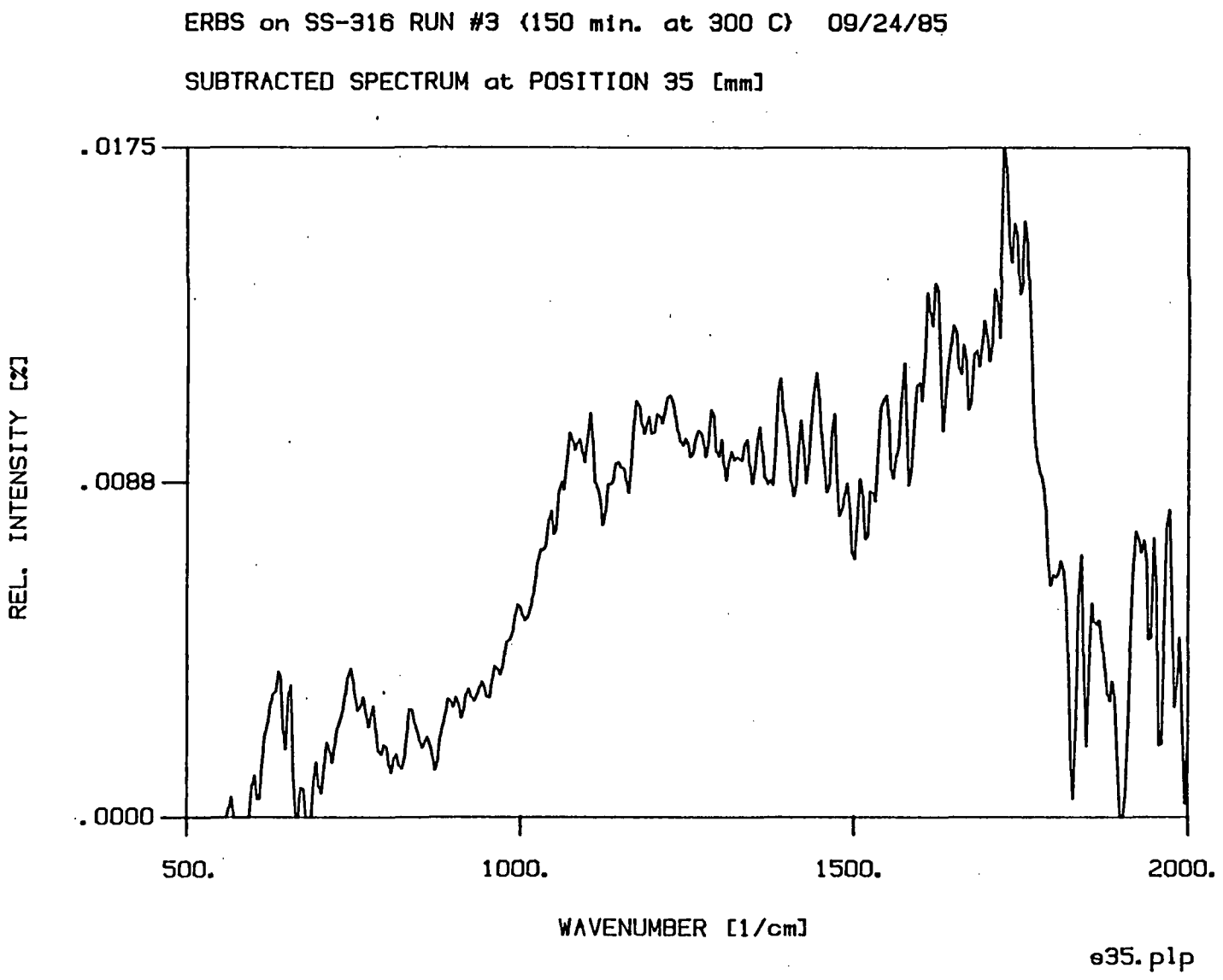
ERBS on SS-316 RUN #3 (150 min. at 300 C) 09/24/85
SUBTRACTED SPECTRUM at POSITION 35 [mm]
.0175
.0088
.0000
REL. INTENSITY [%]
500.
1000.
1500.
2000.
WAVENUMBER [1/cm]
e35.plp

Figure 14

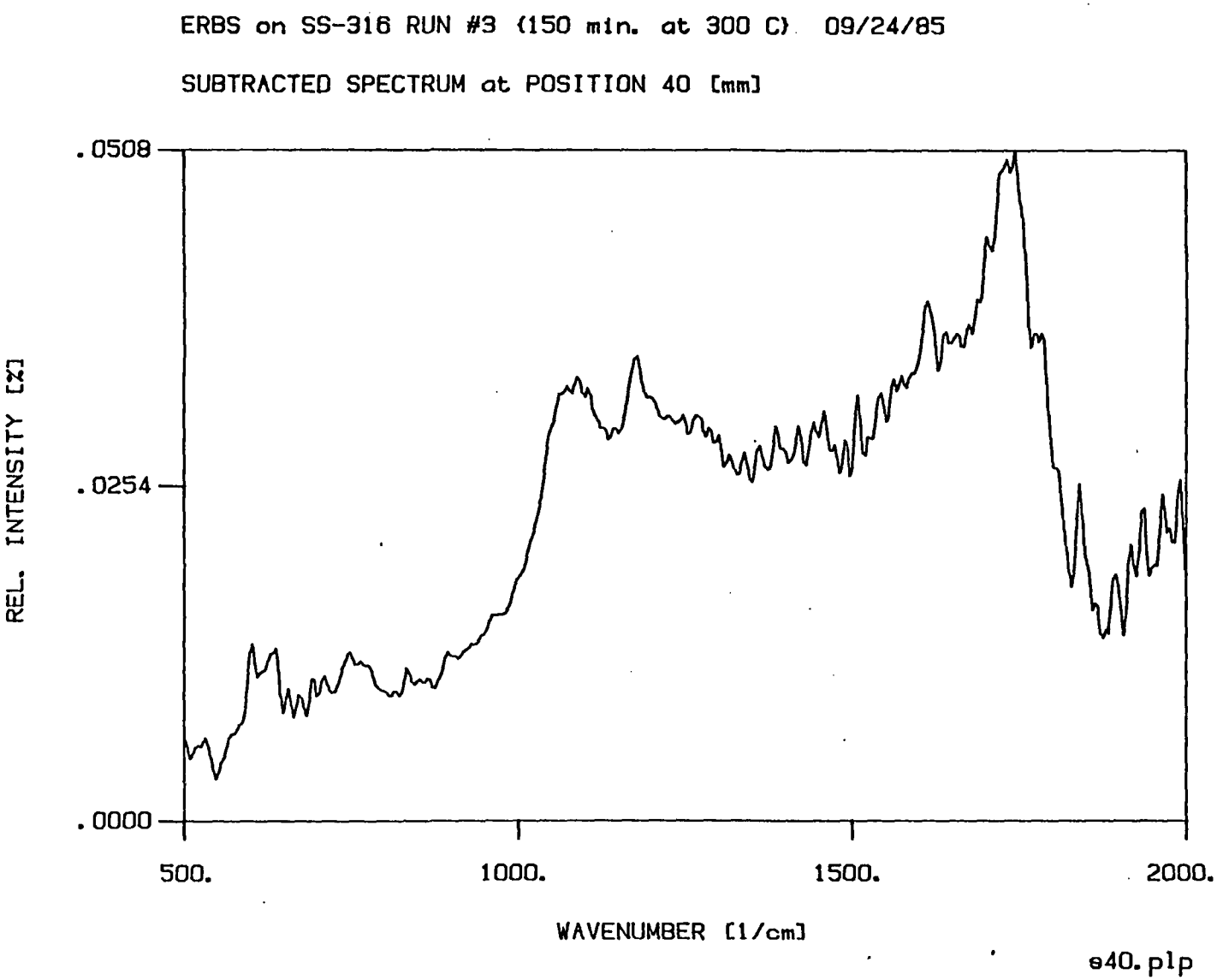
ERBS on SS-316 RUN #3 (150 min. at 300 C) 09/24/85
SUBTRACTED SPECTRUM at POSITION 40 [mm]
.0508
.0254
.0000
REL. INTENSITY [%]
500.
1000.
1500.
2000.
WAVENUMBER [1/cm]
s40.plp

Figure 15

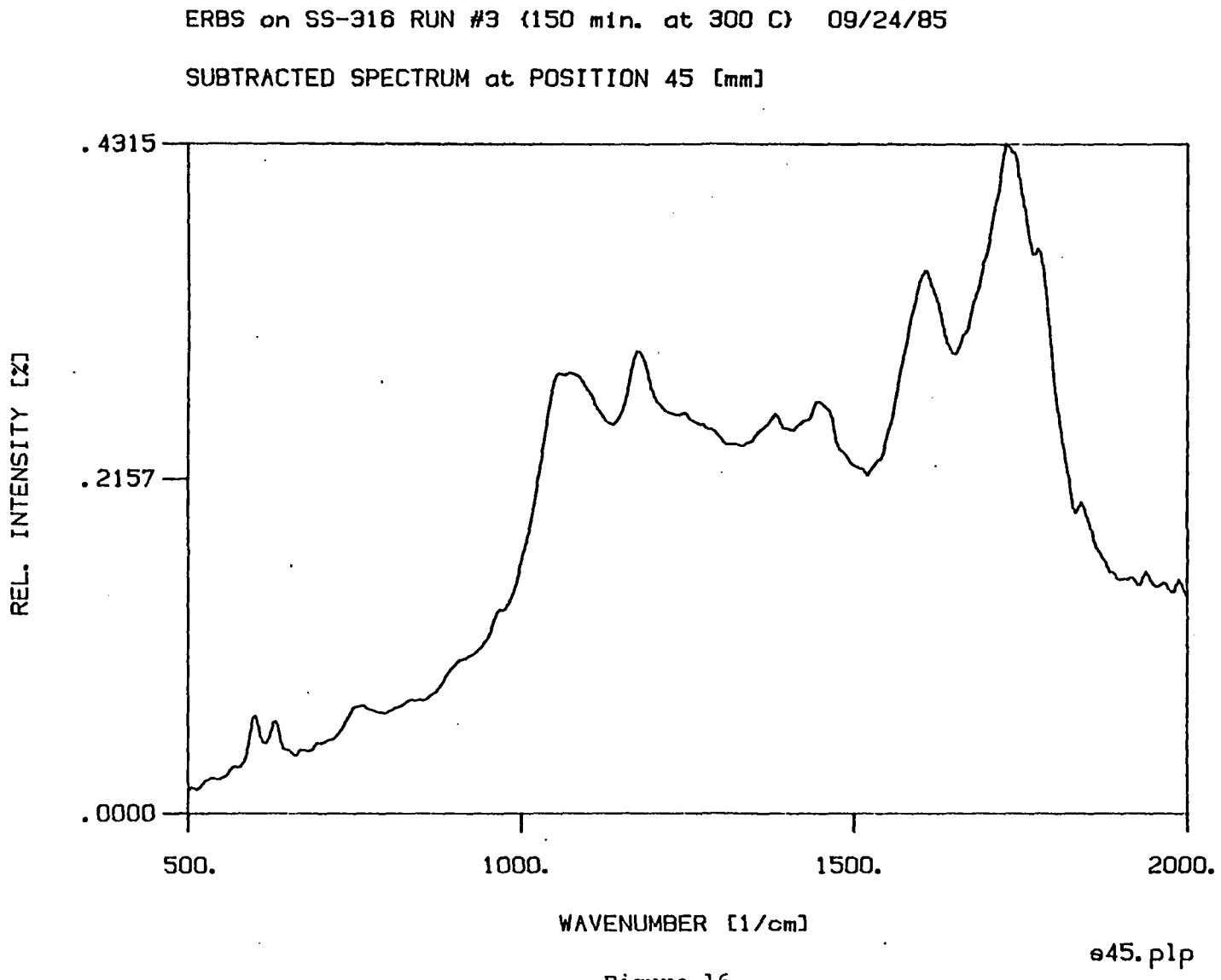
ERBS on SS-316 RUN #3 (150 min. at 300 C) 09/24/85
SUBTRACTED SPECTRUM at POSITION 45 [mm]
.4315
.2157
.0000
REL. INTENSITY [%]
500.
1000.
1500.
2000.
WAVENUMBER [1/cm]
e45.plp

Figure 16

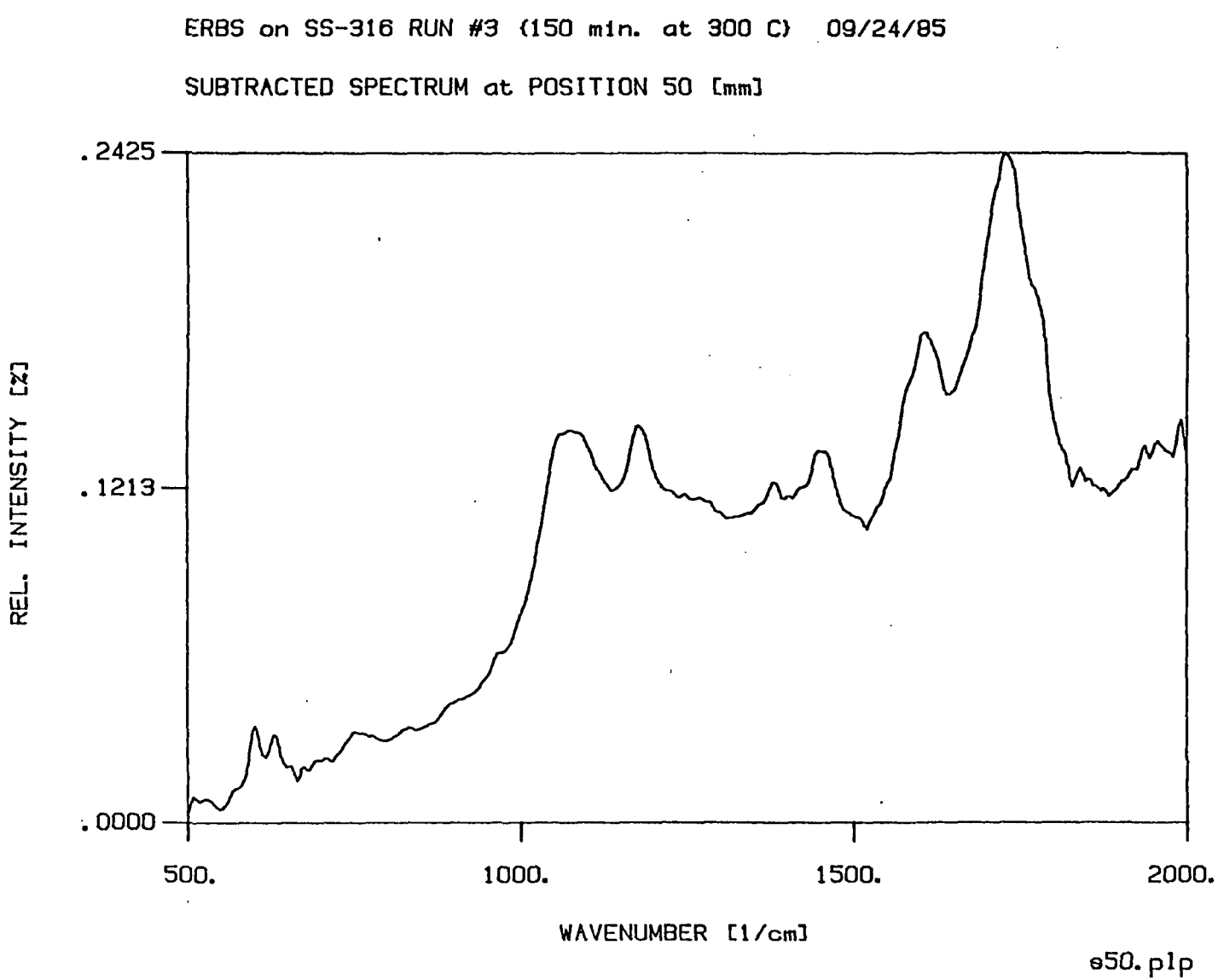
ERBS on SS-316 RUN #3 (150 min. at 300 C) 09/24/85
SUBTRACTED SPECTRUM at POSITION 50 [mm]
.2425
.1213
.0000
REL. INTENSITY [%]
500.
1000.
1500.
2000.
WAVENUMBER [1/cm]
s50.plp

Figure 17

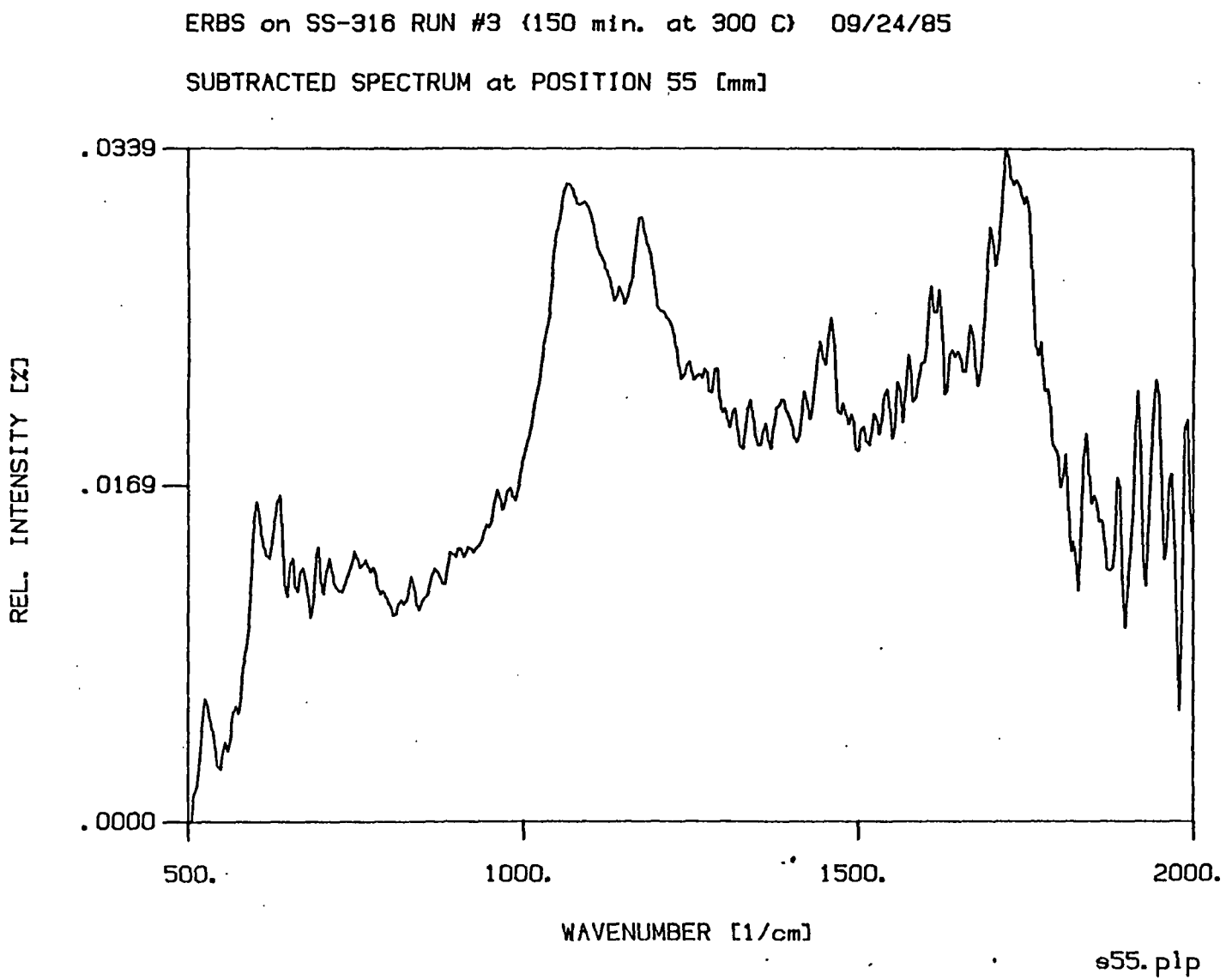
ERBS on SS-316 RUN #3 (150 min. at 300 C) 09/24/85
SUBTRACTED SPECTRUM at POSITION 55 [mm]
.0339
.0169
.0000
REL. INTENSITY [%]
500.
1000.
1500.
2000.
WAVENUMBER [1/cm]
s55.plp

Figure 18

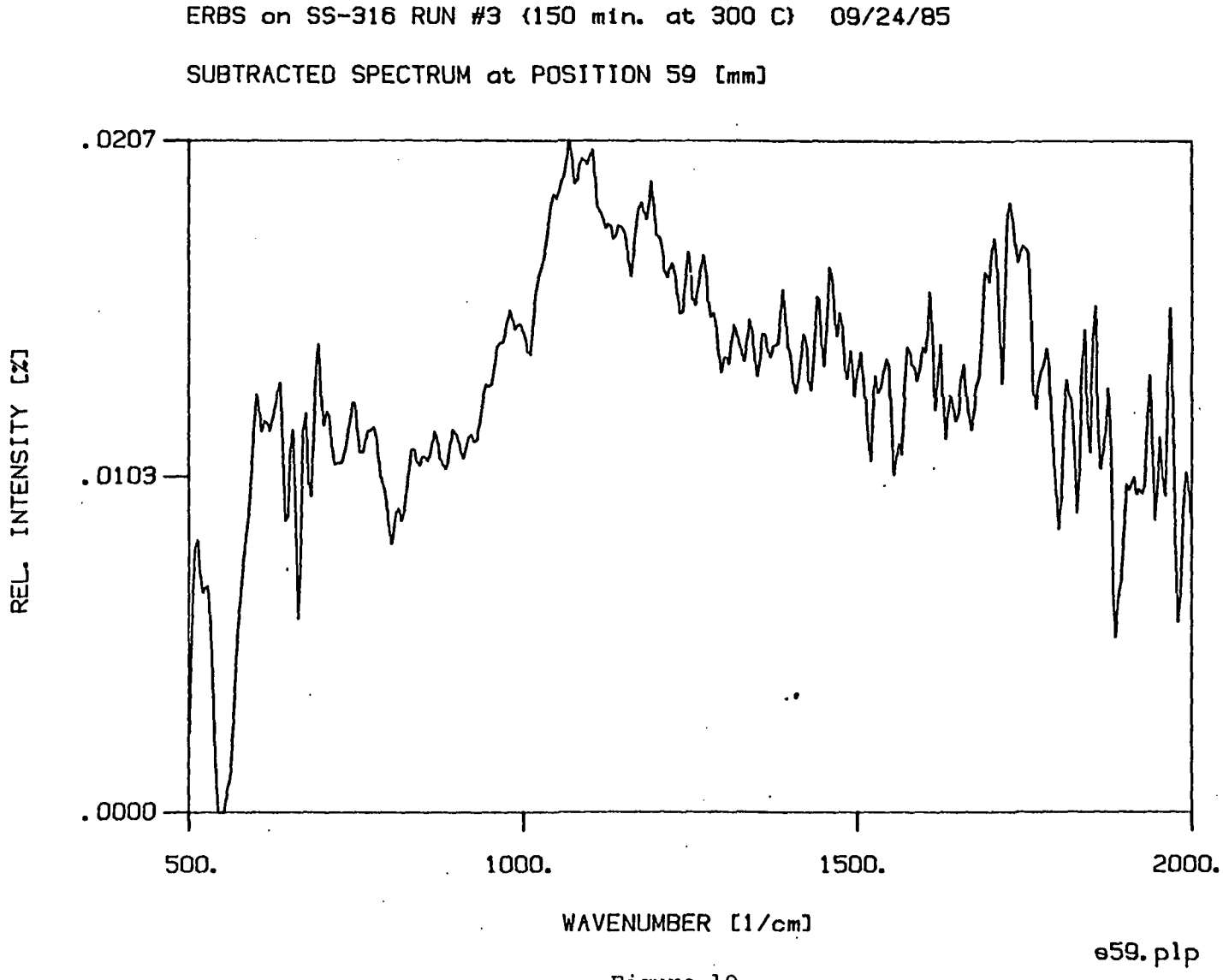
ERBS on SS-316 RUN #3 (150 min. at 300 C) 09/24/85
SUBTRACTED SPECTRUM at POSITION 59 [mm]
.0207
.0103
.0000
REL. INTENSITY [%]
500.
1000.
1500.
2000.
WAVENUMBER [1/cm]
e59.plp

Figure 19

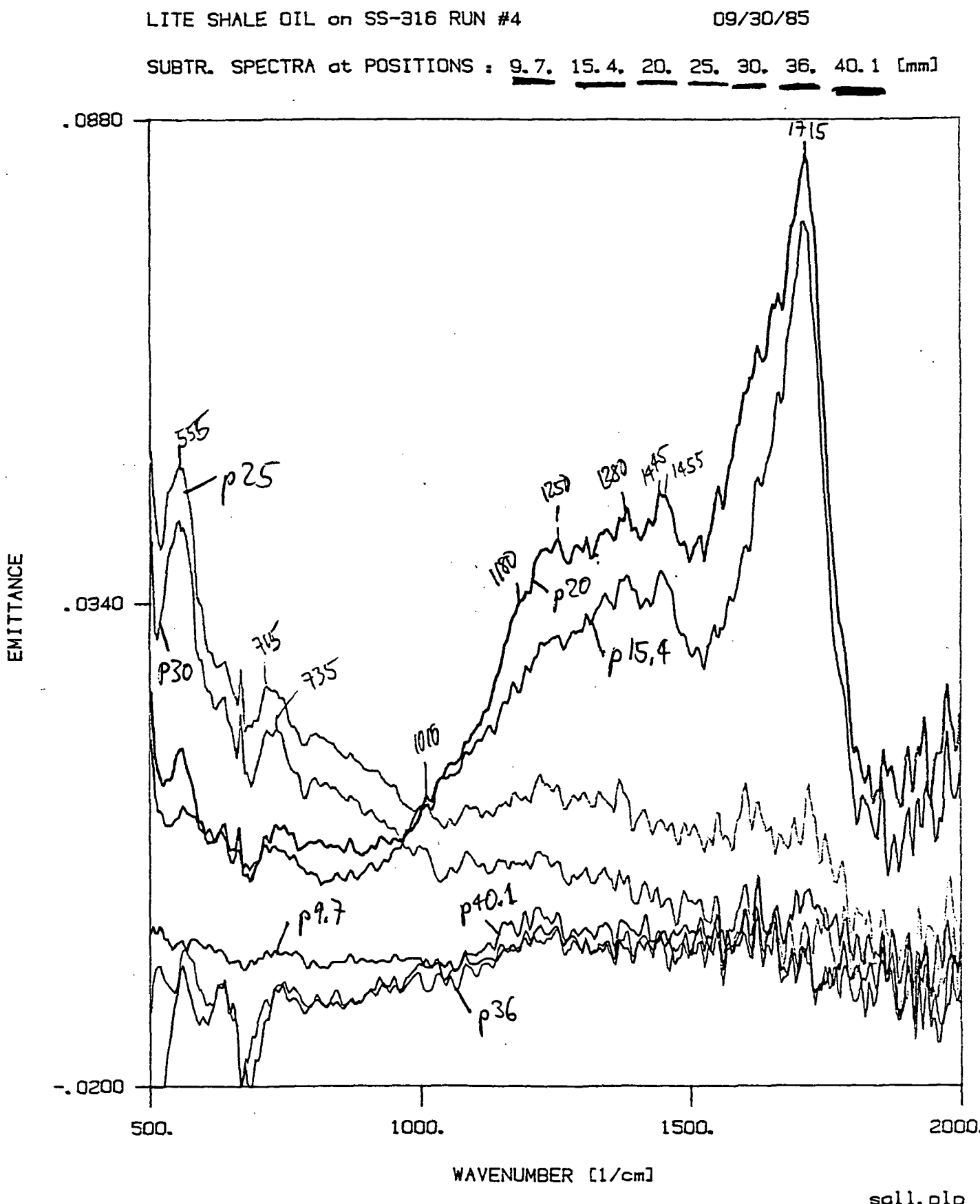


sall.plp

Figure 20

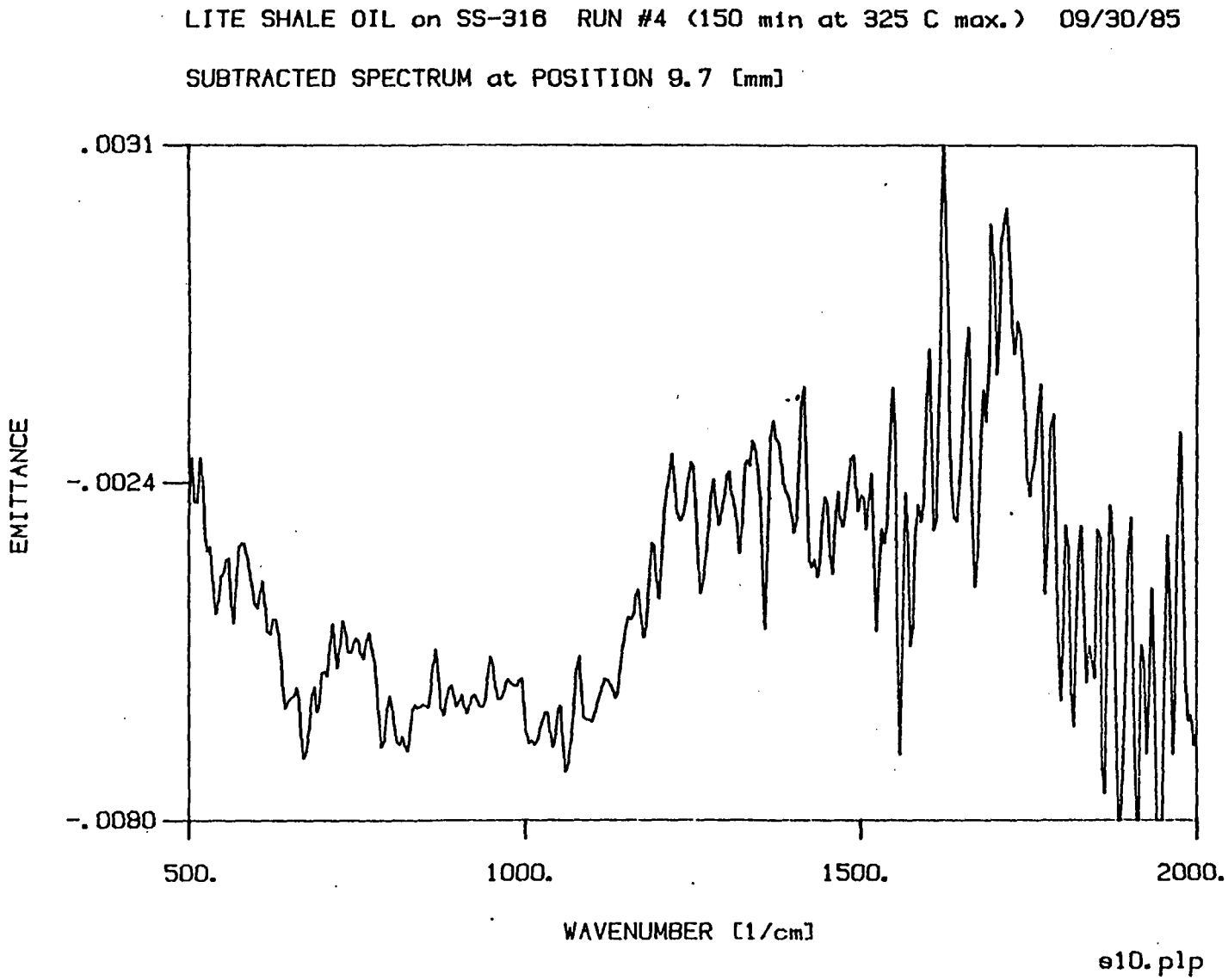
LITE SHALE OIL on SS-316 RUN #4 (150 min at 325 C max.) 09/30/85
SUBTRACTED SPECTRUM at POSITION 9.7 [mm]
.0031
-.0024
-.0080
EMITTANCE
500.
1000.
1500.
2000.
WAVENUMBER [1/cm]
s10.plp

Figure 21

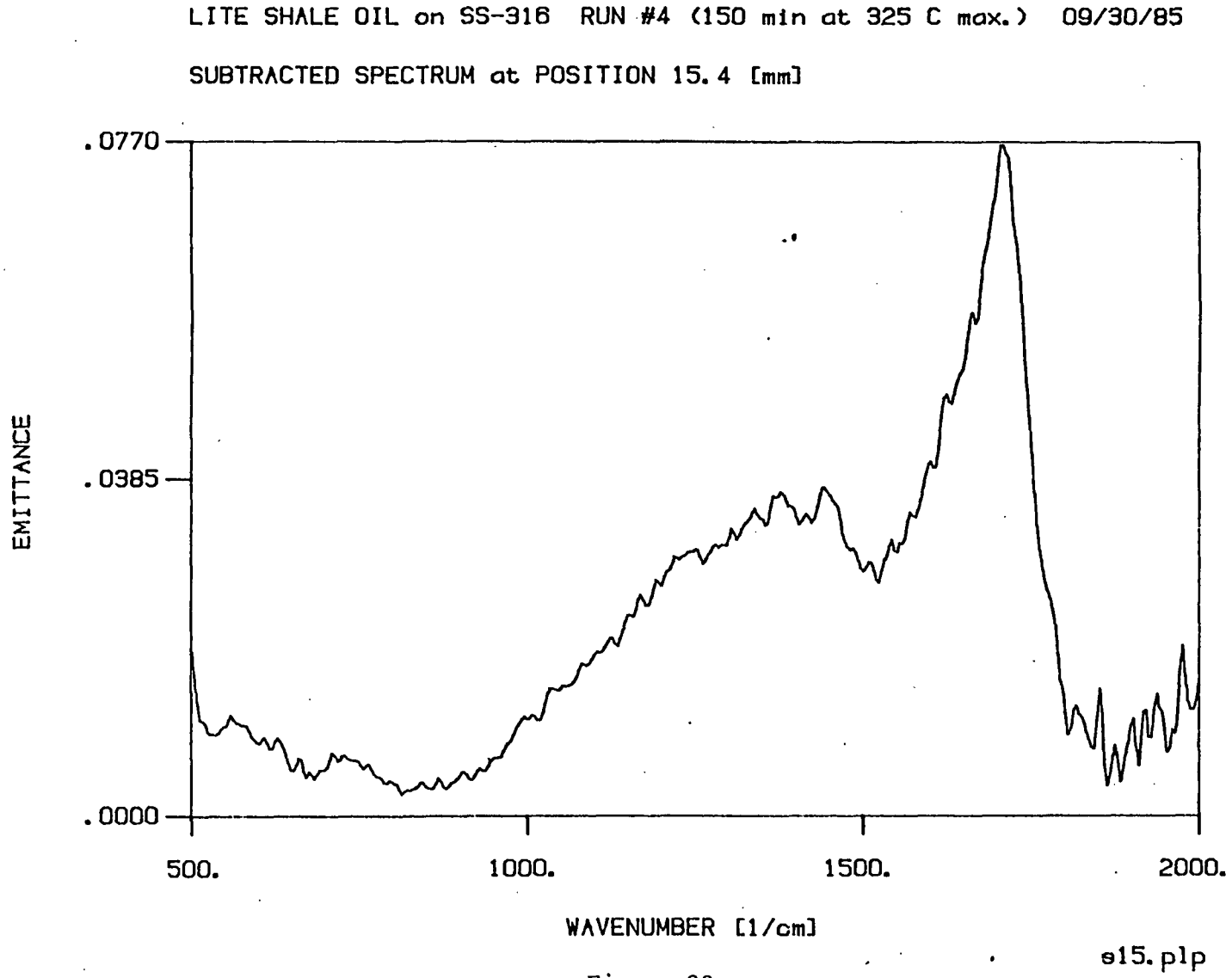
LITE SHALE OIL on SS-316 RUN #4 (150 min at 325 C max.) 09/30/85
SUBTRACTED SPECTRUM at POSITION 15.4 [mm]
.0770
.0385
.0000
EMITTANCE
500.
1000.
1500.
2000.
WAVENUMBER [1/cm]
s15.plp

Figure 22

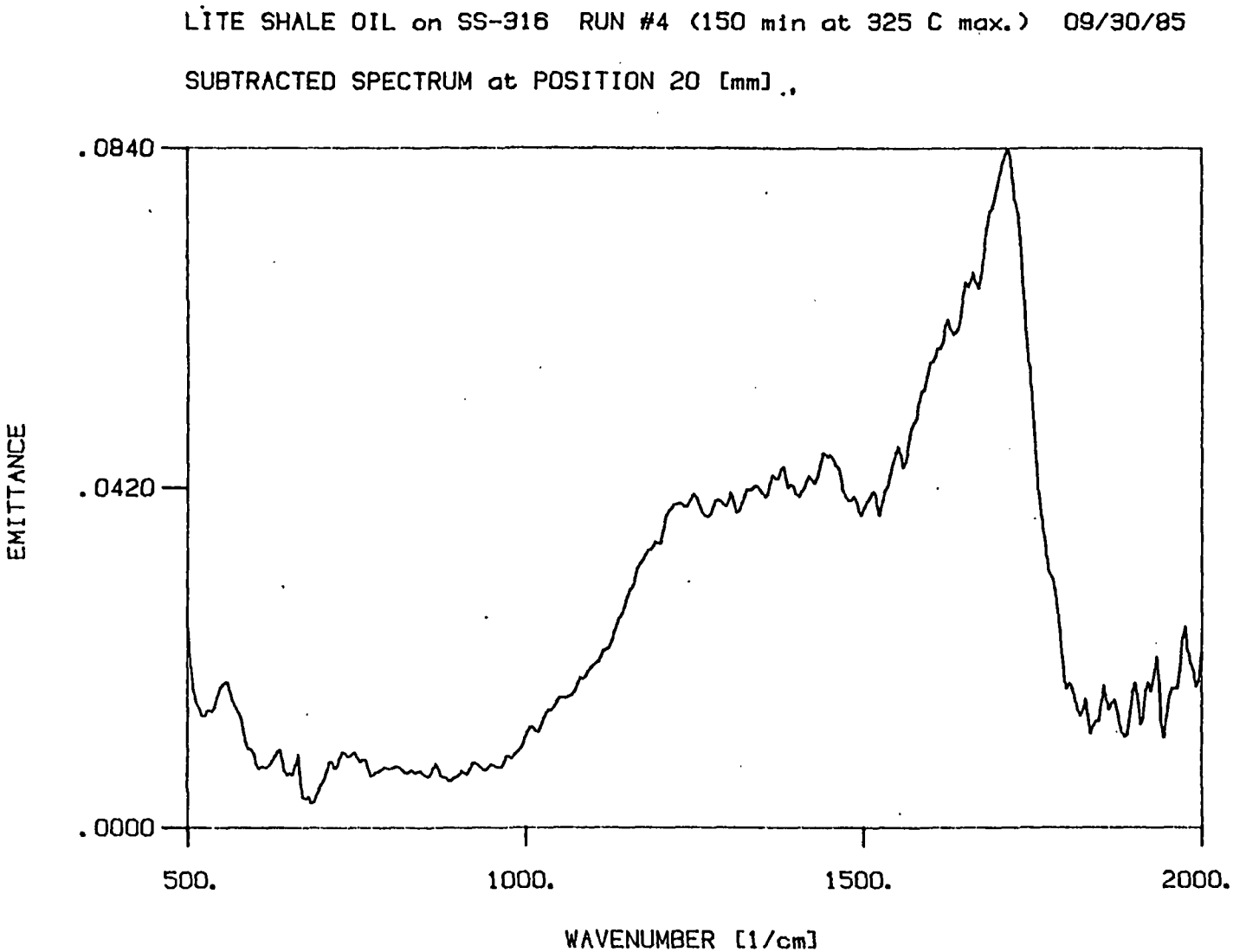
LITE SHALE OIL on SS-316 RUN #4 (150 min at 325 C max.) 09/30/85
SUBTRACTED SPECTRUM at POSITION 20 [mm]
.0840
.0420
.0000
EMITTANCE
500.
1000.
1500.
2000.
WAVENUMBER [1/cm]
e20.plp

Figure 23

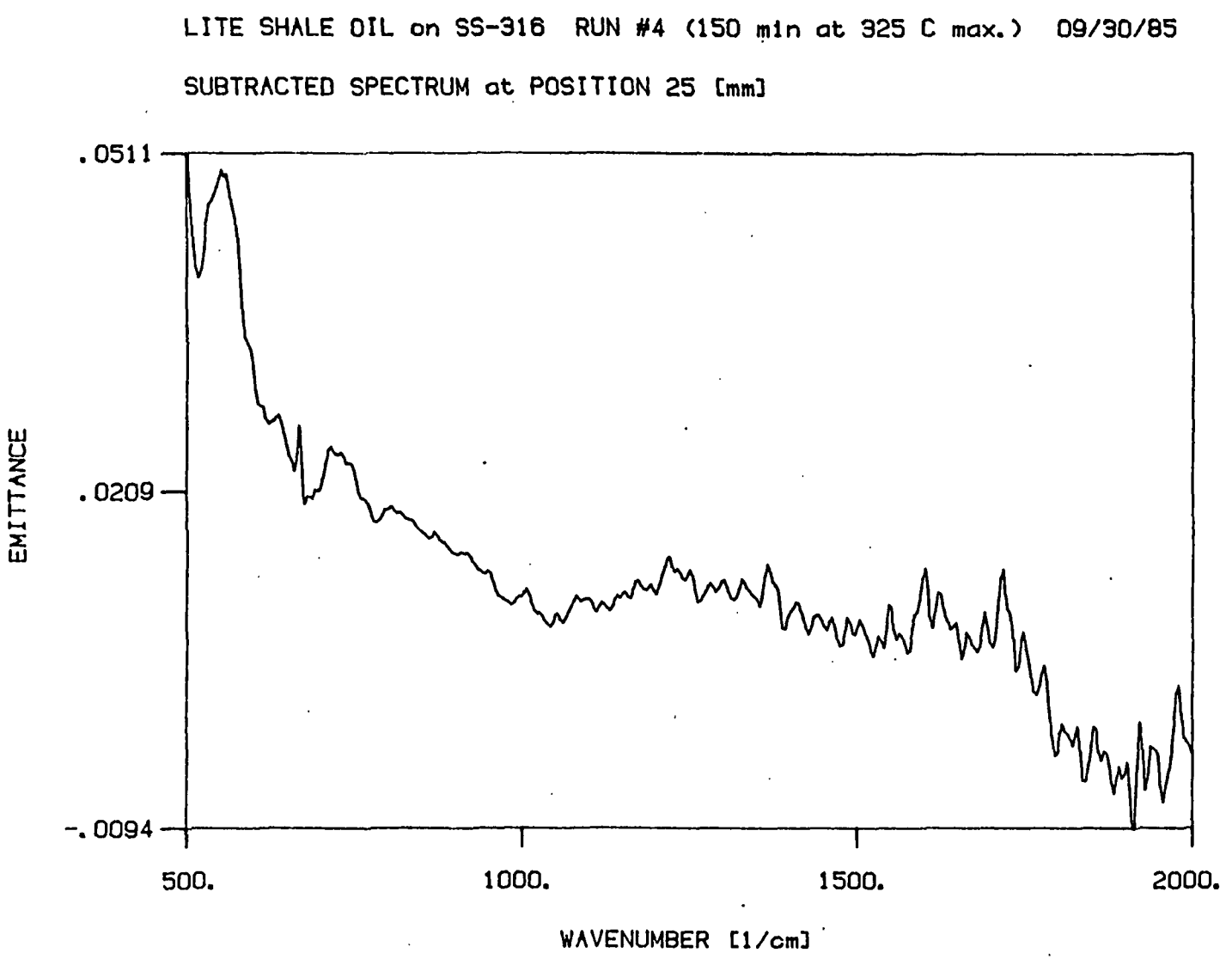
LITE SHALE OIL on SS-316 RUN #4 (150 min at 325 C max.) 09/30/85
SUBTRACTED SPECTRUM at POSITION 25 [mm]
.0511
.0209
-.0094
EMITTANCE
500.
1000.
1500.
2000.
WAVENUMBER [1/cm]
e25.plp

Figure 24

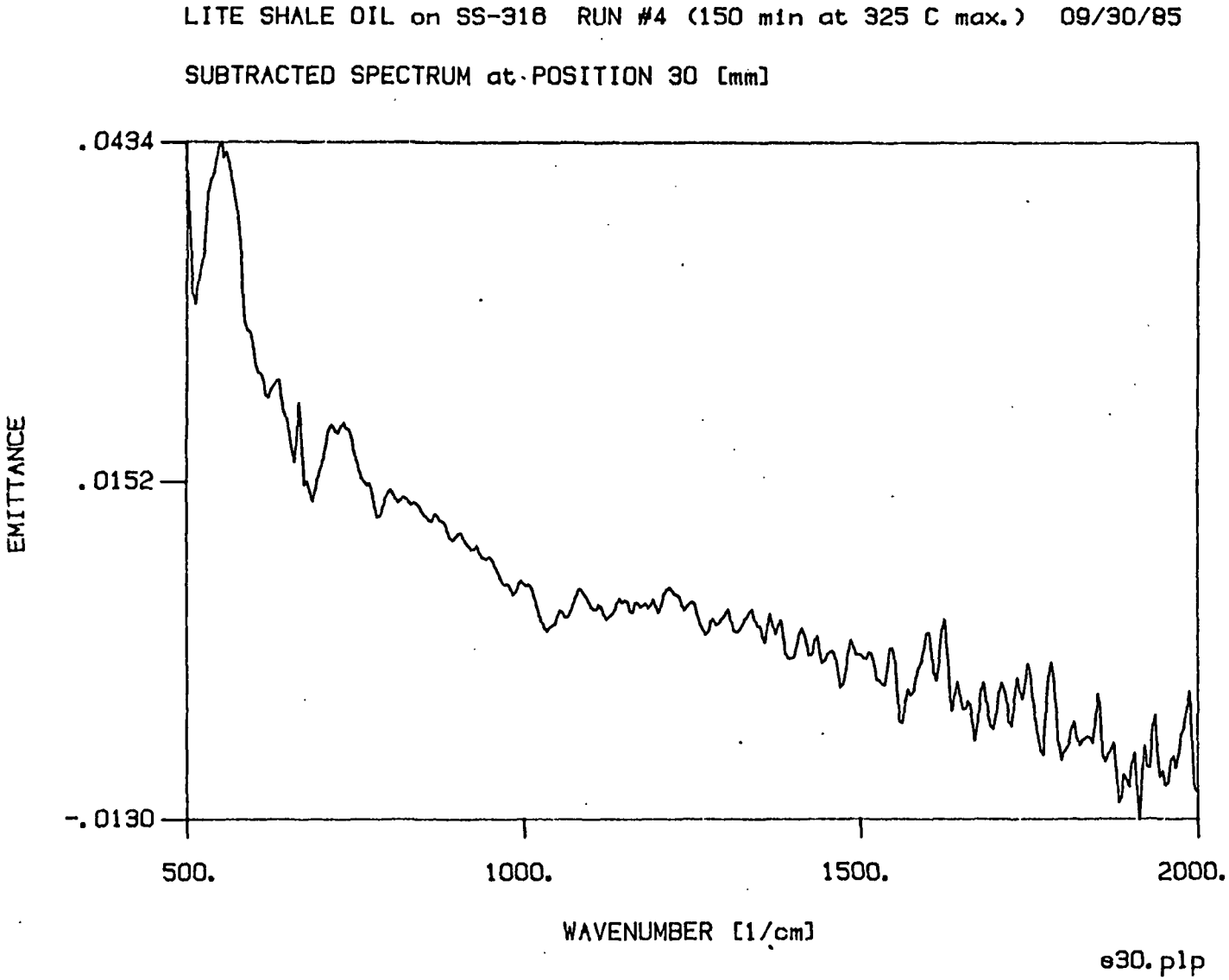
LITE SHALE OIL on SS-316 RUN #4 (150 min at 325 C max.) 09/30/85
SUBTRACTED SPECTRUM at POSITION 30 [mm]
.0434
.0152
-.0130
EMITTANCE
500.
1000.
1500.
2000.
WAVENUMBER [1/cm]
e30.plp

Figure 25

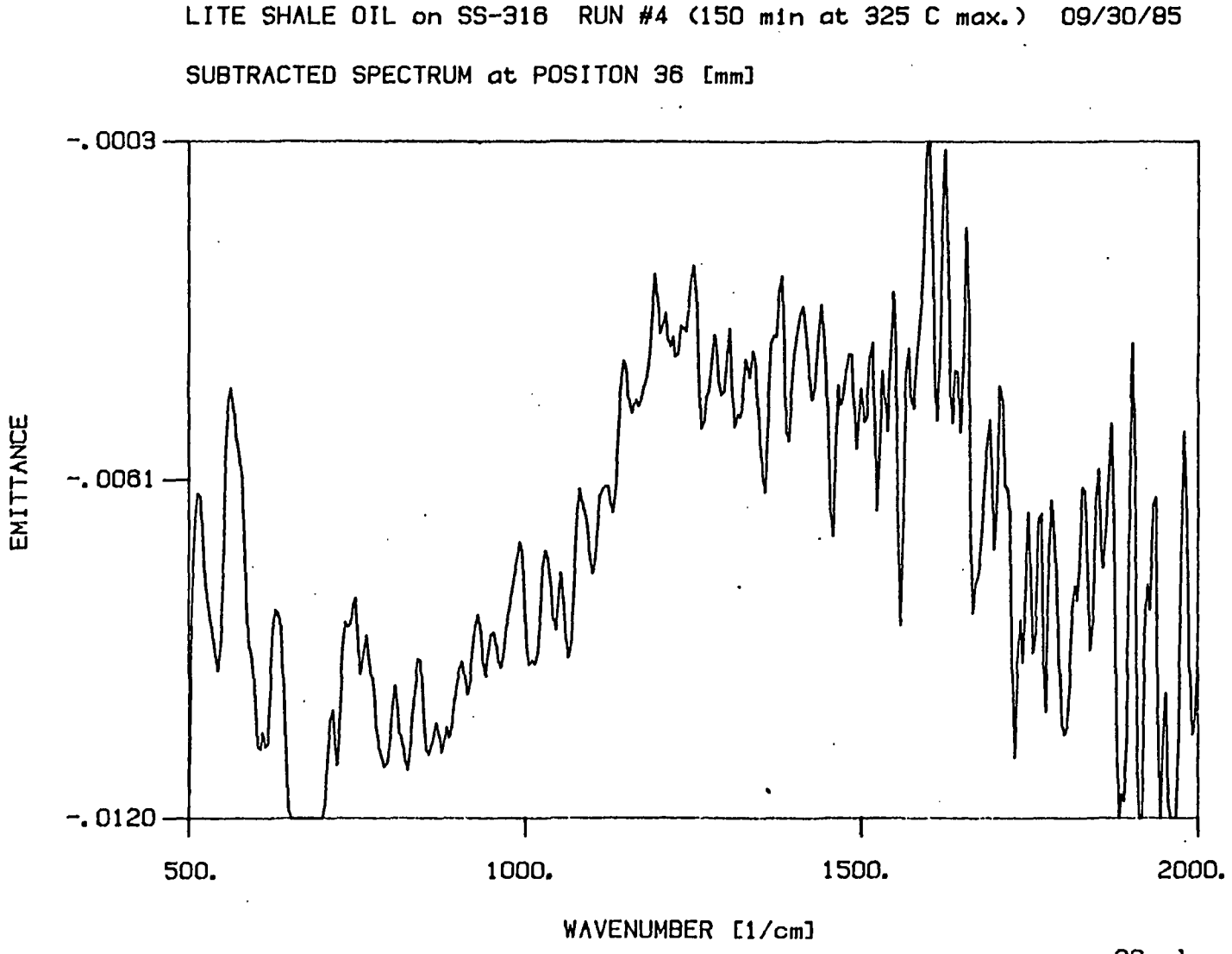
LITE SHALE OIL on SS-316 RUN #4 (150 min at 325 C max.) 09/30/85
SUBTRACTED SPECTRUM at POSITON 36 [mm]
-.0003
-.0061
-.0120
EMITTANCE
500.
1000.
1500.
2000.
WAVENUMBER [1/cm]
e36.plp

Figure 26

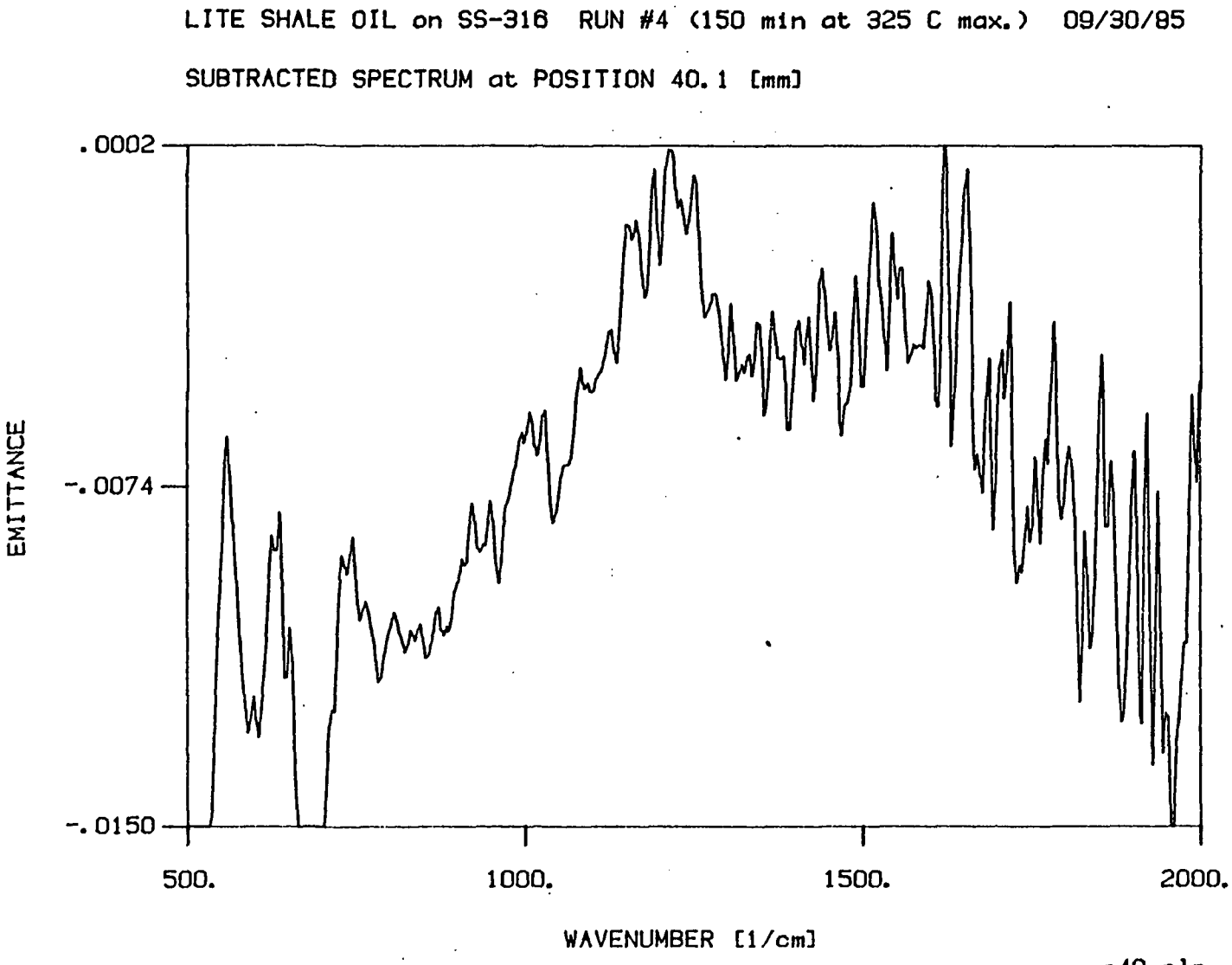
LITE SHALE OIL on SS-316 RUN #4 (150 min at 325 C max.) 09/30/85
SUBTRACTED SPECTRUM at POSITION 40.1 [mm]
.0002
-.0074
-.0150
EMITTANCE
500.
1000.
1500.
2000.
WAVENUMBER [1/cm]
e40.plp

Figure 27

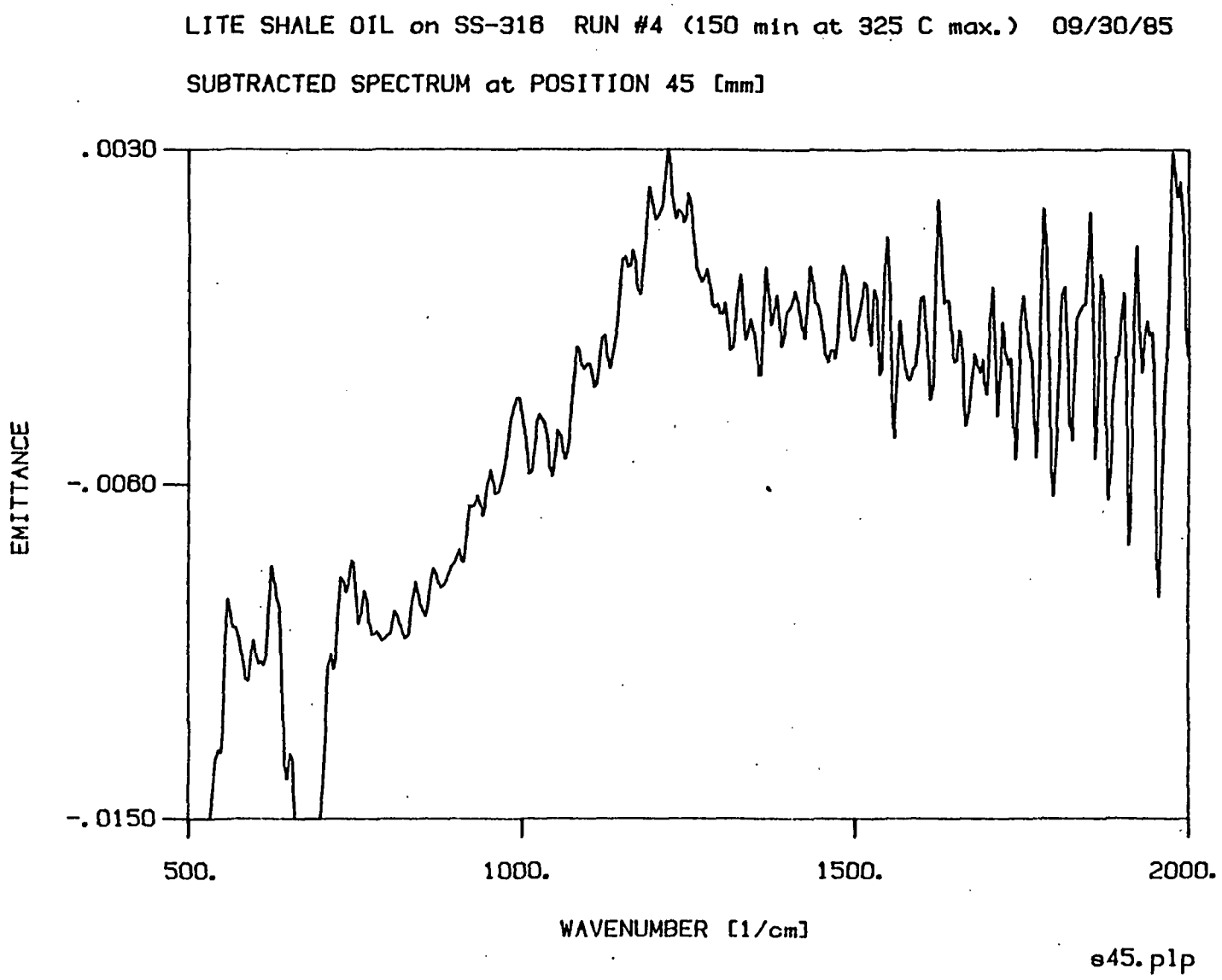
LITE SHALE OIL on SS-316 RUN #4 (150 min at 325 C max.) 09/30/85
SUBTRACTED SPECTRUM at POSITION 45 [mm]
.0030
-.0060
-.0150
EMITTANCE
500.
1000.
1500.
2000.
WAVENUMBER [1/cm]
e45.plp

Figure 28

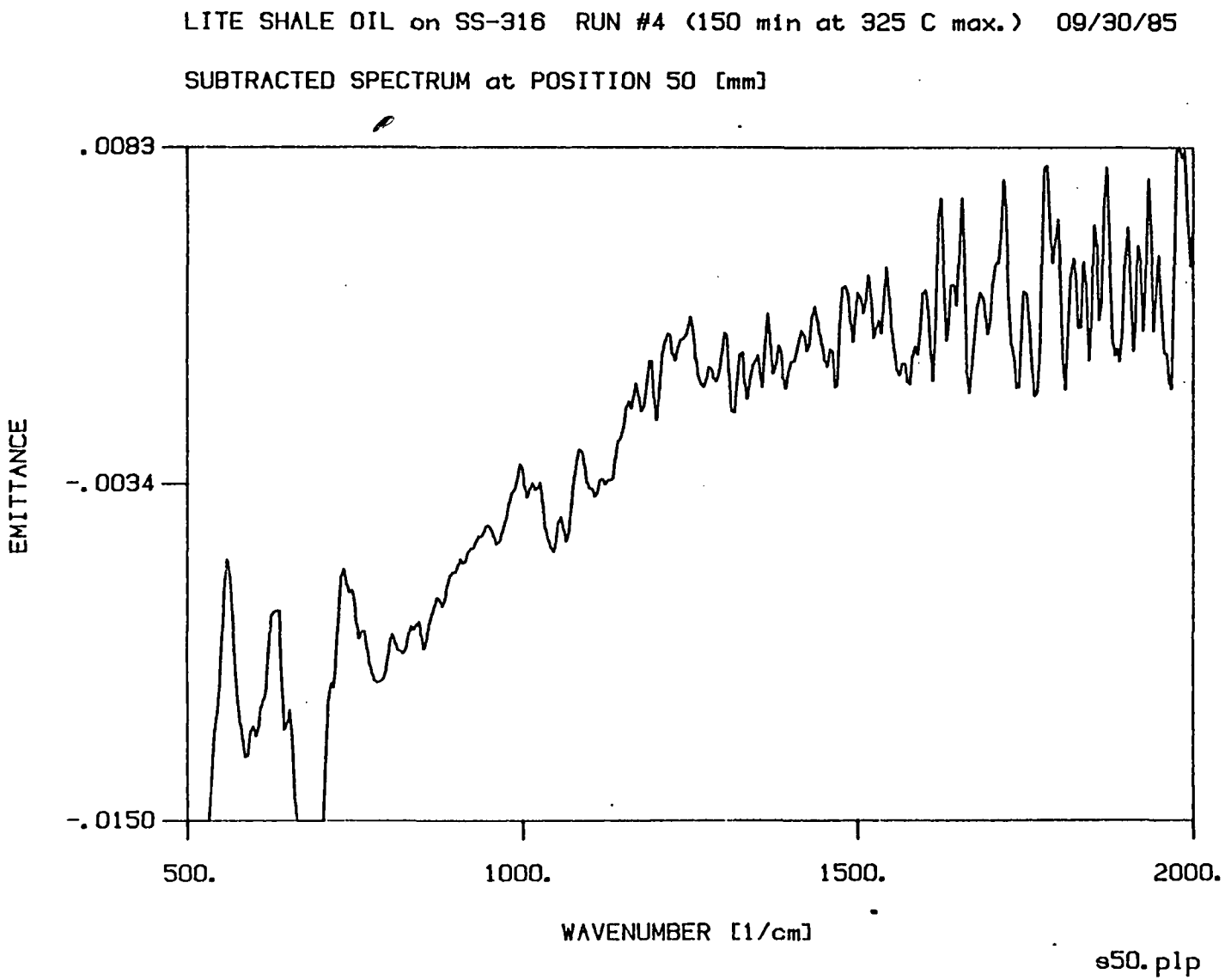
LITE SHALE OIL on SS-316 RUN #4 (150 min at 325 C max.) 09/30/85
SUBTRACTED SPECTRUM at POSITION 50 [mm]
.0083
-.0034
-.0150
EMITTANCE
500.
1000.
1500.
2000.
WAVENUMBER [1/cm]
s50.plp

Figure 29

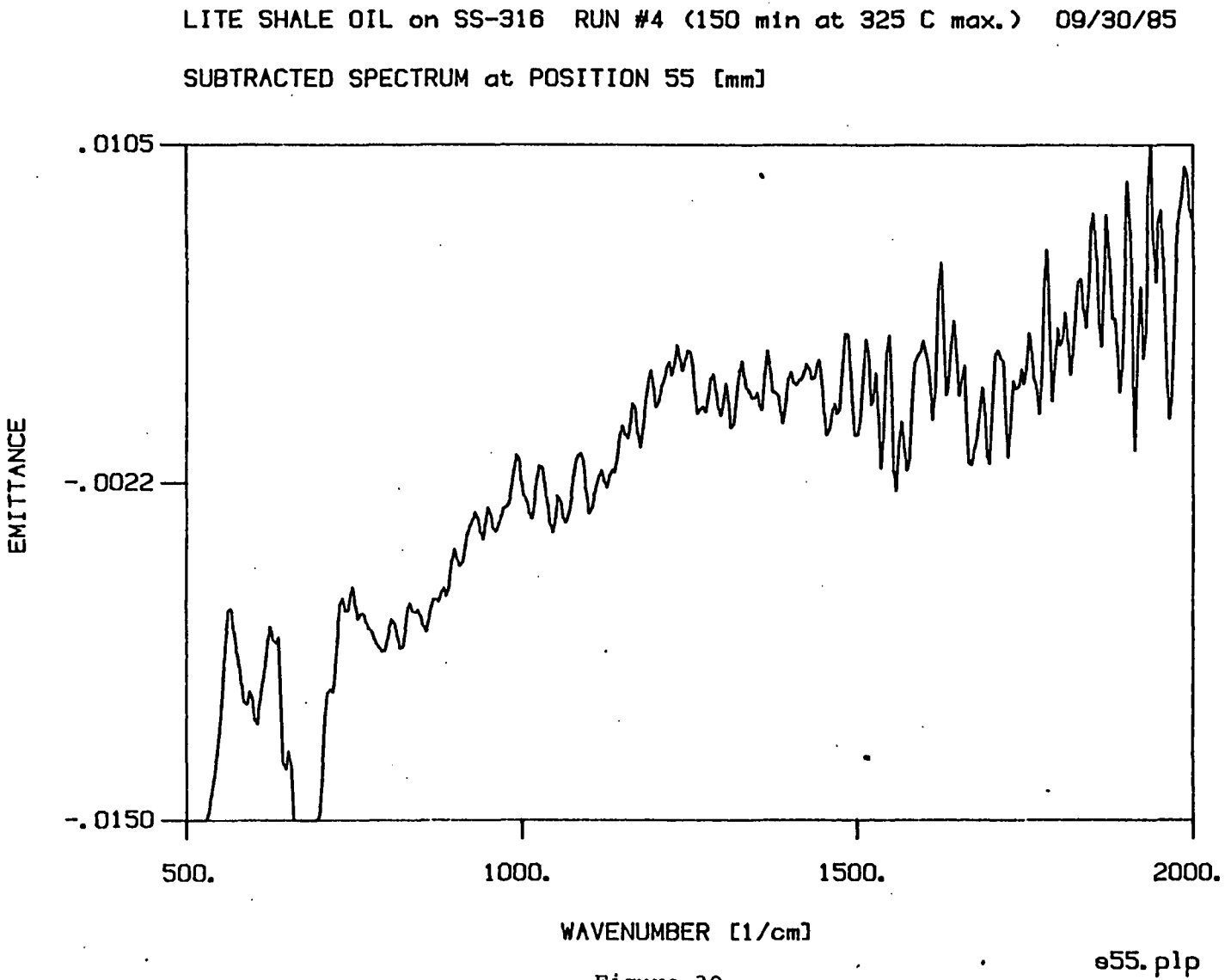
LITE SHALE OIL on SS-316 RUN #4 (150 min at 325 C max.) 09/30/85
SUBTRACTED SPECTRUM at POSITION 55 [mm]
.0105
-.0022
-.0150
EMITTANCE
500.
1000.
1500.
2000.
WAVENUMBER [1/cm]
e55.plp

Figure 30

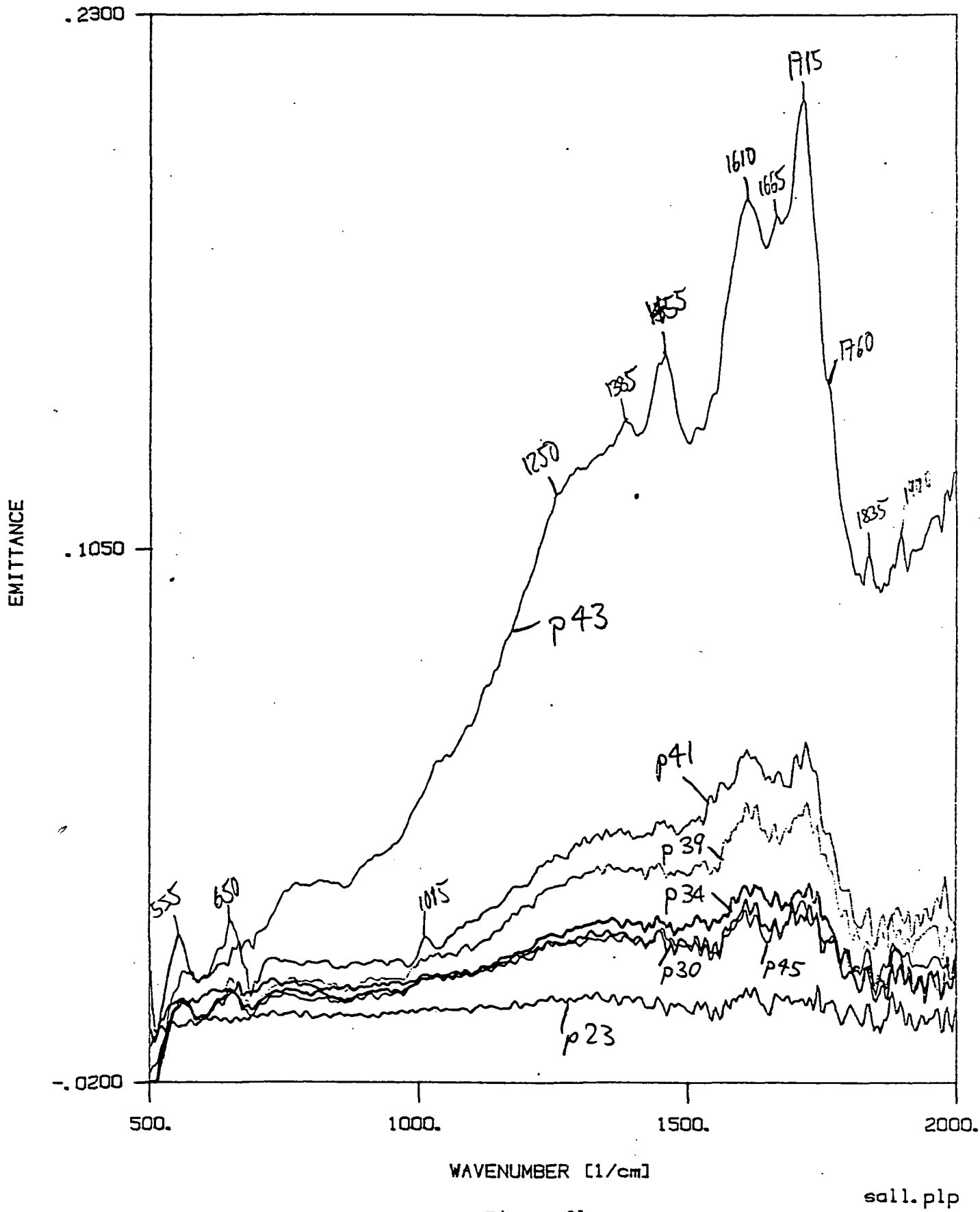
SHALE JP-4 on SS-316 RUN #5 10/01/85
SUBTR. SPECTRA at POSITIONS : 23. 30. 34. 39. 41. 43. 45 [mm]
.2300
.1050
-.0200
EMITTANCE
500.
1000.
1500.
2000.
WAVENUMBER [1/cm]
1715
1610
1655
1760
1455
1385
1250
1835
555
650
1015
p43
p41
p39
p34
p30
p45
p23
sall.plp

Figure 31

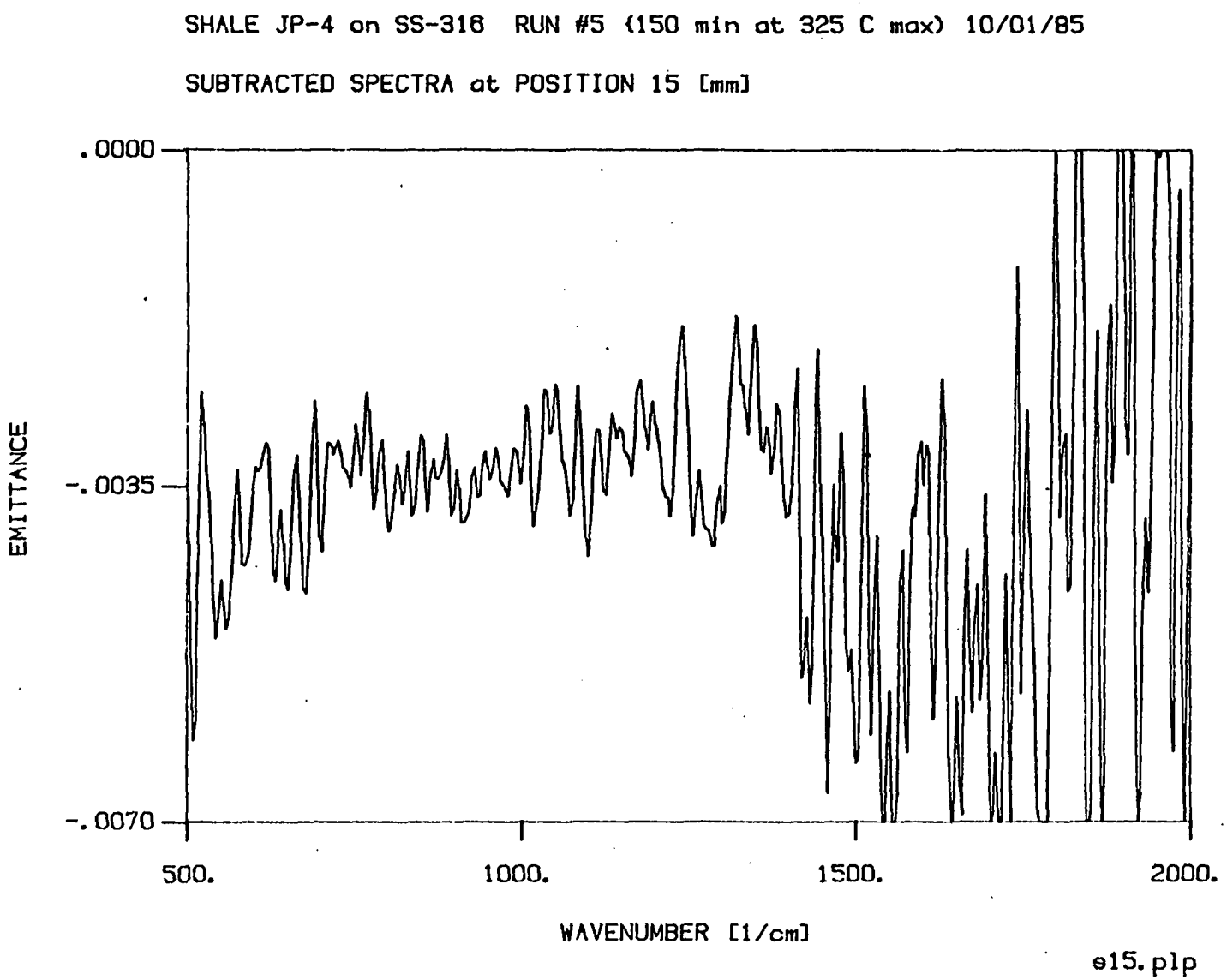
SHALE JP-4 on SS-316 RUN #5 (150 min at 325 C max) 10/01/85
SUBTRACTED SPECTRA at POSITION 15 [mm]
.0000
-.0035
-.0070
EMITTANCE
500.
1000.
1500.
2000.
WAVENUMBER [1/cm]
e15.plp

Figure 32

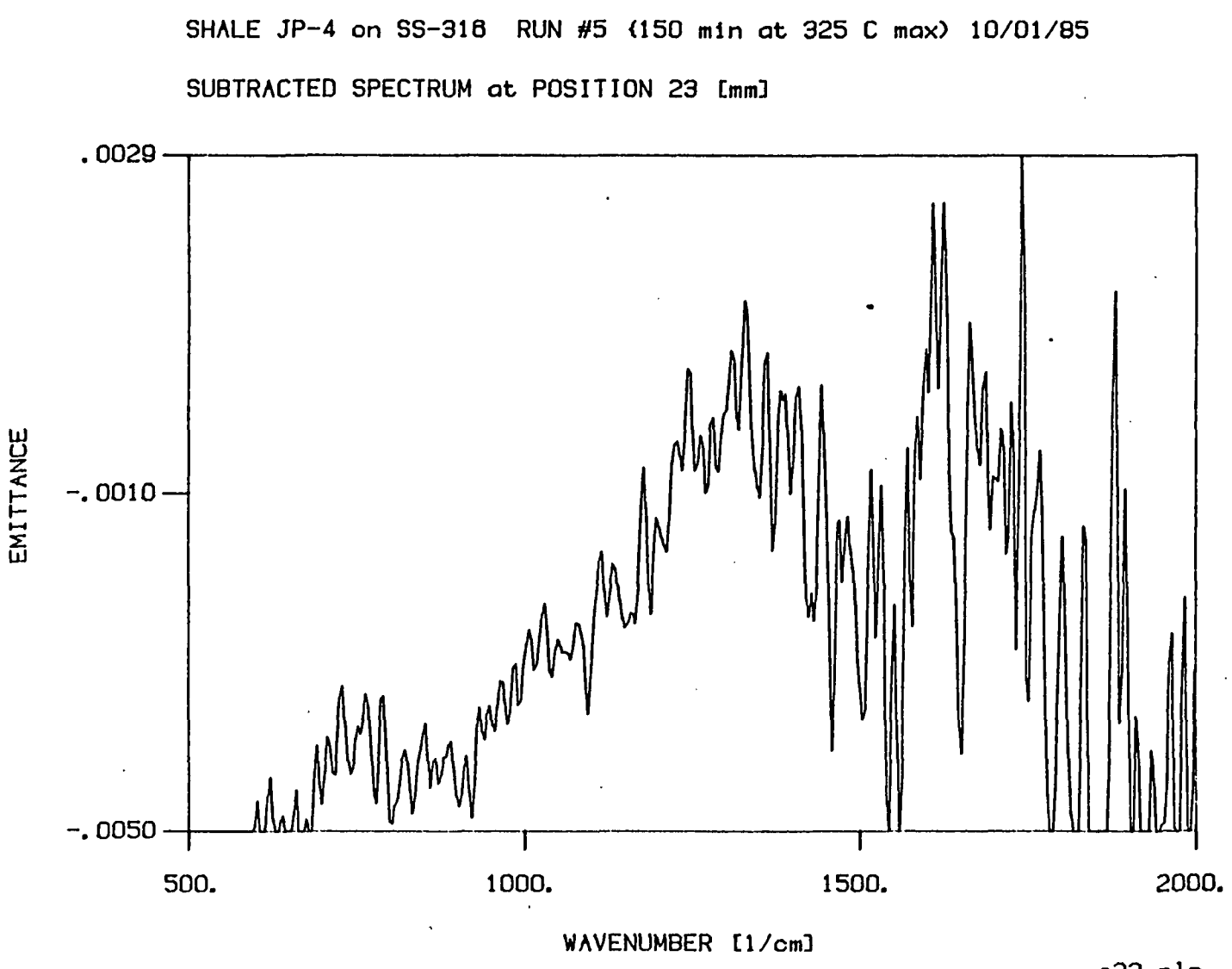
SHALE JP-4 on SS-316 RUN #5 (150 min at 325 C max) 10/01/85
SUBTRACTED SPECTRUM at POSITION 23 [mm]
.0029
-.0010
-.0050
EMITTANCE
500.
1000.
1500.
2000.
WAVENUMBER [1/cm]
e23.plp

Figure 33

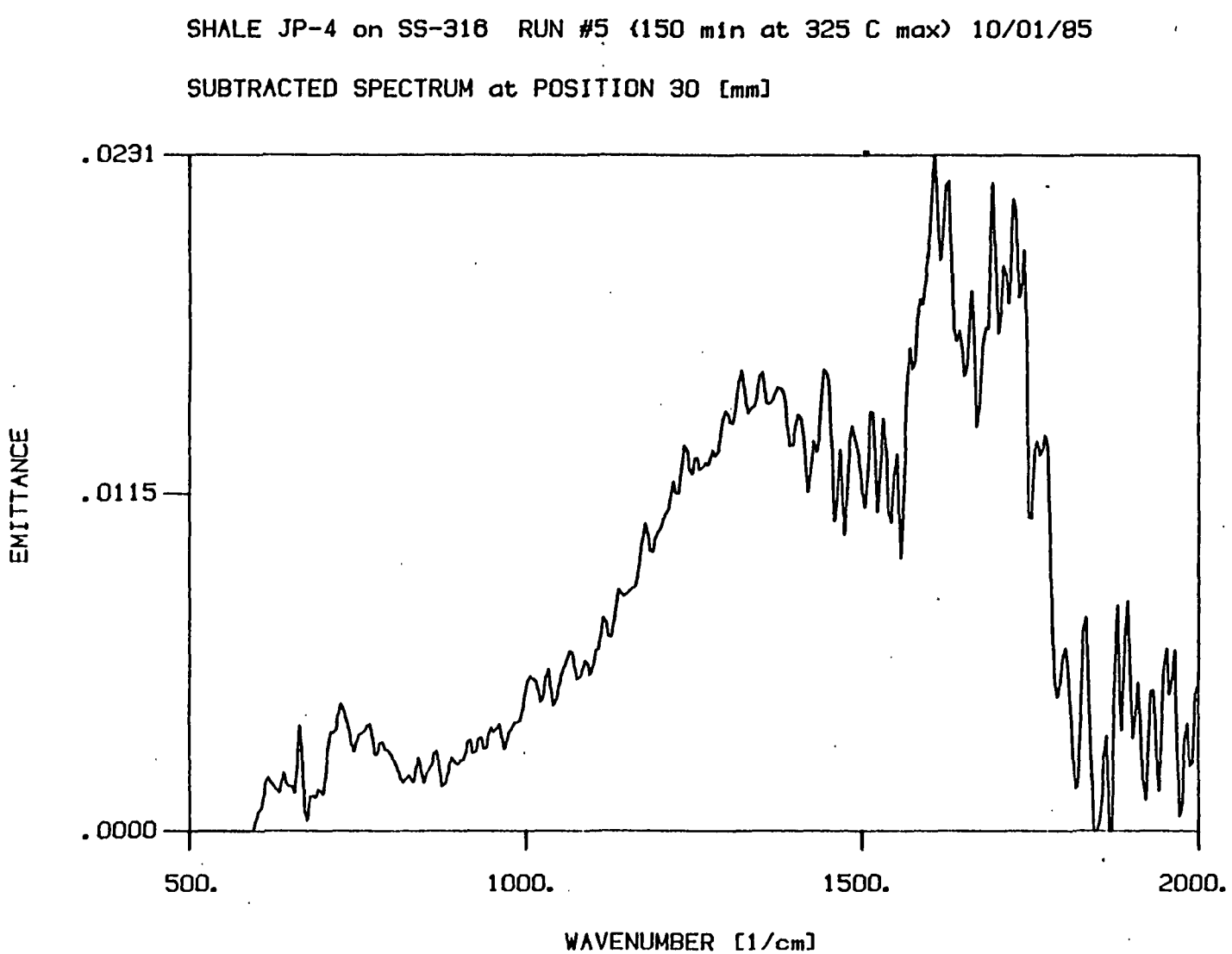
SHALE JP-4 on SS-316 RUN #5 (150 min at 325 C max) 10/01/85
SUBTRACTED SPECTRUM at POSITION 30 [mm]
.0231
.0115
.0000
EMITTANCE
500.
1000.
1500.
2000.
WAVENUMBER [1/cm]
s30.plp

Figure 34

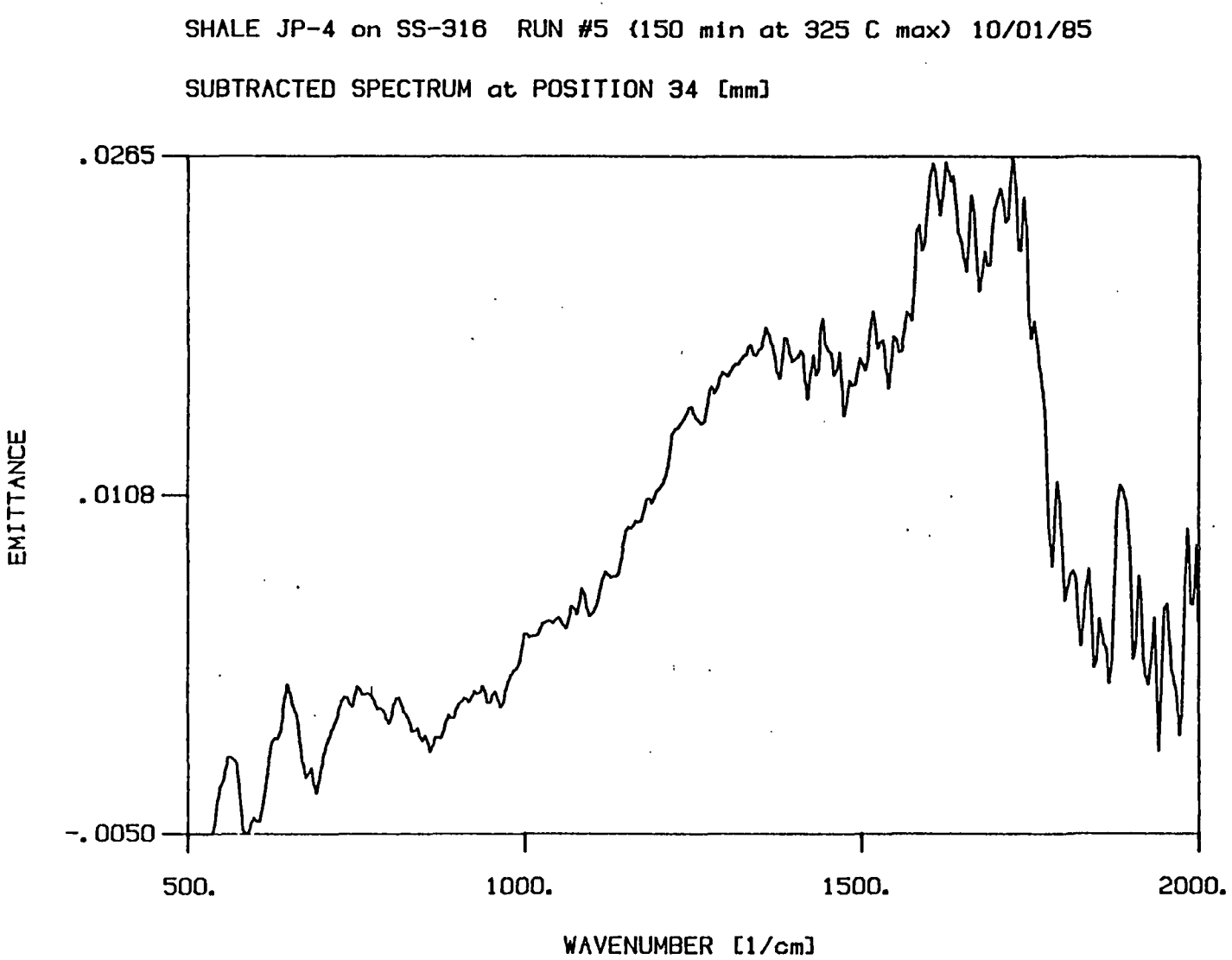
SHALE JP-4 on SS-316 RUN #5 (150 min at 325 C max) 10/01/85
SUBTRACTED SPECTRUM at POSITION 34 [mm]
.0265
.0108
-.0050
EMITTANCE
500.
1000.
1500.
2000.
WAVENUMBER [1/cm]

Figure 35

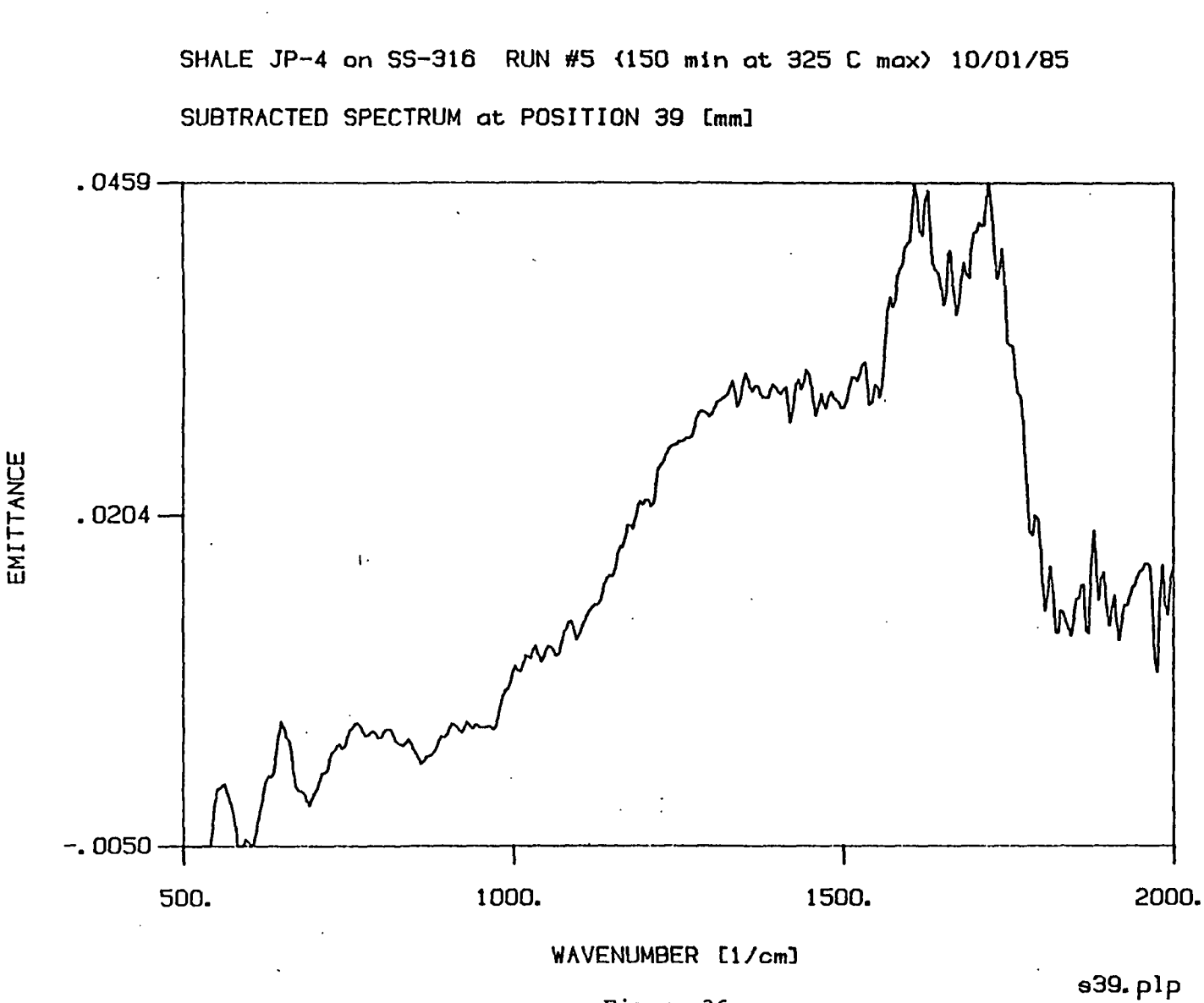
SHALE JP-4 on SS-316 RUN #5 (150 min at 325 C max) 10/01/85
SUBTRACTED SPECTRUM at POSITION 39 [mm]
.0459
.0204
-.0050
EMITTANCE
500.
1000.
1500.
2000.
WAVENUMBER [1/cm]
s39.plp

Figure 36

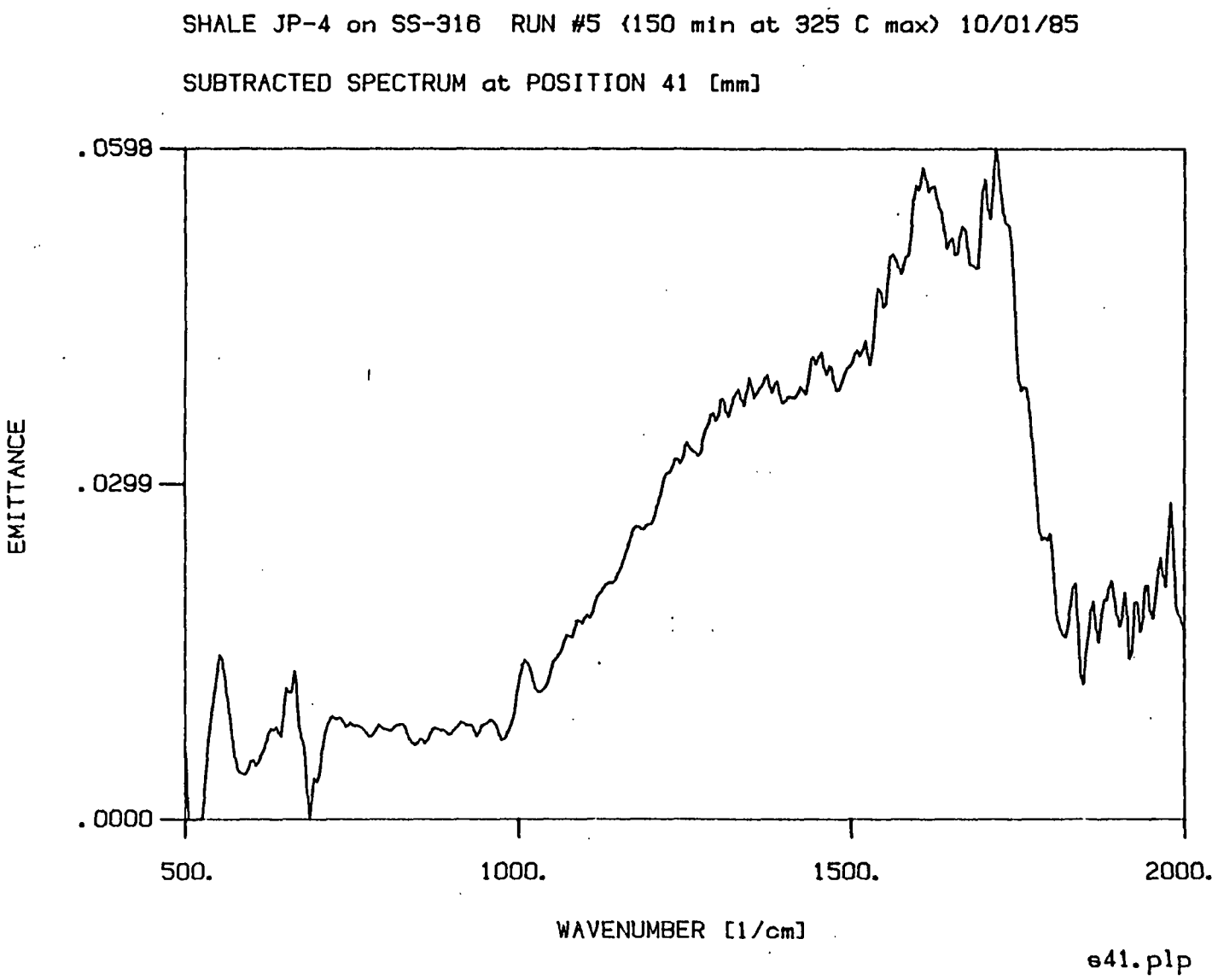
SHALE JP-4 on SS-316 RUN #5 (150 min at 325 C max) 10/01/85
SUBTRACTED SPECTRUM at POSITION 41 [mm]
.0598
.0299
.0000
EMITTANCE
500.
1000.
1500.
2000.
WAVENUMBER [1/cm]
e41.plp

Figure 37

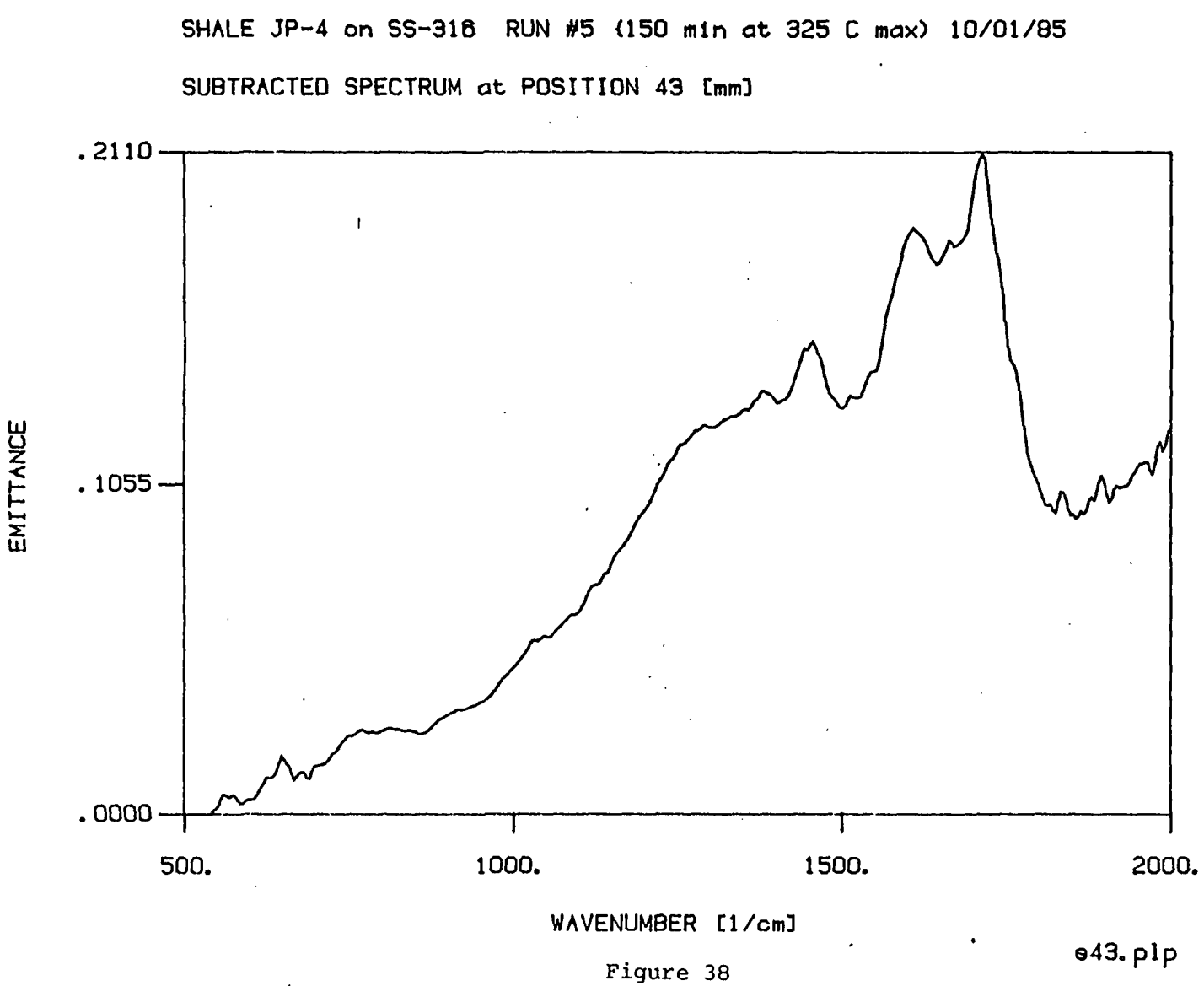
SHALE JP-4 on SS-316 RUN #5 (150 min at 325 C max) 10/01/85
SUBTRACTED SPECTRUM at POSITION 43 [mm]
.2110
.1055
.0000
EMITTANCE
500.
1000.
1500.
2000.
WAVENUMBER [1/cm]
e43.plp

Figure 38

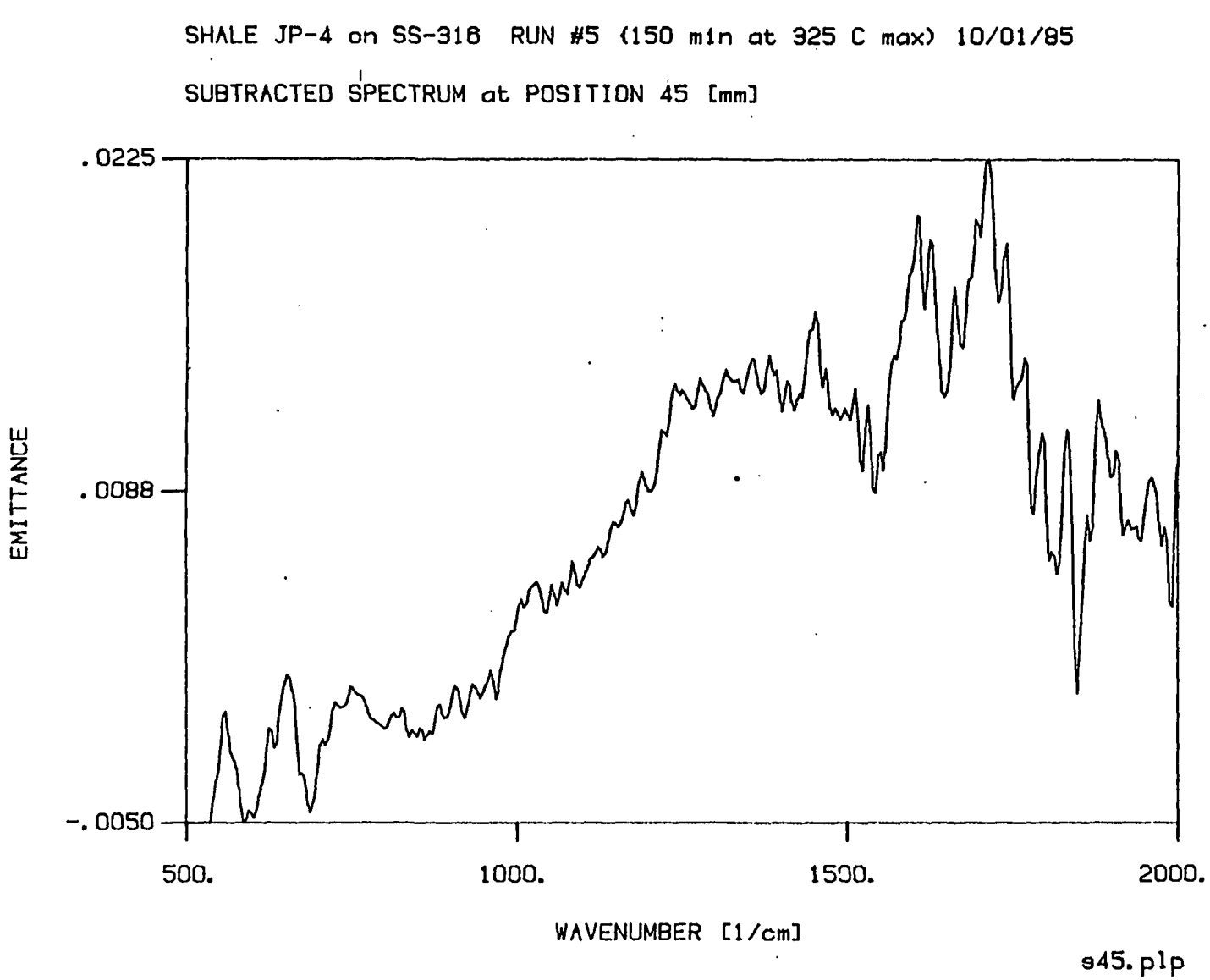
SHALE JP-4 on SS-316 RUN #5 (150 min at 325 C max) 10/01/85
SUBTRACTED SPECTRUM at POSITION 45 [mm]
.0225
.0088
-.0050
EMITTANCE
500.
1000.
1500.
2000.
WAVENUMBER [1/cm]
s45.plp

Figure 39

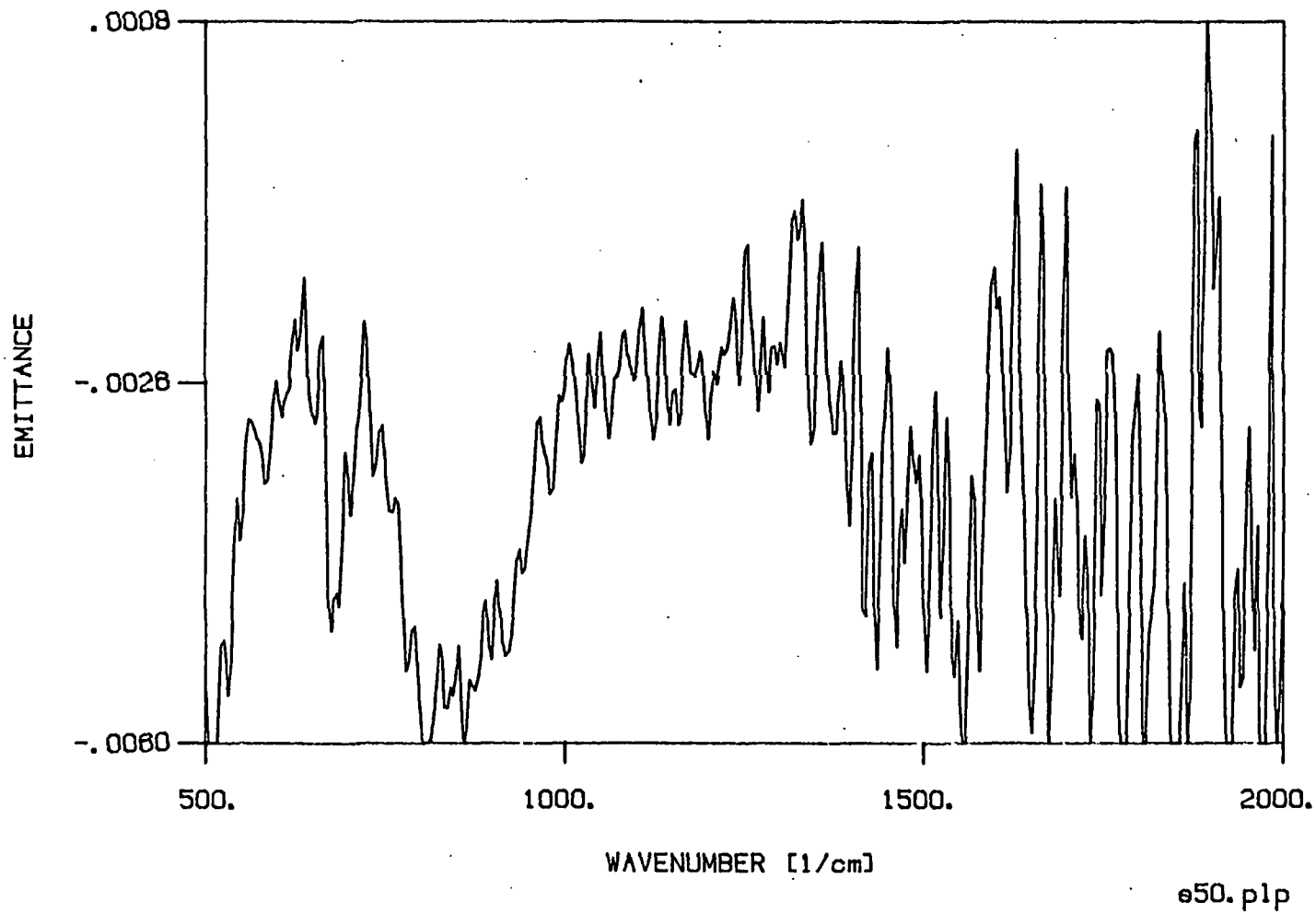
SHALE JP-4 on SS-316 RUN #5 (150 min at 325 C max) 10/01/85
SUBTRACTED SPECTRUM at POSITION 50 [mm]
.0008
-.0026
-.0060
EMITTANCE
500.
1000.
1500.
2000.
WAVENUMBER [1/cm]
e50.plp

Figure 40

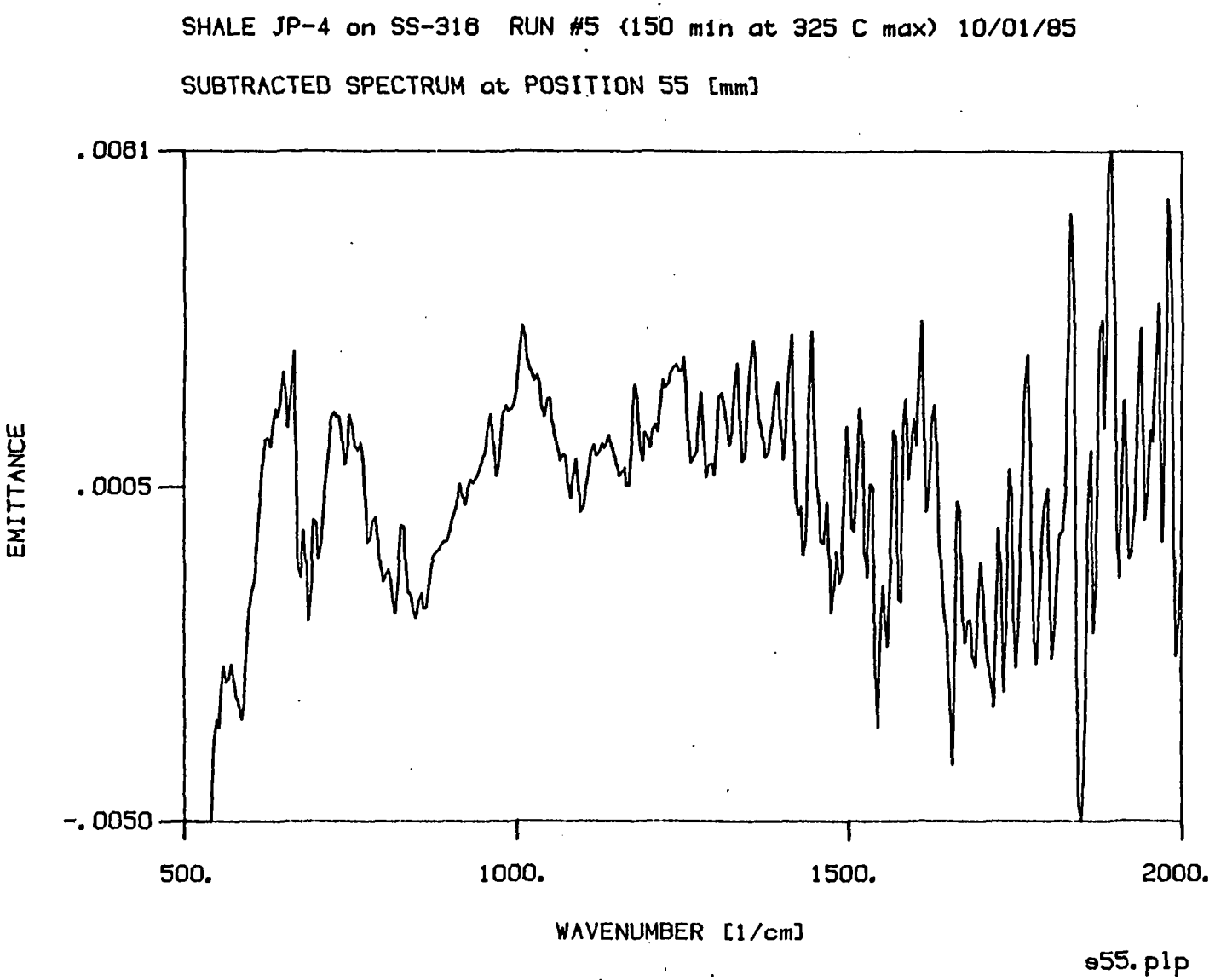
SHALE JP-4 on SS-316 RUN #5 (150 min at 325 C max) 10/01/85
SUBTRACTED SPECTRUM at POSITION 55 [mm]
.0061
.0005
-.0050
EMITTANCE
500.
1000.
1500.
2000.
WAVENUMBER [1/cm]
s55.plp

Figure 41

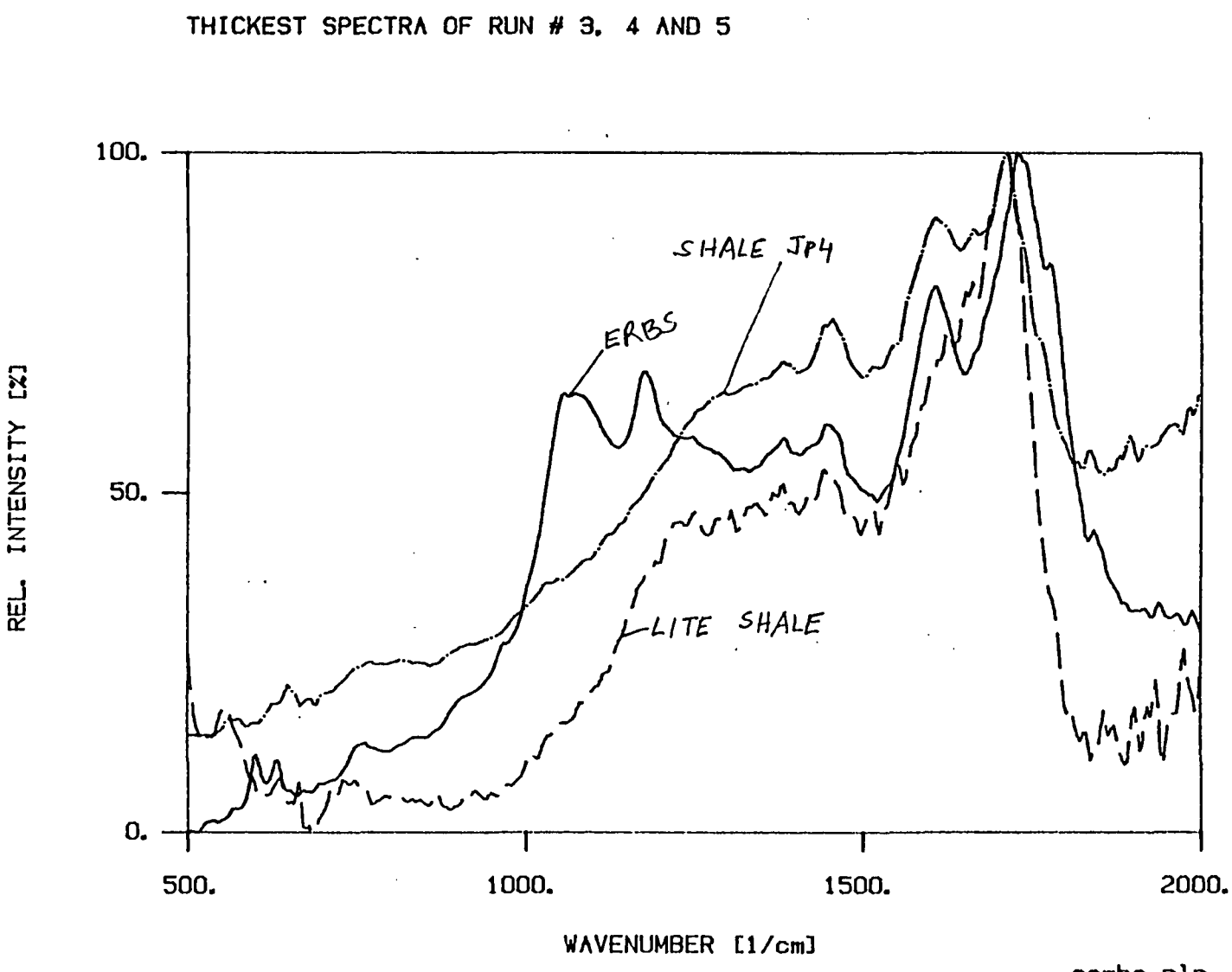
THICKEST SPECTRA OF RUN # 3, 4 AND 5
100.
50.
0.
REL. INTENSITY [%]
SHALE JP4
ERBS
LITE SHALE
500.
1000.
1500.
2000.
WAVENUMBER [1/cm]
combo.plp

Figure 42

## APPENDIX A

### Temperature Profiles

The temperature profiles vary with the material of the JFTOT tube but not with the fluids used. Figures 43 and 44 show almost identical profiles for ERBS and JP-4.

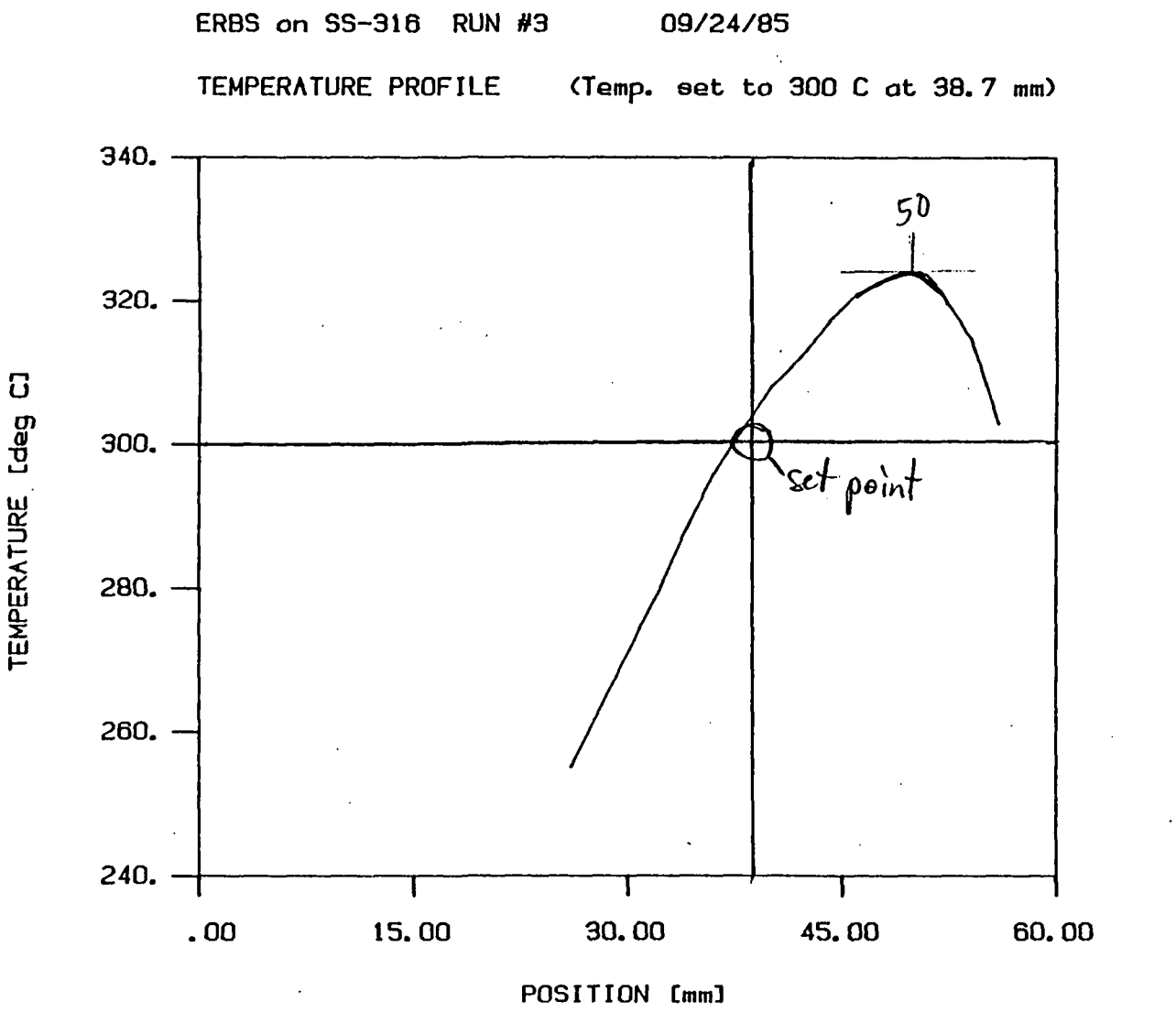
ERBS on SS-316 RUN #3 09/24/85
TEMPERATURE PROFILE (Temp. set to 300 C at 38.7 mm)
340.
320.
300.
280.
260.
240.
TEMPERATURE [deg C]
50
set point
.00
15.00
30.00
45.00
60.00
POSITION [mm]
tempro3.plp

Figure 43

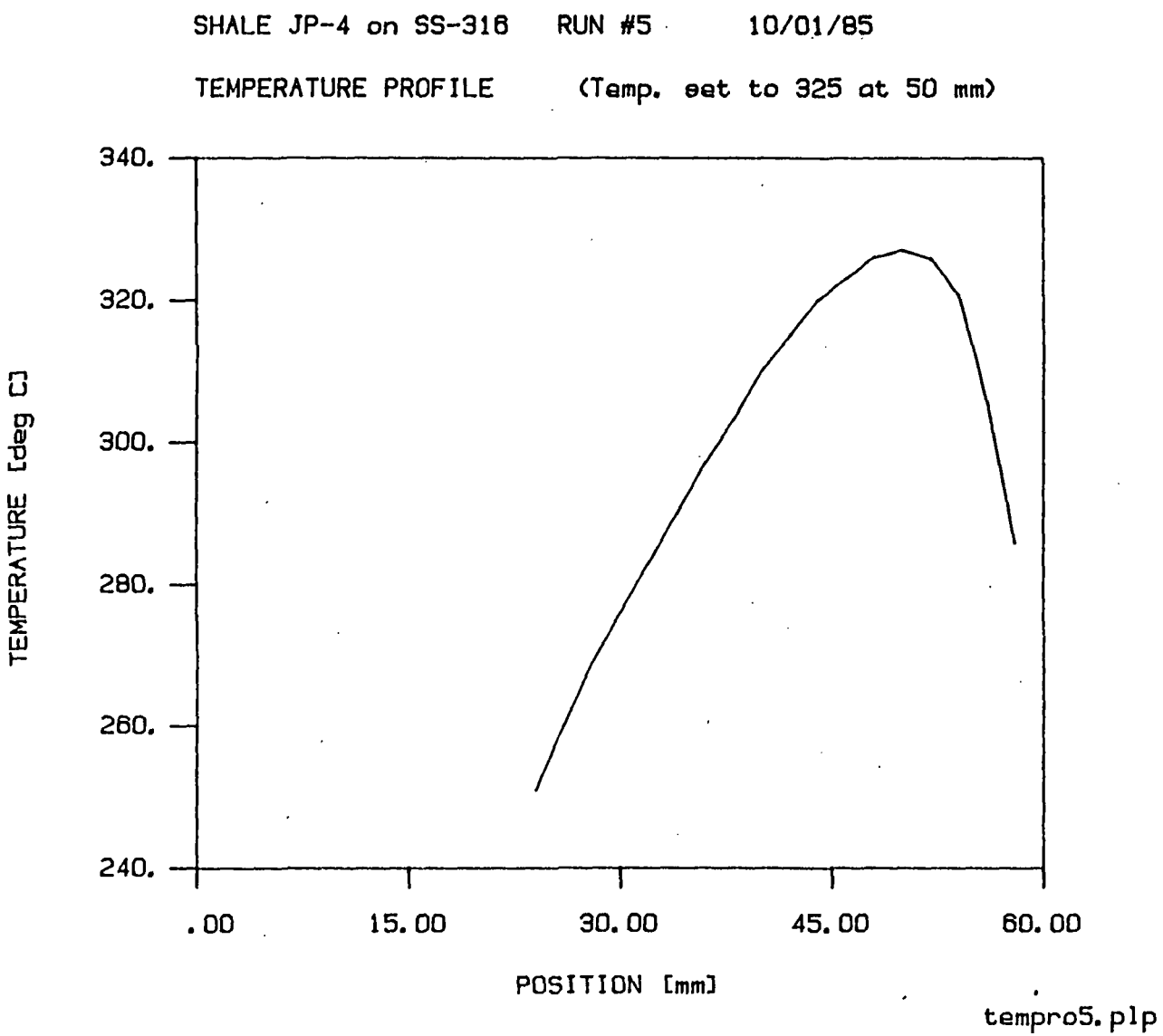
SHALE JP-4 on SS-316 RUN #5 10/01/85
TEMPERATURE PROFILE (Temp. set to 325 at 50 mm)
340.
320.
300.
280.
260.
240.
TEMPERATURE [deg C]
.00
15.00
30.00
45.00
60.00
POSITION [mm]
tempro5.plp

Figure 44